Università degli Studi dell'Insubria

DIPARTIMENTO DI SCIENZA E ALTA TECNOLOGIA

Dottorato di Ricerca in Astronomia ed Astrofisica

Reconstructing the evolutionary path of galaxies: a study of the main properties of early- and late-type galaxies over the redshift range 0.6<z<2.5

Candidate:
Sonia Tamburri

Supervisor:
Dr. Paolo Saracco

November 2014
XXVII Cycle

All'Amore, ai cieli stellati e alla gioia di vivere.

Contents

Abstract

The aim of the analysis carried out in this thesis work is twofold. On the one hand we are interested in addressing whether a sample of morphologically selected early-type galaxies (ETGs) differs from a sample of passive galaxies in terms of galaxy statistics. On the other hand we study how the relative abundance of galaxies, the number density, and, the stellar mass density of different morphological types change over the redshift range $0.6 \leq z \leq 2.5$. Furthermore, we investigated if these galaxies and their properties can provide evidences on the possible variation of the abundance of low-to-high mass stars in galaxies, i.e. the variation of the IMF, with redshift, stellar mass and colours.

From the 1302 galaxies brighter than Ks(AB)=22 selected from the GOODS-MUSIC catalogue, we classified the ETGs, i.e. elliptical (E) and spheroidal galaxies (E/S0), on the basis of their morphology and the passive galaxies on the basis of their specific star formation rate (sSFR$\leq 10^{-11}$ yr^{-1}). Since the definition of a passive galaxy depends on the model parameters assumed to fit the spectral energy distribution of the galaxy, in addition to the assumed sSFR threshold, we probed the dependence of this definition and selection on the stellar initial mass function (IMF). We find that spheroidal galaxies cannot be distinguished from the other morphological classes on the basis of their low star formation rate, irrespective of the IMF adopted in the models. In particular, we find that a large fraction of passive galaxies (> 30 %) are disc-shaped objects and that the passive selection misses a significant fraction (~ 26 %) of morphologically classified ETGs.

Using the sample of 1302 galaxies morphologically classified into spheroidal galaxies (ETGs) and non-spheroidal galaxies (LTGs), we find that the fraction of these two morphological classes is constant over the redshift range $0.6 \leq z \leq 2.5$, being 20-30 % the fraction of ETGs and 70-80 % the fraction of LTGs. However, at $z < 1$ these fractions change among the population of the most massive ($\mathrm{M}_* \geq 10^{11} M_\odot$) galaxies, with the fraction of

massive ETGs rising up to 40 % and the fraction of massive LTGs decreasing to 60 %. Parallel to this trend, we find that the number density and the stellar mass density of the whole population of massive galaxies increase by almost a factor of ~ 10 between $0.6 \leq z \leq 2.5$, with a faster increase of these densities for the ETGs than for the LTGs. Finally, we find that the number density of the highest-mass galaxies both ETGs and LTGs ($M_* > 3 - 4 \times 10^{11} M_\odot$) does not increase from $z \sim 2.5$, contrary to the lower mass galaxies. This suggests that the most massive galaxies formed at $z > 2.5 - 3$ and that the assembly of such high-mass galaxies is not effective at lower redshift.

From the analysis of the galaxy SEDs, reproduced with different IMFs, we found that the bulk ($> 80\%$) of the 1302 galaxies are best-fitted with IMFs that contain a greater relative number of low-mass stars compared to a Salpeter IMF. This trend is constant with redshift and galaxy mass, testifying that from our data we do not observe an IMF variation as function of the cosmic time, galaxy mass and galaxy morphology.

Introduction

Understanding how galaxies formed and assembled their mass along the cosmic time is a critical and not completely resolved issue of modern observational cosmology. Many studies have focused their attention on the population of early-type galaxies (ETGs), i.e. elliptical (E) and spheroidal galaxies (E/S0), since these galaxies contain most of the stellar mass and host the most massive galaxies in the local Universe (e.g. Baldry et al. 2004, Fukugita et al. 1998). For these reasons they are thought to be of fundamental importance in order to trace the history of stellar mass assembly and to explain the physical processes driving galaxy evolution. Early-type galaxies in the local Universe form an almost homogeneous family of systems mainly characterized by negligible star formation, relatively old stellar populations, red colours (e.g. Bernardi et al. 2003, Faber et al. 2007), and tight correlations among observed quantities such as luminosity, colour, size, and velocity dispersion (Renzini 2006, and references therein). Despite their apparent simplicity, the physical processes involved in the formation and evolution of ETGs are still unclear and many attempts have been done to solve this issue starting from the analysis of the galaxy morphology. In fact, the different morphology of galaxies results from the different processes with which their stellar mass has been assembled.

If visual morphological classification at low redshift is not challenging, at higher redshift morphological classification was not always feasible because of observational limits. Moreover, the increasing sizes of galaxy samples has favoured the development and the use of classification methods faster than the visual one and often based on the photometric properties of local galaxies. Accordingly, multi-colour classifications were adopted to split red galaxies with an old stellar population, in principle ETGs, from the complementary population of blue star forming galaxies, which should be predominantly discs (e.g. Strateva et al. 2001, Bell et al. 2004, Ilbert et al. 2010). However, a rigid galaxy classification starting from the bimodality of the

colour-magnitude diagram cannot take into account events that alter the galaxy colours, such as dust extinction of star forming galaxies (Williams et al. 2009) or quenched star formation in late-type objects (Bell 2008). Another technique aimed at distinguishing ETGs from late-type galaxies (LTGs) makes use of the star formation activity of the galaxies, dividing passive and active galaxies according to the efficiency of their star formation rate with respect to their mass (e.g. Feulner et al. 2005, Drory et al. 2005, Fontana et al. 2009, Cassata et al. 2011). However, as shown by Szomoru et al. (2011), while at $z \sim 2$ galaxies with low specific star formation rate (sSFR) are predominantly spheroids, in local Universe, a contamination of spiral-blue star-forming galaxies is evident and can clearly affect the interpretation of the result in term of mass assembly history of a specific galaxy population. Alternatively, the shape parameter n related to the Sérsic profile has been also used to separate disc-like surface brightness profiles ($n < 2-2.5$) from elliptical ones ($n > 2 - 2.5$) (e.g. Shen et al. 2003, Cassata et al. 2005, Buitrago et al. 2013). However, since there is not a one-to-one correspondence between the photometric properties of a galaxy and its shape, all these methods fail to distinguish the morphology of galaxies, producing mixed samples of ETGs and discs. Moreover, the photometric properties of the ETGs observed in the local Universe are not necessarily those characterizing the ETGs at high-z. Hence, the differences and the contaminations among the various selection criteria clearly show that, mixing and comparing results obtained from different selections is misleading.

As I will show in this thesis, a robust analysis should disentangle the evolutionary phases of spheroids and/or discs, since their different dynamic and shape suggest a different mass assembly history. In the current hierarchical scenario, ETGs should appear later in time as the product of mergers between small subunits of disc-like or irregular galaxies, following a hierarchical build-up similar to that of their host dark matter halos (De Lucia et al. 2006). However, from an observational point of view, ETGs seem to escape the scheme provided by the hierarchical paradigm, showing that a more complex scenario must characterize their formation and evolution. Thus, to have insight into how the matter aggregates in the galaxies we see today, it is important to keep progenitors separate from descendants. This way we can trace the evolutionary path followed by the two classes of objects, analysing the mean properties of

each morphological type and constraining the mechanisms characterizing their growing and shaping.

The aims of this thesis is twofold. On one hand I am interested in addressing whether a selection of passive galaxies select approximately the same galaxies of a morphological selection of ETGs, and hence if they can be used interchangeably or instead they produce samples significantly different whose properties cannot be compared. Moreover, I am interested in testing the dependence of the selection criterion based on the specific SFR on the different model assumptions, in particular on the choice of the stellar initial mass function (IMF). On the other hand, I am also interested in describing how the composition of the population of galaxies is changed with time both in terms of relative abundance of different morphological types and in terms of comoving number densities of ETGs and LTGs. These analysis are performed for galaxies with different masses, hence the study will also focused to understand how the baryonic matter was distributed in the two morphological classes along the time passed between $z \sim 0.5$ and $z \sim 2.5$. To further quantify the evolution of spheroidal and disc-shaped galaxies, for a complete sample of massive galaxies ($M_* \geq 10^{11}$ $M_\odot$), the analysis of the comoving mass density with redshift and the comparison of the formation epochs of the stellar components will be performed. I used the above analysis also to verify whether a variation of the relative number of low and high mass stars formed in a burst of star formation, i.e. a variation of the IMF, occurred in the last 9-10 Gyr. Indeed, the properties of galaxies (e.g. stellar mass, mean age of the stellar population, etc.) are derived from the comparison of the observational data (mainly multiwavelength photometry sampling the continuum emission) with stellar population models, that assume an a priori fixed IMF. It follows that any change of the mass distribution of stars, would drastically modify such basic properties and their evolution.

This thesis is organized as follow:

- **Chapter 1** presents an overview on the current knowledge of galaxy formation both from observational and theoretical points of view. The attention is focused on the population of ETGs and on their fundamental role in: - tracing the history of the stellar mass assembly, - understanding the evolutionary path of the baryonic matter across the cosmic time, - providing important insight into the physics of the early Universe.

- **Chapter 2** describes the main properties of the data set on which this thesis is based, the GOODS-MUSIC catalog, and the selection of the magnitude-limited sample of galaxies used in the analysis. In this chapter, the methodologies used to derive the main physical properties of the galaxies are also discussed. In particular, we focused on the analysis of the galaxy surface brightness profiles to determine the structural parameters (i.e. effective radius and axial ratio) and, on the best fitting of the spectral energy distributions through the use of synthetic models, to retrieve the main physical parameters: stellar mass, age of the stellar populations and star formation rate.

- **Chapter 3** presents a comparison of samples of galaxies selected according to the most common criteria used to select, in principle, samples of early-type galaxies. In particular, in this chapter I describe the morphological classification performed and the criteria used to define and select passive and no-passive galaxies. Then, it is shown an accurate comparison of the two selection criteria aimed at understanding if they select approximately the same galaxies or rather they produce samples significantly different. Moreover, a study of the dependence of the selection of passive galaxies on the assumed IMF is also presented.

- **Chapter 4** focuses on the evolution with redshift of the population of galaxies both in terms of relative abundance of different morphological types and in terms of their numerical growth. It is also considered the evolution of the stellar mass content of early- and late-type galaxies, focusing in particular on the most massive galaxies, to put constrains on their mass assembly. The discussion is sustained also with a study of the stellar population age and, of the formation epoch of massive galaxies, to connect the history of the galaxy mass assembly to the their stellar component.

- **Chapter 5** presents an analysis aimed at investigating whether any significant variation of the relative number of low-to-high mass stars occurred in the last 9 Gyr, i.e. whether the IMF has changed across the time. Furthermore, it is also studied if exists a variation of the stellar IMF with the galaxy stellar mass, since galaxies with different mass could have had a different history of star formation that could have influenced

their IMF. Finally, the variation of the abundance of low-to-high mass stars is studied by means of observable scaling relations, that have no dependence on any assumptions or models.

- **Conclusions** reviews and summarizes the main results of the thesis work.

Most of the analysis presented in chapters 2, 3, and 4 has been published in a refereed paper appeared on Astronomy and Astrophysics journal:
Tamburri et al. 2014, DOI: 10.1051/0004-6361/201423495

Chapter 1

A brief overview of galaxy formation and evolution

In this chapter I briefly describe the main theoretical and observational achievements of the modern extragalactic astronomy, and the questions still unsolved. The aim is not to give an extensive and complete review, but rather to introduce this thesis in the context of the galaxy formation and evolution, to allow a better understanding of the fundamental goals of this work.

1.1 The ΛCDM model

The current and accepted cosmological model to explain the different theories and phases of the Universe, from the hypothesised Big Bang and Inflation theories to the observed Cosmic Microwave Background (CMB), from the growth of the structures to the present-day accelerated expansion, is the Λ Cold Dark Matter model (ΛCDM). The concordance model, ΛCDM, assumes that the Universe is composed only for a small fraction of baryonic material, i.e. visible matter formed by standard particles: the baryons (e.g. protons, neutrons, electrons, photons, etc.). The remaining part of the Universe is permeated by *i)* dark energy (DE), represented by the cosmological constant Λ, that produces the accelerated expansion of the Universe, and by *ii)* a particular form of non-baryonic material, the Cold Dark Matter. One of the last evaluation of the composition of the Universe has been done studying the hot and cold regions of the CMB map produced by Planck. From this analysis the Universe seems to be composed by ~ 4.9 % of ordinary matter, by ~ 26.8 % of Dark Matter (DM), and by ~ 69 % of Dark Energy (ref. Planck Collaboration, Fig. 1.1).

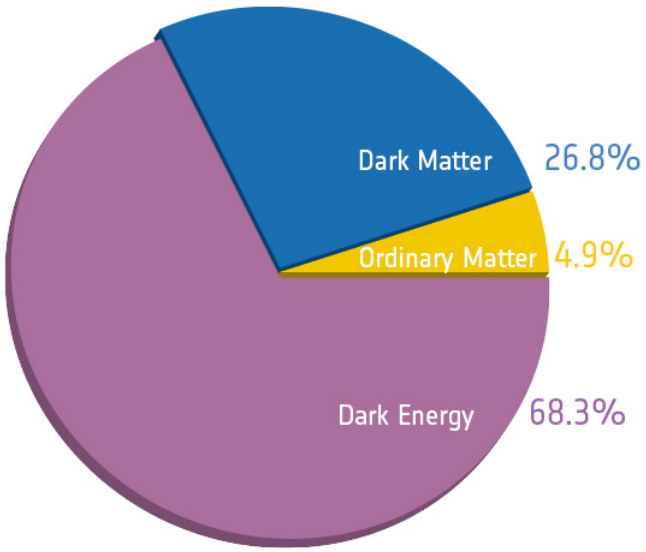

Figure 1.1: The relative amounts of the different constituents of the Universe. Image credit: ESA/Planck

The first evidence of the presence of dark energy came from the observation of SNe Type Ia, that presented a dimming larger than the expected, ascribable to the accelerated expansion of the Universe (Riess et al. 1998, Perlmutter et al. 1999). However the real essence of the DE is still matter of debate, and new methods like Baryon Acoustic Oscillations and Weak Lensing have been developed to measure the cosmic acceleration (e.g. Euclid Mission, Laureijs et al. 2011; Weinberg et al. 2013 for a review).

The other controversial Universe component is the dark matter. Its existence was initially posited by Zwicky (1933), that studying the galaxies in the Coma cluster hypothesised the presence of a large amount of invisible matter, required to hold the cluster together. After this study many observables have been proposed to sustain the DM existence, and likely one of the most famous involved the issue of the rotational curve of spiral galaxies (Ostriker et al. 1974, Rubin et al. 1978). After the general acceptance of the presence of dark matter in the Universe, the still debated problem has involved its nature and composition. Among the several options, the cold dark matter (CDM), made by collisionless massive particles with non-relativistic speed ($v/c < 0.1$), has been ascribable as the most plausible candidate to explain the observed phenomena of the luminous matter.

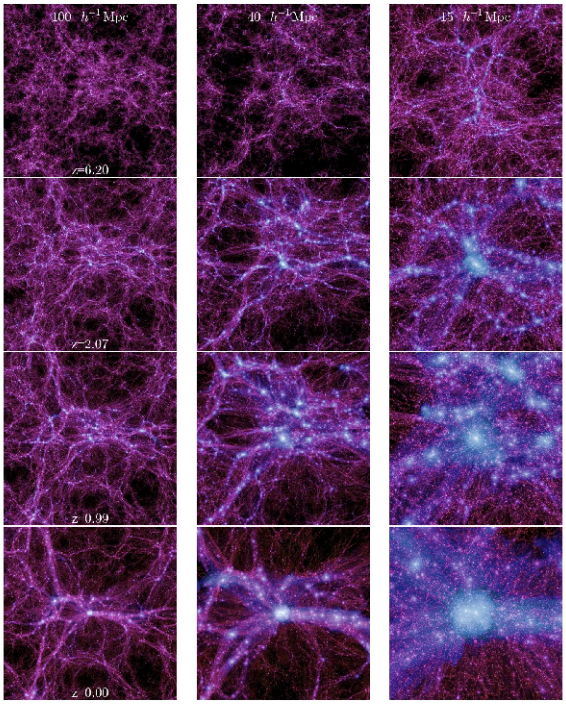

Figure 1.2: Time evolution of the formation of the most massive halo from $z \sim 6$ (*top*) to $z = 0$ (*bottom*). Zoom sequence from left to right: 100, 40, and 15 Mpc/h. Image credit: Boylan-Kolchin et al. 2009.

The dark matter is the key ingredient to explain the origin of cosmic structures and the assembling of the baryonic matter. Indeed, in a ΛCDM Universe, the formation of cosmic structures is driven by the dissipationless gravitational collapse of DM halos. These halos of CDM merge together under the effects of gravity in a hierarchical way (i.e. from smaller haloes to bigger ones), dragging with them the baryonic matter. The baryons follow the hierarchical accretion of DM halos, inside which dissipate their energy and collapse to form the luminous systems.

The scenario has been widely verified through the numerous cosmological simulations (e.g. the Millennium Simulations Fig. 1.2, Springel et al. 2005, Boylan-Kolchin et al. 2009), that describe the DM haloes formation, from the growth of the initial small fluctuations in the CMB via gravitational instability, to the formation of the filament-dominated large structures we see today.

If the processes involving the growth of dark matter haloes appear convincingly understood, the physical processes related to the baryonic matter are not fully clear. Indeed, the evolution of the DM component is reasonably well understood mostly because it involves gravitational physics (see e.g.

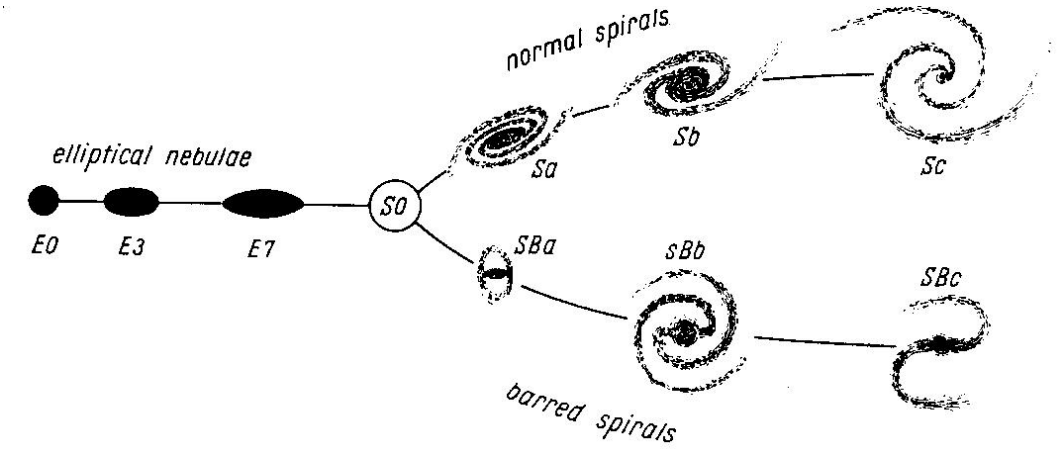

Figure 1.3: The Hubble's Tuning Fork diagram for morphological galaxy classification. Reproduced from Hubble (1936).

Wechsler 2008 for a review). On the other hand, the general scheme of the evolution of the baryons - the visible matter - is much more intricate to draw, as it depends on a complex physics. What is not totally understood at present is how from the onset of the gas accretion onto DM haloes, all the mechanisms connected with it, such as gas cooling, star formation trigger, and feedback processes lead to the assembled mass we observe today.

1.2 Galaxy classification

Historically, the first step towards an understanding of galaxy formation and baryons assembly has involved the observational approach of galaxy classification, since the morphology of a galaxy (that is its apparent shape and structure) is strictly connected to the processes involved in its formation.

Edwin Hubble in 1936 presented one of the first galaxy classification scheme, the so called *Hubble Tuning Fork* (Fig. 1.3, Hubble 1936). The Hubble's scheme was based on the optical appearance of galaxies onto photographic plates, that were separated in two main groups:

- Ellipticals (E): with a regular form, divided in 7 sub-types depending on the eccentricity of the elliptical isophote;
- Spirals (S): with thin disk and spiral arm structures.

Between ellipticals and spirals there was an intermediate class, the Lenticulars (S0), thought to be an intermediate phase in the evolution from ellipticals

to spirals. In fact, Hubble considered his classification as an evolutionary sequence with galaxy on the left changing into the morphological class on the right with time. This idea is now believed to be wrong, and if any evolutionary sequence is present on the tuning fork it could be in the opposite direction, with spirals that transform in ellipticals (see Sec. 1.3, hierarchical scenario). However, even today, the precise process describing the galaxy formation and evolution with cosmic time, from high redshift galaxies to the Hubble sequence identified in the local Universe, is still an open issue.

In the current morphological classification the spheroidal galaxies in the tuning-fork diagram are identified as early-type galaxies (ETGs), while the spiral and the irregular galaxies are called late-type galaxies (LTGs). These definitions are connected to the typical properties observed for these two classes in the local Universe. In particular, the LTGs are generally forming stars, are gas rich, present nebular emissions in the spectra, and have typical blue colours. Conversely, the ETGs have older stellar populations, have typical red colours and, a regular shape.

In this thesis the issue of the baryonic mass assembly will be treated through the study of the early-type galaxies (ETGs). As shown in Sec. 1.4, they are considered to have a crucial role in the understanding of how the baryonic matter assembled in the galaxies we observe today, since they contain a significant fraction of the total mass in stars in the local Universe, despite they numerically are only the 25-30% (Fukugita et al. 1998), they are the most massive objects at any redshift and, they have homogeneous properties from recent to distant cosmic epochs. For this reason, the understanding of their build up and growth is of paramount importance to trace the history of the stellar mass assembly in the Universe, to study the physics of the baryonic component of the Universe and, to reconstruct the star formation history at high redshift.

1.3 Formation scenarios of early-type galaxies

Historically, two main scenarios have been proposed in order to reproduce the formation and evolution of the ETGs across the cosmic time (Fig. 1.4):

- the **Monolithic scenario**: (Eggen et al. 1962, Larson 1974, Zeldovich 1970, Arimoto & Yoshii 1987, Bressan et al. 1994) in which galaxies formed in a single intense event of star formation through the collapse

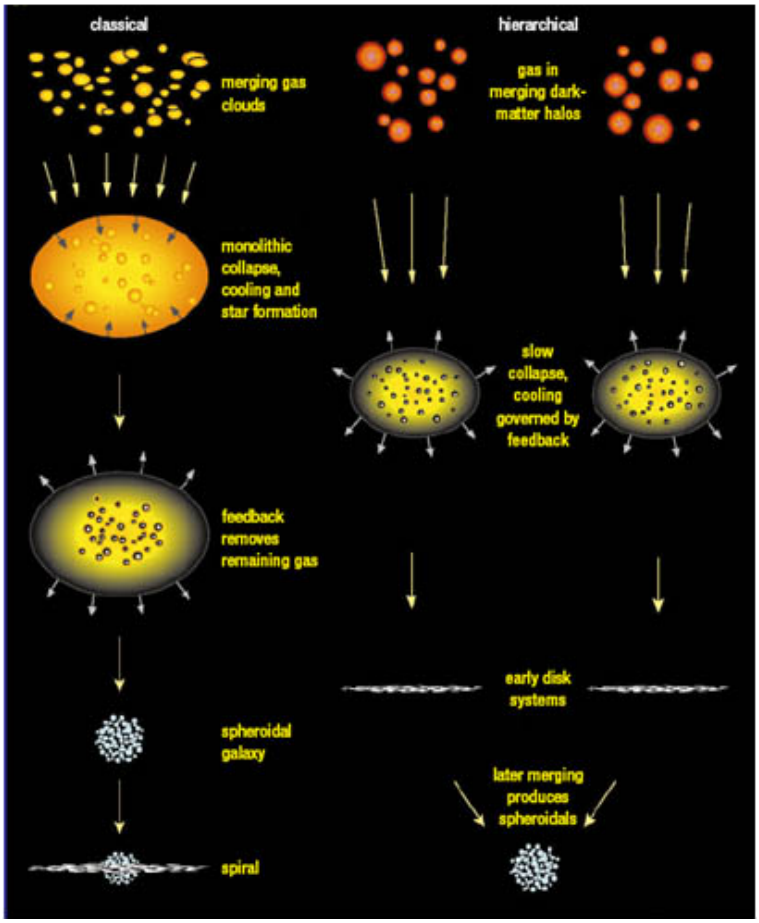

Figure 1.4: Reproduction of the two principal models of galaxy formation and evolution: the monolithic "top-down" scenario and the hierarchical merging "bottom-down" model.

and the virialization of the proto-galactic clouds, occurred on short time scale and, at very high redshift. In this scenario, the early-type galaxies rapidly stop the star formation after the collapse, and each of them evolves independently, with a passive evolution of their stellar component. This model has the peculiarity to postulate a simultaneous formation of the stars contained in the galaxy and of its mass assembly, and it is usually considered a "top-down" scenario, in which the bigger structures form early in time;

- the **Hierarchical scenario**: (White & Rees 1978, Blumenthal et al. 1984, Cole et al. 1994) in which less massive galaxies are the first to form, reflecting the hierarchical evolution of the small DM haloes at early epochs. In this scenario, the elliptical galaxies result from the continuous merging of smaller gas-rich progenitor disks over time scales comparable to the Hubble time (Kauffmann & White 1993, Kauffmann et al. 1993b), with very massive ETGs formed at lower redshift after many generations of merging; for this evolutionary path, the hierarchical merging model is labelled as "bottom-up" scenario. In such model, the star formation is not limited at the earliest time, but is diluted in a wide range of redshift. Moreover, the star formation and the galaxy mass assembly are not concomitant processes (e.g. De Lucia et al. 2006).

The monolithic collapse was able to reproduce several observational ETG properties, such as the tightness of the colour-magnitude relation and of the fundamental plane, as well as their redshift evolution (Kodama et al. 1998, van Dokkum & Standford 2003). Furthermore, it justify the high star formation rates (10-1000 $M_{\odot}$ yr^{-1}) observed in high redshift galaxies, such as sub-millimetres galaxies. However, it fails to explain some observations (Ellis 1998). For instance, it fails to reproduce the evolution of luminosity function (LF) and mass function (MF), that support the idea that new galaxies formed at $1 < z < 3$ (Fontana et al. 2006) and it fails to reproduce the presence of structures, such shells and ripples, that are clear signatures of merger events happened in later epochs. Moreover, in the monolithic scenario the evolution of stars and dark matter proceeds similarly, giving to this component a similar space distribution that is in contradiction with the observations. Finally, from the analysis of the star formation history (SFH; e.g. Ellis 1998, Madau et al. 1996, Hopkins & Beacom 2006) less of the 20 % of the observed star formation

(SF) would have occurred before $z \sim 3$, inconsistently with a single epoch of SF at high redshift.

Conversely, numerous evidences in favour of the hierarchical scenario come from both observations and from numerical simulations. Di Matteo et al. (2005) have shown that ellipticals are formed through major mergers of gas-rich disk galaxies; indeed the tidal forces developed with merger lead gas to fall in the galaxy centre, triggering the star formation and feeding the growth of central black hole (Barnes & Hernquist 1991, 1996). Subsequently, the star formation ceases, part of the gas is expelled through galactic winds, and the result is the formation of a "red and dead" elliptical galaxy. This scenario seems acceptable, because at least in the local Universe, the bulk of the star formation is located in disk-shaped or irregulars galaxies and numerous evidences of merger events are presented. However, some considerations about the kind of merger and, about the merger rate are necessary. In the current view of the hierarchical scenario the ETGs formation is probably a combination of "wet" and "dry" merger episodes. The first occurred at very high redshift, $z > 4 - 5$, concurrently with large episodes of star formation (e.g. Khochfar & Silk 2006, Naab et al 2007), the second occurred at later epochs through the coalescence of pre-existing old stellar systems, that aggregated their mass mostly in the spheroids outskirts, keeping the central part and the total stellar mass of the galaxies nearly unchanged (e.g. Naab et al. 2009, Bezanson et al. 2009, Hopkins et al. 2010).

These formation scenarios were widely testified through the development of a huge number of models, that reproduce the accretion of DM haloes, account for the transformation of gas in stars, consider mechanisms of feedback (e.g. supernova and/or AGN feedback) able to trigger and stop star formation, and reproduce the observed population of ellipticals and their properties (mass, age, metallicity, etc.). Among these analysis, the research led by De Lucia et al. (2006) using semi-analytical models, applied to both dark and baryonic matter, collected a great approval, since it was able to reproduce many observables, such as the colour/morphology distribution of low-redshift galaxies and the high metal abundance of massive ellipticals. However, unless a specific feedback mechanism was included, these models fail in reproduce the observed abundance of massive red galaxies (De Lucia & Blaizot 2007, De Lucia & Borgani 2012). In fact, the collapse of the DM haloes in a "bottom-

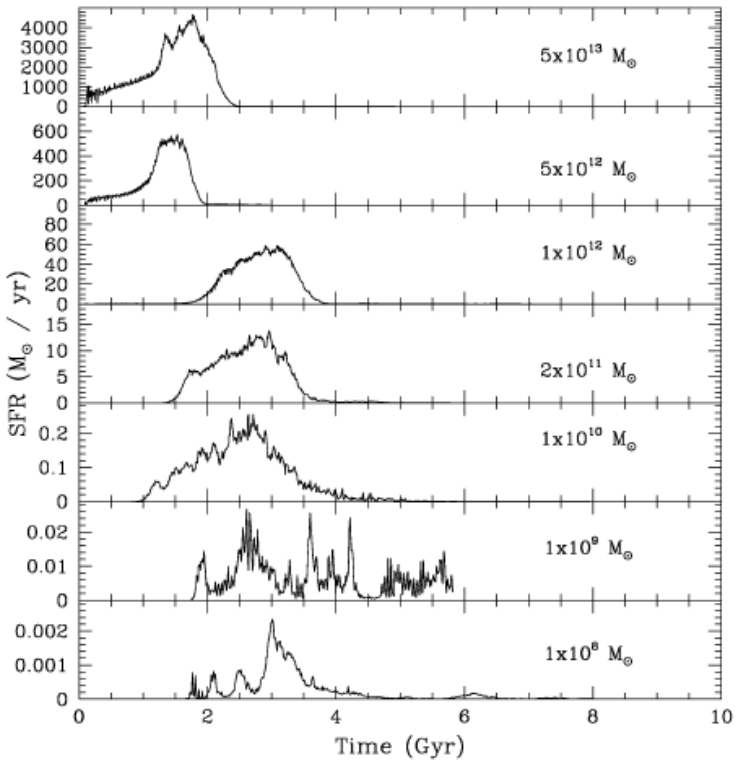

Figure 1.5: Star formation histories as model prediction from massive galaxies (top) to dwarf galaxies (bottom). Chiosi & Carraro (2002)

up" fashion is followed by an "up-sizing" in the assembly of the baryonic mass. This means that the massive ETGs assembled most of their stellar mass only at $z < 1$ and that, they are the youngest systems of the Universe, in contradiction with the observed LF and mass density findings, that predict the presence of the bulk of the massive ETGs already at $z \sim 1$.

Cowie et al. (1996), in order to solve the problem of the hierarchical scenario, introduced a model, the "*downsizing scenario*", in which the baryonic matter has a mass-dependent assembly history, with most massive systems ending their SF and their assembly first and, less massive systems that have prolonged SF extended to later epochs. This idea was postulated by Cowie et al. (1996) after the results collected studying a Ks-selected sample of galaxies. They found that the massive galaxies formed their stars within short and highly peaked star formation interval at earlier cosmic time, while the less massive galaxies extended their SF over longer period until more recent epoch.

A similar result was obtained analytically by Chiosi & Carraro (2002), that using an N-body-tree simulation found that the star formation of massive

galaxies was characterized by a singular episode of star formation that happened at very early epochs, while the smaller galaxies presented irregular and intermittent SF episodes prolonged in time (Fig. 1.5).

This trend was then observationally confirmed, studying the specific star formation rate (sSFR) as a function of the stellar mass, that showed as the massive galaxies became progressively more star forming as redshift increase (Perez-Gonzalez et al. 2005, Papovich et al. 2006, Jimenez et al. 2007). Fontana et al. (2004) found that the typical M/L ratio of massive ETGs in the K20 survey was greater than that of less massive one, indicating that their stars formed at higher redshift. Also Thomas et al. (2005, 2010), presented evidences in favour of the downsizing scenario, derived from the analysis of the star formation histories of local ETGs, that showed formation epoch (z_{form}) much higher for more massive ETGs, $z_{form} \sim 3-5$ for $M_{ETG} \sim 10^{12}$ $M_{\odot}$ versus $z_{form} \sim 1$ for $M_{ETG} \sim 3 \times 10^{10}$ $M_{\odot}$. Treu et al. (2005) analysing the M/L ratio, derived from the study of the fundamental plane, arrived at a similar conclusion, $z_{form} > 2$ for high-mass spheroidal and, $z_{form} \sim 1.2$ for less massive systems.

Reconciling the downsizing scenario in a ΛCDM Universe is not a trivial operation, since it can appear an anti-hierarchical assumption, in which the galaxy formation epochs are progressively moved at higher redshift as the mass of the galaxies increases. Several authors managed this contradiction (e.g. Granato et al. 2004, De Lucia et al. 2006, Rasera & Teyssier 2006) separating the formation of the main galaxy stellar population from the assembly of the galaxy mass. In this context the downsizing in star-formation (i.e. stars in more massive galaxies are older) is a natural consequence of mechanisms that rapidly suppress the SF (e.g. SN or AGN feedback) at earlier time in massive galaxies (Menci et al. 2006, Schawinski et al. 2006, Daddi et al. 2007). With this consideration, the local massive galaxies are formed by stars born at earlier epoch that only afterwards merged to form the massive structures we see today. However, downsizing in mass assembly seems to be more difficult to explain in this models and the existence of an old population of passive and massive ETGs already assembled at $z > 2$ remains a critical issue. Indeed, as shown in Fig. 1.6, reproduced from the Fig. 3 of Cimatti et al. (2006), the predictions of De Lucia et al. (2006) (dashed line) based on the Millennium Simulation show that the brightest and most massive ETGs are those whose space density

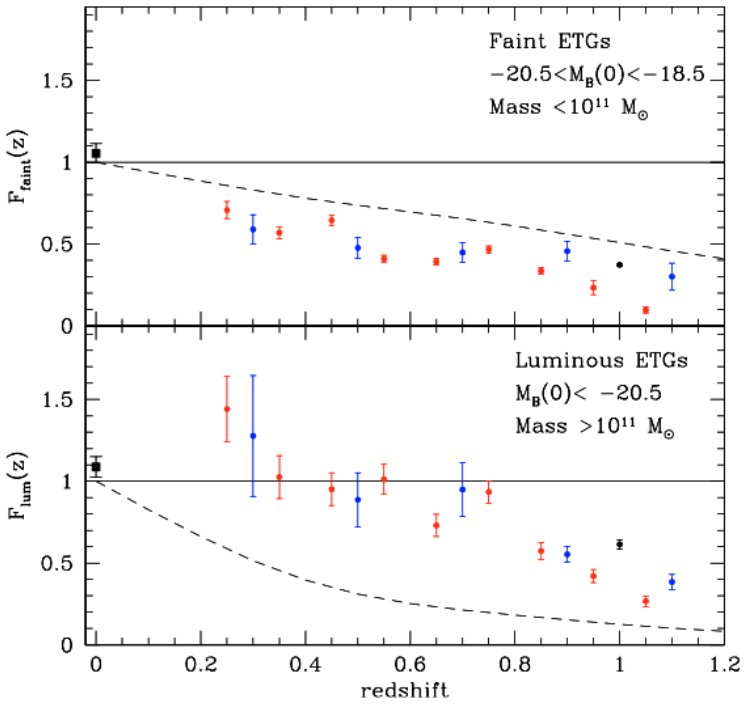

Figure 1.6: Reproduced from Fig.3 of Cimatti et al. (2006). The evolution of the fractional number density for low and high luminosity ETGs. The coloured points refer to different observations, the dashed line correspond to the prediction of De Lucia et al. (2006).

most rapidly drops with increasing redshift, contrary to the observed evolution of their luminosity function (Cimatti et al. 2006).

The results analysed until now, show that the crucial redshift interval in which the strongest evolution and assembly of massive ETGs occurred is at $1 < z < 3$ (Cimatti 2009). However, a coherent picture for explaining the observed MF of massive ETGs and the number density evolution of small galaxies is still lacking. The main problem in the description of the formation scenario is due to the difficult treatment of the stellar component and in the consideration of numerous ingredients difficult to reproduce in hierarchical model of galaxy formation, such as the star formation histories time scales, the AGN feedback, the dust content, and the stellar Initial Mass Function (IMF).

1.3.1 The cold-accretion scenario

The only convincing alternative to the hierarchical formation of spheroids is the cold-accretion scenario (Dekel et al. 2009). In this context, the formation of

ETGs is driven by cosmological cold streams and violent disk instability rather than by merger. After the hierarchical collapse of DM haloes, the primordial gas starts to falling in the DM potential wells at a rate of about 100 $M_{\odot}$/yr at the highest z, forming a rotating disk. When the surface density is high enough and the circular velocity dispersion is sufficiently low, the disk breaks up into several giant clumps, of about 1 kpc in size and up to a few times 10^9 $M_{\odot}$ each (van den Bergh et al. 1996, Elmegreen & Elmegreen 2005, Genzel et al. 2008, Bournaud et al. 2008), that migrate into the centre and dissipatively merge, forming a spheroid over short time-scales (< 1 Gyr). In this way, the galaxies acquired their gas through a continuous stream-fed of cold gas, that ensures instability and new clump formation in the disk as the older clumps migrate inward. During the gravitational collapse, the gas with high metallicity should flows towards the galaxy centre, producing a spheroids more metal-rich in the centre than in the external regions.

A systematic change in the stream properties is expected after $z \sim 1$, where the cosmological accretion rate becomes slower and the steady, narrow, cold streams no longer penetrate very effectively through the massive DM halos (Keres et al. 2005; Dekel & Birnboim 2006; Cattaneo et al.2006). The subsequent evolution of the spheroids should be mainly characterized by the ageing of their stellar populations, with small new episodes of star-formation at $z < 1$, that can derive from the minor merger with the capture of satellites. Hence, some of spheroids can further grow through inside-out accretion as in the hierarchical scenario, with the limitation to reproduce both the local scaling relations and their scatter (e.g. Nipoti et al. 2012, Saracco et al. 2012).

1.4 ETGs: ideal candidate in understanding galaxy evolution

The population of ETGs have been widely studied in the last fifty years and many correlations have been found among their physical properties, that provided some constraints about their formation. The ETGs are considered a crucial population in the observational cosmology, since they contain most of the present-day stars and baryons (e.g. Fukugita et al. 1998). Therefore, understanding the build-up and growth of ETGs allows us to trace the assembly of the baryonic mass of galaxies in the Universe. Moreover, at any redshift, they are rather homogeneous systems in terms of morphology,

colours and scaling relation (Roberts & Haynes 1994, Renzini 2006). Hence, following their evolution over the cosmic time can give important insights in understanding the physical origin of the Hubble morphological types, the history of assembly of the stellar components, and the evolution of the large structures in the Universe. As follows, it will be presented an overview of the most crucial relations observed for the ETGs from low to high redshift, that make them an excellent probe to investigate the history of the stellar mass assembly of galaxies over cosmic times.

One of the first correlation found was the tight relation between colour and magnitude (C-M) of ETGs observed firstly by Baum (1959), and then definitely established studying 9 local cluster of galaxies and other groups by Visvanathan & Sandage (1977) and, Sandage and Visvanathan (1978a, 1978b). In their analysis, they found the same correlation between all the analysed systems, arguing that both ellipticals and S0 passively evolved in the last 1 Gyr and that the universality of the C-M could be used as distance estimator. Subsequently, Bower et al. (1992, 1999) studying the slope of the C-M of ETGs in the Coma and Virgo clusters (top panel of Fig. 1.7), provided constraints for the first time on the age of the stars in ETGs, concluding that the bulk of the stellar component of ETGs must have formed at $z > 1$.

At the same time, Bower et al. (1992) found a tight relation with a small scatter between the colour-σ (where σ is the central velocity galaxy dispersion) of the ellipticals in Virgo and Coma clusters (bottom panel of Fig. 1.7). The colour-σ relation added a further support to the idea of early formation of stars in ETGs, and placed constraints to the mergers rate occurred in ETGs, through the study of the colour variations and the luminosity changes.

These studies were then extended also for galaxies at higher redshift. Stanford et al. (1998) followed the colour evolution in cluster up to $z \sim 0.9$, showing that the small scatter of the C-M relation observed for local cluster was re-found also at higher redshift. This small dispersion was the proof that the star formation in cluster ETGs was highly synchronized.

For what concerns the field ellipticals, many investigations (e.g. Schade et al. 1999, Baldry et al. 2004, Kodama et al. 2004) recovered the same C-M relation observed for cluster galaxies both at low and high redshift. Some of these studies found that, the field ellipticals could be ~ 1 Gyr younger that their cluster counterpart, and that up to $z \sim 1$ the C-M relation of ellipticals

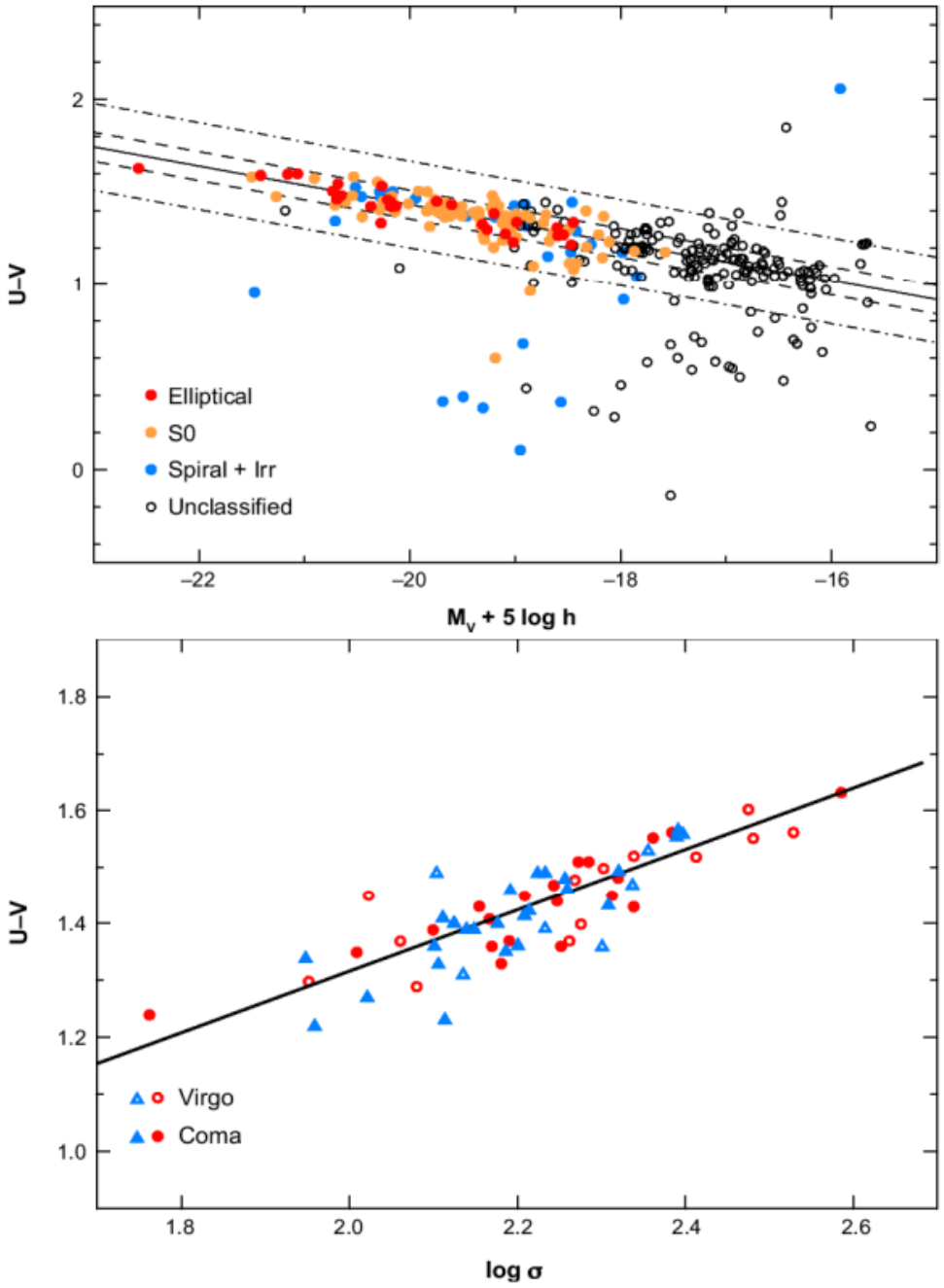

Figure 1.7: *Top:* Figure 2 from Bower et al. 1999, (U-V)-M_V colour-magnitude for spectroscopically confirmed galaxies of the Coma cluster. Different colours refer to different morphological types. *Bottom:* Figure 3 from Bower et al. 1992, (U-V) colour versus velocity dispersion (σ) for ellipticals (red) and lenticulars (blue) in the Virgo and Coma clusters. Figures with colours reproduced from Renzini 2006.

evolves in a manner that is consistent with a pure passive evolution of the stellar component. Moreover, it was noticed that early and late morphological types occupy different locations in the C-M diagram, defining a "red sequence" and a "blue-cloud" that represent the different populations of galaxies that are produced by two different formation processes (Bell et al. 2004, Faber et al. 2007, Franzetti et al. 2007).

Another crucial discovery, that help to put several constraints on the ETG formation, was the observation of the Fundamental Plane (FP), that is an empirical relation between the effective radius (R_e), the central velocity dispersion (σ) and the luminosity intensity (I_e) within R_e of elliptical galaxies, with $R_e \propto \sigma^a I_e^b$ and, a and b depending on the band used to measure the luminosity (Dressler et al. 1987, Djorgovski & Davis 1987). The existence of the FP derives directly from the virial equilibrium of the ellipticals ($\sigma^2 \approx GM/R$), it is connected to their self-similar structures, and to the properties of their stellar populations (e.g. Binney & Tremaine 2008, for a review). Bender et al. (1992) were the first to found a tiny scatter in the plane and a tilt, that was explained by a smooth variation of the mass-to-light ratio (M/L) with mass, that does not imply a departure from virialization of ETGs. Renzini & Ciotti (1993), through the study of the small scatter of the FP, showed that ellipticals assembled their mass via regular mechanisms, that implied small age dispersion and high formation redshift. Bernardi et al. (2003) through a complete comparison of the FP in clusters and field, for a sample of $\sim$ 40000 SDSS morphology- and colour-selected ETGs, estimated that the average surface brightness of ETGs in low density environment was $\sim$ 0.08 mag brighter than in cluster. This difference implies that the ages of the field ellipticals are on average $\sim$ 1 Gyr younger than those in high density clusters, hence the environment regulates the time-scale of the star formation histories.

From all these studies a picture seems to have emerged. The ETGs formed the bulk of their stars at high redshift and then undergone a passive evolution with few new SF events; moreover, the environment in which they have been observed seems to influence the formation epoch of their stars that appear $\sim$ 1 Gyr younger in the field than in the cluster.

However, the caveat to remember is that all these evidences prove that at least some ETGs evolved passively from $z \gtrsim 1$ to $z = 0$, but other local ETGs may have progenitors that at high redshift have a different morphology

("progenitor bias", van Dokkum & Franx (1996)). These progenitors are hence not considered when the evolution of the C-M or of the FP of local ellipticals is treated.

1.4.1 The luminosity and mass function

Another important tool to study the evolution of the ETGs through the cosmic time is provided by the study of the luminosity function (LF) and of the galaxy stellar mass function (GSMF) from the local Universe up to higher redshift. Both the LF and the GSMF represent the galaxy comoving number density in a luminosity/mass interval, and can be parametrized, at least as a first approximation, by a Schechter function (Schechter 1976),

$$\phi(L) = \phi^* \Big(\frac{L}{L^*}\Big)^{\alpha} \, exp\Big(-\frac{L}{L^*}\Big), \tag{1.1}$$

where ϕ^* is the normalization factor, L^* is the luminosity cutoff between the exponential law and the power-law shape, and α is the slope of the power-law.

At low redshift the LF has been carefully determined thanks to the availability of numerous surveys of galaxies (e.g. SDSS, York et al. 2000, 2dF, Colless et al. 2001), that have enabled to find a steepening of the faint end slope of the LF at bluer wavelengths, probably consequence of an increased number of LTGs, that have a typical lower luminosity with respect to the ETGs (Jones et al. 2006). Baldry et al. (2004), analysing the LF of red and blue galaxies in SDSS, selected according to the colour bimodality of the C-M relation, found that the red LF as a brighter characteristic luminosity L^* and a shallower faint-end slope compared to the LF of blue galaxies. Salimbeni et al. (2008), with a similar approach and, thanks to the availability of the deep observations of the GOODS-survey (Grazian et al. 2006), followed the LF evolution of blue and red galaxies up to $z \sim 3$. They found for the total sample and for the blue galaxy sample a mild luminosity evolution in the redshift interval $z = 0.2 - 1$, and no evolution at higher redshift (Fig. 1.8). While they constrained the LF of red galaxy only up to intermediate redshift founding an excess of faint red dwarfs.

The galaxy LF at intermediate and high redshift has been studied by many authors (e.g. Ilbert et al. 2004, 2005, Saracco et al. 2006, Willmer et al. 2006, Faber et al. 2007), some differences can be found between these studies, but a general trend shows that the population of local bright galaxies was already

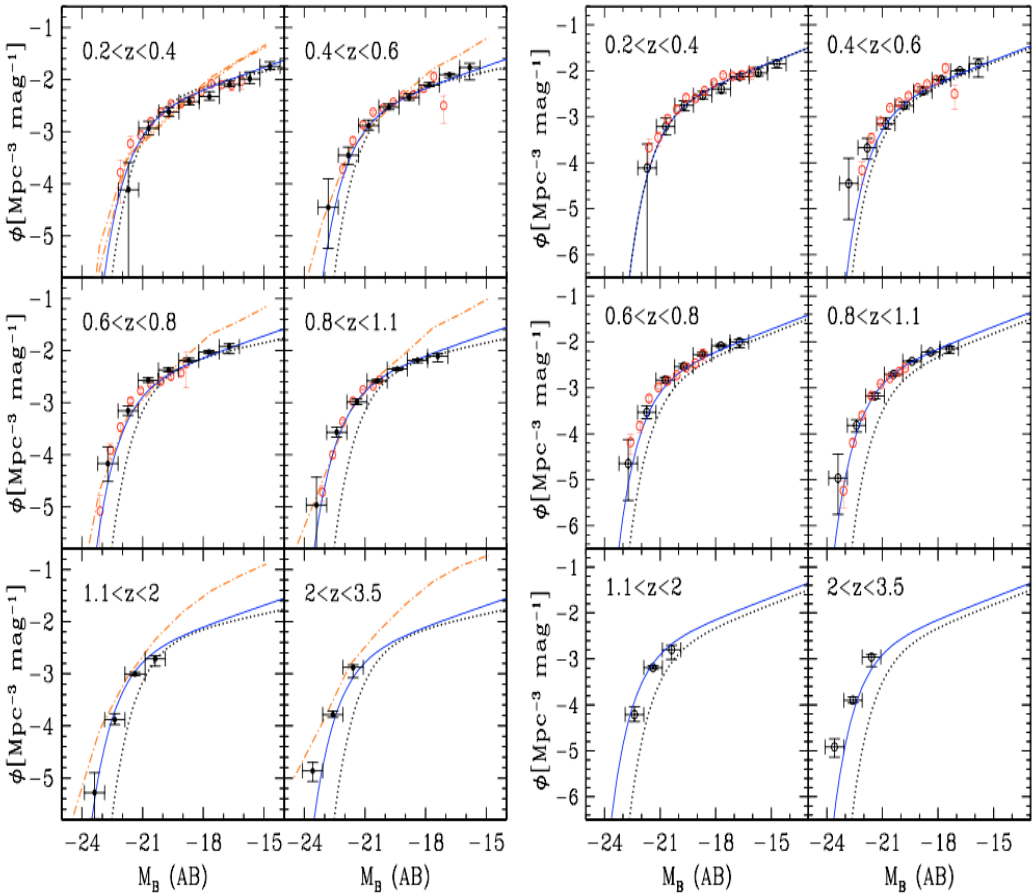

Figure 1.8: *Left:* total LF as a function of redshift. The dotted line is the local LF (Norberg et al. 2002). The filled circles are the points obtained with $1/V$ MAX method. The empty circles come from the DEEP2 survey (Willmer et al. 2006). The dashed-point line is the model of Menci et al. (2006). *Right:* LFs of the blue galaxies as a function of redshift. Lines and points as right panel. The two figures are reproduced by Salimbeni et al. (2008).

formed at $z < 0.8$ and that, the total LF is mainly dominated by the blue/late population, indeed although the blue galaxies have a lower L^* they dominate the volume redshift at any redshift. On the other hand, the red galaxies present a flatter slope of the LF compared to the global LF but, for $z \lesssim 1.5$ they contribute significantly to the bright part of the LF (Bell et al. 2004, Cimatti et al. 2006, Zucca et al. 2009, Fritz et al. 2014). Moreover, Cimatti et al. (2006), through the study of the number density evolution of a sample of massive ETGs, showed that the ETGs on the bright-end of the LF ($M \gtrsim 10^{11}$ $M_{\odot}$) were already all in place at $z \sim 0.8$, hence no new massive ETGs were formed at lower redshift and major merger must be relatively limited (López-Sanjuan et al. 2012). This result favours the hypothesis that the massive ETGs

assembled their mass at high-redshift, and as I showed in Sec. 1.3 (*downsizing scenario*), putting several constrains on the galaxy formation scenarios.

The other important tool to probe when galaxies formed and assembled their mass derives from the study of their stellar mass content through the analysis of the GSMF. Follow the GSMF across the cosmic time can reveal the evolutionary path followed by different galaxy populations at different epochs, and can help to understand if the galaxy mass assembly is mainly driven by mergers events or in-situ star formation.

In the local Universe the characteristic mass of the GSMF has been found larger for ETGs than for LTGs, while the faint end slope was steeper for late-type galaxies. At higher redshift, following the evolution of the GSMF up to z=1 in the 1.4 deg^2 of the zCOSMOS survey (Lilly et al. 2007, 2009), Pozzetti et al. (2010) found a rapid increase in the global GSMF for galaxies with $M < 10^{11}$ $M_{\odot}$ and a slower increase for $M > 10^{11}$ $M_{\odot}$ galaxies. This trend was observed in a more pronounced way for the ETGs, this implies an earlier build up of stars and mass in the massive galaxies compared to the lower mass ETGs. Ilbert et al. (2013) studying the stellar mass assembly out to z=4 in the COSMOS field, confirmed that the global GSMF is strongly mass-dependent, i.e. the low-mass end evolves more rapidly than the high-mass end. However, the contribution of low-mass galaxies to the GSMF remains still uncertain due to the observational limits associate to less bright galaxies.

From the GSMF several authors derived the evolution of the stellar mass density as a function of redshift, however the results are controversial. Arnouts et al. (2007) and Ilbert et al. (2010) found that the stellar mass density of red galaxies increased by an order of magnitude between $z \sim 2$ and $z \sim 1$, this rapid evolution was interpreted as an increase in the star-formation quenching, that caused a galaxies transformation from active SF to passive galaxies. Instead, Brammer et al. (2011) found a halved evolution of the mass density in the same redshift interval without appealing to a morphological transformation. The inconsistencies can probably due to a different method of galaxy selection.

The study of GSMF help to understand how galaxies assembled their stellar mass, however, despite all the progresses made to understand the mass assembly of ETGs, the models adopted to predict the galaxy mass assembly, are unable to correctly reproduce the observed GSMF. For instance, some

models tend to underestimate the high-mass contribution and overpredict the rate of its evolution (Fontana et al. 2004, 2006), and others tend to overpredict the number density of low-mass galaxies (Fontanot et al. 2009, Marchesini et al. 2009).

1.4.2 The evolution of the number and mass density

In order to establish the evolutionary path of ETGs it is fundamental to determine which are the properties undergoing evolution and to accurately trace their variation back in time. A powerful tool to study the galaxy evolution of a morphological type of galaxies is to analyse how evolves its number and mass density (ρ_N and ρ_*) as a function of redshift, since they can give ideas of the mechanism and of the time-scales involved in the galaxy evolution.

The number density of the ETGs has been widely studied by many authors, from these studies a similar scenario emerged, in which the most massive ETGs are already in place at $z \sim 1$ while less massive ones appear later (e.g. Pozzetti et al. 2003, 2010, Bundy, Ellis & Conselice 2005, Zucca et al. 2006, Franceschini et al. 2006, Scarlata et al. 2007, Brammer et al. 2011, Ilbert et al. 2013, Muzzin et al. 2013). Scarlata et al. (2007) analysing the evolution of the number density of a sample of bright ETGs ($L > 2.5L*$) in the ~ 2 deg^2 of the COSMOS field (Scoville et al. 2007), found no significant evolution in the range $0 < z < 0.7$, with only a 30% of possible increase if different star formation histories were considered. Pozzetti et al. (2010) studying the zCOSMOS survey (Lilly et al. 2007) found an almost negligible evolution in the number density of quiescent massive galaxies ($M > 10^{11}$ M$_\odot$) between $0.25 < z < 0.85$. Ilbert et al. (2013), with the analysis of quiescent galaxies selected according to a two-colour selection technique in the UltraVISTA project (McCracken et al. 2010), did not find any significant evolution of the ρ_N of massive galaxies at $z < 1$, while observed an increase by a factor grater than 5 for the low-mass quiescent galaxies ($log(M/M_\odot) \sim 9.5$), that was interpreted as due to the continuous quenching of galaxies between $z \sim 1$ and $z \sim 0.1$. Moreover, Ilbert et al. (2013) found an increase in the stellar mass density of all quiescent galaxies (independently from their stellar mass) between $1 < z < 3$ of a factor almost 10, and an increase of a factor ~ 40 for the massive quiescent galaxies between $2.5 < z < 3$, due to the quenching of star-forming galaxies.

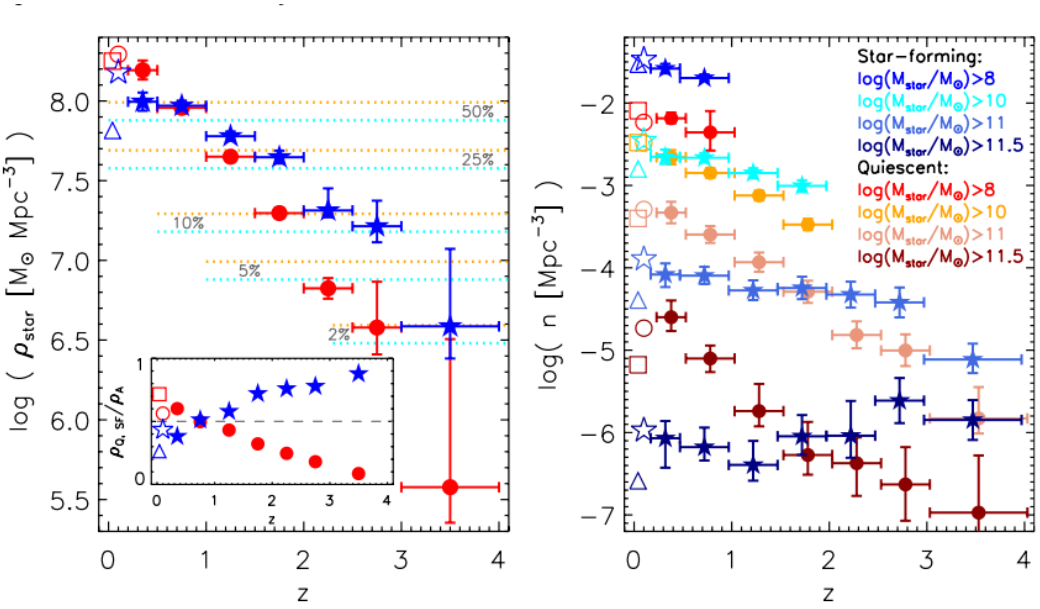

Figure 1.9: Reproduced from Muzzin et al. (2013). Evolution of the stellar mass density of star-forming (blue) and quiescent (red) galaxies as a function of redshift (left panel). Evolution of the number densities of the two morphological classes at a fixed mass limit as a function of redshift.

Brammer et al. (2011) analysing the number density of quiescent galaxies in the NEWFIRM Medium-Band Survey, find also an evolution of the quiescent population at $1 < z < 2$, but with an halved rate compared to Ilbert et al. (2013). Moresco et al. (2013) studying sample of ETGs selected according different criteria in zCOSMOS survey confirmed a low increase (< 10 %) in the number density of massive ETGs at $0.2 < z < 0.65$, while an increase of a factor $\sim 2-4$ for the lower massive ETGs in the same redshift range. Muzzin et al. (2013), using a K_S selected catalogue of the COSMOS/UltraVISTA field, found that the stellar mass density of the quiescent galaxies grows twice as fast as the star-forming population at all redshift, and that the number density of massive quiescent galaxies ($log(M/M_{\odot}) > 11.5$) steady increase at $z < 3.5$ (Fig. 1.9). Furthermore, they found that the stellar mass density of the Universe was only 50 %, 10 % and, 1 % of its current value at $z \sim 1.0$, 2.0, and 3.5, respectively.

A significant uncertainty remains on the contribution of low mass galaxies, which could have effect on the stellar mass density at high redshift ($z > 2$; Mortlock et al. 2011). Moreover the different selection criteria adopted to identify spheroidal galaxies (e.g. red colours, quiescence of their

stellar component, two-colours selection) can induce a gap between different measurements (Cassata et al. 2011). Indeed, it is worth emphasizing that even a low-level of ongoing star formation can make spheroidal galaxies drop out of the ETG samples and, a low level of dust obscuration can make LTGs enter in the ETG samples, hence the number density evolution of the ETGs could be under/over-predicted.

We have seen that the evolution of the comoving number and mass density of galaxies are some of the quantities most frequently used to describe the rate at which galaxies assembled their stellar mass across the time (e.g. Pozzetti et al. 2010). These quantities and distributions are fundamental since they are usually compared with the predictions of hierarchical models of galaxy formation and evolution. However at high redshift, the properties of galaxies (e.g. luminosity, stellar mass, mean age of stellar population, etc.) are derived from the comparison of the observational data (mainly multiwavelength photometry sampling the continuum emission) with stellar population models. All the models used so far are based on the stellar initial mass function derived from the properties observed in local galaxies and assumed a priori independent of time, environment, metallicity, galaxy morphology. As shown in the next section this could be a strong assumption, that needs to be considered when the different phases of the mass assembly want to be constrained.

1.5 The importance of the stellar initial mass function in constraining the evolution of ETGs

The most widely adopted approaches to constrain the assembly history of galaxies pass through the analysis of their stellar population properties (e.g. stellar mass, age, star formation history and time-scale) over cosmic time. These properties are derived, at different redshift, by comparing observations with stellar population synthesis (SPS) models strictly dependent on the stellar initial mass function (IMF). Hence, an intrinsic degeneracy exists between the assumed IMF and the derived properties of a stellar population, and several discrepancies in the understanding of the galaxy evolution can derive from the poor knowledge of the IMF.

The IMF is the mass distribution of stars which form in a star-formation event and provides the relative number of low- and high-mass stars in a

galaxy. Since the evolution with time of stars depends primarily on their mass, it follows that the IMF is of fundamental importance in determining the properties of galaxies and how they evolve with time. Actually, the stellar mass of a galaxy is mainly determined by the long-lived low-mass stars (≤ 1 $M_{\odot}$), while intermediate and high-mass stars (≥ 1 $M_{\odot}$) principally contribute to the total luminosity. Moreover, the short-lived massive stars control the quantity of heavy elements in the IGM and the evolution of gas content (Larson 1998). Thus, any change in the IMF would drastically modify the basic galaxy properties and their evolution.

Up to now, the widely adopted stellar IMF can be approximated by a declining power law as originally suggested by Salpeter (1955) even if other studies suggested that it may overestimate the number of low-mass stars (≤ 1 $M_{\odot}$ e.g. Kroupa 2001). Currently, both observational (e.g. Treu et al. 2010) and theoretical (e.g. Larson 2005) arguments strengthen the hypothesis of an IMF described by a power law posing the central problem of determining the relative number of low-to-high mass stars, i.e. its slope.

The implicit assumption in models of galaxy formation and evolution is that the IMF is a universal function, i.e. it does not vary with time and place: the relative distribution of low-to-high mass stars has been always and anywhere the same. This assumption stems from the fact that the IMF has been found not vary, within uncertainties, among Milky-Way stellar clusters and OB associations (e.g. Kroupa et al. 2013). Intuitively, there is no reason to suppose the IMF of galaxies independent of galaxy morphology, environment, metallicity, and redshift, but until the last years works in favour of a universal IMF, i.e. in agreement with the set of values proposed by Salpeter/Kroupa/Chabrier (Bastian 2010 for a review), alternate with some others supporting an IMF with variable slope (Elmegreen 2009, Conroy & van Dokkum 2012, Spiniello et al. 2012, Ferreras et al. 2013).

Assuming a priori that the local IMF is representative also of the IMF of galaxies at high redshift, for instance of galaxies at $z \sim 1.5$, 9-10 Gyr younger with most of their life and evolution not yet occurred, or even representative of the very early phases of galaxy formation, seems a very strong assumption. Indeed, galaxies in the local Universe have behind 13 Gyr to form and assemble their stellar content. Their stars can be formed through subsequent episodes of star formation, through merging events or a combination of the two.

Each episode of star formation, indeed, produces a population of stars which enhances the metallicity of the gas at disposal to the subsequent burst. The higher metallicity increases on average the minimum mass needed by a gas cloud to collapse lowering the probability that very low-mass stars (< 0.4 $M_{\odot}$) form. These mechanisms affect substantially the resulting stellar mass function since change the relative fraction of low-mass and high-mass stars.

If on one hand the validity of the local IMF at high redshift does not seem a robust assumption due to the unknown long mass assembly history of local galaxies, there are also some reasons to think that at high redshift the IMF was actually dominated by massive stars contrary to the local IMF. The first reason is that the first stars are expected to contain no heavy elements (e.g. Abel et al. 2002; Bromm et al. 2002). However, no metal-free low-mass stars, those long-lived able to survive up to now, are observed. Thus, the first stars had to be short-lived high-mass stars to rapidly evolve and die. A similar problem, a deficiency of metal-poor stars called G-dwarf problem, is also observed in the solar neighbourhood. Another reason is the large total mass of heavy elements observed in high-redshift clusters. This fact points toward a higher proportion of high-mass stars than in the present-day IMF. Furthermore, the evolution of the IMF with cosmic time have been suggested to reconcile also the integral of the observed star formation history with the observed mass density history (Wilkins et al. 2008). Finally, the strong evolution of the cosmic luminosity density resulting from the studies of high-redshift galaxies suggest a top-heavy early IMF (e.g. Baugh et al. 2005). However, in spite of these considerations, the IMF is always considered universal and assumed that locally observed.

In the last years it has been diffused the idea that the ETGs are the best candidates to prove the mass distribution of the earliest stars (i.e. the IMF), since at any redshift they host the oldest stellar population and are the most massive among the galaxies (e.g. Renzini 2006). The oldest age of the stellar population maximizes the probability that the relevant burst is the earliest one, i.e. the initial one. The high-mass content means that ETGs started to assemble their mass earlier than the other galaxies and that the resulting IMF is probably closer to the initial one than in the other galaxies. The negligible star formation assure that the contribution from young stars to the integrated light and mass is negligible, contrary to the other star forming galaxies at high redshift. Moreover, their high-mass content represent almost 70% of the

stellar mass in the local Universe (Fukugita et al. 1998). Thus, constraining their IMF means to constrain the distribution in mass of 70% of the stars in the universe.

Several recent studies, that involve the analysis of the IMF in the ETG population through the use of new techniques (e.g. spectral analysis, strong lensing, dynamics), have recently pointed to a varying IMF with velocity dispersion σ_v (i.e. with total mass and/or mass density) in ETGs, the so called IMF-σ_v relation: ETGs having higher velocity dispersion have a bottom-heavier IMF, i.e. an enhanced fraction of low- to high-mass stars. Other dynamical and lensing studies have offered a new indirect method to probe the IMF, constraining the mass-to-light ratio, rather than the IMF shape (e.g. Cappellari et al. 2012). van Dokkum & Conroy (2010) studying gravity-sensitive features in the galaxies' unresolved light of local massive ETGs, concluded that their IMF is bottom-heavier than Kroupa/Chabrier IMF; however these studies can be lead only at low redshift given the necessity of spectra with high S/N (> 100 per Å).

In a recent study Shetty & Cappellari (2014) using dynamical models, found that the IMF of massive ETGs at $z \sim 0.8$ is similar to that of local galaxies. This result is consistent with the evidence that, on average the stellar content of ETGs passively evolve from $z \sim 0.8$ to $z = 0$. Hence, if a variation of the IMF of massive ETGs occurs with time, it should be detectable at $z > 1$. However, constraining the IMF at high redshift is very challenging due to observational limits. In fact, most of the observations of local galaxies and of the information acquired on them were not feasible and accessible for galaxies at high-z; this is the reason why up to now the local IMF has been assumed universal.

The above discussion lead to a scenario in which both the IMF functional form and its knowledge across the cosmic time still remain an open question. For this reason, constraining the different proportion of low-to-high mass stars in galaxies with different morphology and at different redshift will be one of the goals of this thesis. This target will be performed through the comparison between the observed properties of high- and low-redshift galaxies and thanks to the availability of a suited set of stellar population models able to reproduce the spectral energy distribution of galaxies with different proportion of low-to-high mass stars (see Chapter 5).

1.6 Selection criteria adopted to select ETGs

Not all the results on the ETG evolution showed in the previous sections fully agree with each other (e.g. Schiavon et al. 2006). These discrepancies are based on several motivations, among which the necessity of a detailed knowledge of the stellar IMF, as shown in Sec. 1.5. Other discrepancies can be due to the bias deriving from the different selection of ETG samples, from the incompleteness of the selections or, from the use of stacked data, that can include heterogeneous galaxy populations. Moreover the comparison between high-z and low-z is usually done on the basis of different analysis, parameters, rest-frame wavelength and spatial sampling.

In the local Universe, ETGs have been historically identified by means of their visual morphology that have permitted a good census of the local population. Conversely, the identification of ETGs for redshift higher than $z = 1$ was more fragmentary than that at $z < 1$, at least before the availability of the deep surveys performed with the Hubble Space Telescope (HST; e.g. COSMOS, GOODS, CANDELS). At very high$-z$ ETGs were usually identified in flux limited samples, using colour selections such as the passive-Bzk criterion at $1.4 < z < 2.5$ (Daddi et al. 2004) or the Distant Red Galaxy (DRG) criterion for galaxies at $z > 2$ (Franx et al. 2003) or appealing to stellar properties observed in local ETGs and then adopted also for high-z ETGs (e.g. passivity, colours, spectral features). These were only few methods among the numerous adopted to recognize and select ETGs, and most of them were developed to overcome the observational limits that did not allow to observe faint and distant sources.

The necessity to morphologically classify galaxies derived from the tight correlation between the physical properties of a galaxy and the way in which it was formed. In fact, the shape of a galaxy reflects its dynamical status; disc-shaped galaxies are described, at first approximation, by exponentially declining light profiles and their dynamics its due to the ordered motion of stars around the azimuthal axis. They have a relatively high angular momentum, that supports the disc structure, and are usually classified cold systems because of their low velocity dispersions. Spheroids, instead, have centrally peaked light profiles, that extend at greater radii and, their dynamics and shape are supported by the chaotic motions of the stars within the galaxy. They have a high velocity dispersion (hot systems, $\sigma_v \sim 100 \div 300$ km/s)

and a low angular momentum. Hence, study the galaxy structure provides information for understanding the formation and evolution of galaxies. Thus, the morphological analysis of large and unbiased samples of galaxies allows to discriminate between the prediction of different formation scenarios (Sec. 1.3).

Nowadays, analytic methods to morphologically classify galaxies have been usually preferred to the standard visual classification, both to speed the classification process because of the large number of observed galaxies, and to skip the observational limits presented at higher redshift.

One of the first method for galaxy classification recurs to the use of fitting formulae to describe the galaxy light profile. The de Vaucouleurs profile (de Vaucouleurs 1948) and the exponential profile (Freeman 1970) were used for a long time to analytically describe the morphology of ellipticals and discs, respectively. The generalization of these laws was made by Sérsic in 1968 (Sersic 1968), who proposed a more general law to describe the surface brightness as a function of the radius and of an index connected with the galaxy shape, both for bulges and spirals (see Sec. 2.3.1). The light profile of each galaxy were then fitted with this law, and the galaxies were divided in morphological classes following a separation criterion fixed a priori.

Among the non-parametric methods to derive galaxy morphology one of the most adopted appeals to the use of the "CAS" parameters, namely *concentration*, *asymmetry* and *clumpiness* (Abraham et al. 1994, 1996a, 1996b, Conselice 2003). The concentration is the ratio between two radii containing a fraction of the total light; the asymmetry quantifies the degree of rotational symmetry of the light distribution; the clumpiness describes the fraction of the galaxy light contained in clumpy structures.

Two further parameters that are frequently used as structural measurement systems are the Gini coefficient G and the M_{20} parameter (Abraham et al. 2003, Lotz et al. 2004). Both of these parameters estimate the light distribution within pixels, and are used to find galaxies of broad morphological classes, also those that underwent merging processes.

The advantage of the non-parametric methods is that they are applied to a large number of galaxies without human intervention, however they have a strong dependence on the S/N ratio of the galaxies (Lisker 2008), hence especially for distant galaxies they can lead to a misclassification of the galaxy morphology.

All this methods used to morphologically classify galaxies are very heterogeneous and their application can lead to a different classification of the same galaxies (Moresco et al. 2013). However to follow the evolution and to constrain the formation of a particular galaxy population, such as the ETGs, is of fundamental importance well-characterizing the galaxy types. Only studying sample of strictly defined ETGs, it would be possible to compare results achieved until now, to reconcile inconsistencies still present in the understanding of the galaxy evolution and to try to answer at still open questions.

Did the galaxy change their morphology through cosmic time? When did the Hubble sequence appear? How is the impact of the selection criteria in studying the evolution of a galaxy population?

In the present thesis project, morphological classification, global parameters (stellar mass, age, star formation time-scales) and photometric quantities will be derived following the same recipe, from low ($z \sim 0.5$) to high ($z \sim 2.5$) redshift. This will provide a solid set of observables and a good sampling of their evolution over $\sim$9 Gyr of cosmic time, necessary to constrain the build-up and the shaping of the ETGs.

Chapter 2

Observational data and methods of analysis

In the next sections I will describe the GOODS survey, and the catalogue from which the samples of galaxies used in my analysis have been extracted. Then, it will be introduced the techniques used to derive the principal physical and structural parameters of the galaxies.

2.1 The GOODS-South survey and the GOODS-MUSIC catalogue

The Great Observatories Origins Deep Survey (GOODS, Giavalisco et al. 2004) is a project aimed at collecting some of the best and deepest observations over a wide area of the sky with the most powerful space-based and ground-based facilities, to gather multi-wavelength data to study the formation and the evolution of the galaxies across the cosmic time.

The survey is composed of two target fields of $\sim$140 arcmin^2 each. The first one centred on the Hubble Deep Field North (GOOODS-North) and the second one on the Chandra Deep Field South (CDFS, GOODS-South), see Fig. 2.1 for details. The two fields were observed with the NASA's Hubble, Chandra and Spitzer space-based telescopes and the ESA's XMM-Newton observatory, the 8.2 m-aperture Very Large Telescopes (VLT) at the ESO Paranal Observatory, the twin 10-m Keck Telescopes, the 8.2-m Subaru Telescope, and the 8-m telescopes of the Gemini Observatory.

The sample of galaxies studied in this work has been extracted from the GOODS-South field.

For what concerns the GOODS-South field, as part of an ESO Large

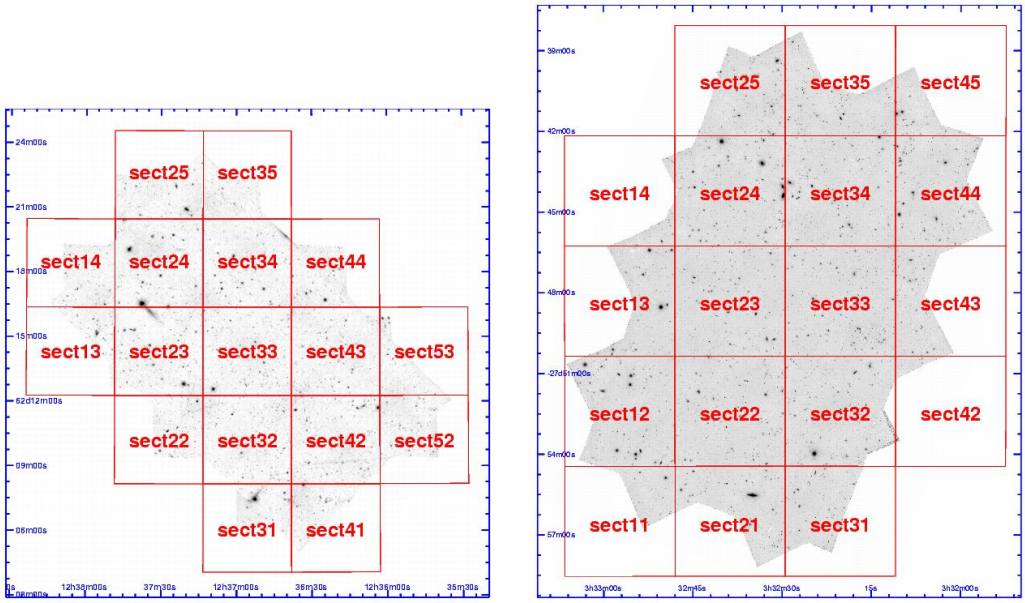

Figure 2.1: GOODS-North (left) and GOODS-South (right) fields divided in sections.

Programme, near infrared imaging in the J, H, Ks filters (Retzlaff et al. 2010), very deep U-band imaging with VLT-VIMOS (Nonino et al. 2009) and an extensive spectroscopic campaign (ESO-GOODS) with FORS2 and VIMOS which has yielded ∼2700 redshift (Vanzella et al. 2008, Popesso et al. 2009, Balestra et al. 2010), have been carried out. In addition to the ESO-GOODS spectroscopic survey, many spectroscopic campaigns have been carried out in the CDFS area. These campaigns produced over 4000 redshift collected into a Spectroscopy Master Catalog made available by ESO Web Site. In Table 2.1 a summary of the observations and of the images' properties for the GOODS-South field are reported. The limited magnitudes at 90% completeness are the mean values on the field, averaged on the position and areas of every object (Grazian et al. 2006).

This thesis work is based on a multicolour catalog, the GOODS MUlticolour Southern Infrared Catalog v2 (GOODS-MUSIC, Grazian et al. 2006, Santini et al. 2009) extracted from the GOODS-South field. The GOODS-MUSIC catalogue consists of 14999 sources selected in either the z band or the Ks band. It includes photometry in 15 bands, two U band images (3590 Å and 3680 Å) from the ESO 2.2 m telescope, an U image from the VLT-VIMOS (3780 Å), four bands photometry from the HST-ACS camera (B_{435},

Filter	λ_c Å	$\Delta\lambda$ Å	FWHM arcsec	Pixelscale arcsec/px	Area arcmin^2	MAGLIM 90%
U_{35}	3590	222	0.90	0.23	143.2	25.5
U_{38}	3680	170	1.10	0.23	143.2	24.5
U_{VIMOS}	3780	197	0.80	0.20	90.2	26.5
B (F435W)	4330	508	0.12	0.05	143.2	27.5
V (F606W)	5940	1168	0.12	0.05	143.2	27.5
i (F775W)	7710	710	0.12	0.05	143.2	26.5
z (F850LP)	8860	554	0.12	0.05	143.2	26.0
J_{ISAAC}	12550	1499	0.45	0.15	143.2	24.5
H_{ISAAC}	16560	1479	0.45	0.15	78.0	24.3
K_{ISAAC}	21630	1383	0.45	0.15	143.2	23.8
$3.6\mu m$	35620	3797	1.60	0.60	143.2	24.0
$4.5\mu m$	45120	5043	1.70	0.60	143.2	23.4
$5.8\mu m$	56860	6846	1.90	0.60	143.2	22.0
$8.0\mu m$	79360	14797	2.00	0.60	143.2	22.0
$24.0\mu m$	237000	47000	5.20	1.20	143.2	—-

Table 2.1: Characteristics of the photometric data in the GOODS-South field (Grazian et al. 2006).

V_{606}, i_{775} andz_{850} hereafter), three NIR images (J, H and Ks) from the VLT-ISAAC telescope and five Spitzer photometry at 3.5, 4.5, 5.8, 8 and 24 μm. All the magnitudes in the catalog are given in AB scale. The object detection in the GOODS-MUSIC catalogue was first done in the ACS-F850LP images, using a modified version of `Sextractor` (Bertin & Arnouts 1996). In addition to this, the detections that escaped in the F850LP images but that were bright in the Ks band were done in the latter images. This double procedure produced a catalogue from which a z-selected or a Ks-selected subsample can be extracted. A detailed set of simulations was executed to estimate the completeness limits of the samples (Grazian et al. 2006). Since the depth of the images used for the galaxy selection varies across the area, a single magnitude limit cannot be defined in each band, so the z-selected sample and the Ks-selected sample have been divided in six independent catalogs, each with a well defined magnitude limit. The z-selected catalogs have magnitude limits in the range 24.65-26.18, while the magnitude limits in Ks-selected sample range from 21.60 to 23.80. The completeness of the detection is discussed in Grazian et al. (2006), where the authors evaluated, for elliptical and spiral galaxies of different half-light radii and bulge/disk ratios, a 90% completeness level from simulation in z and Ks bands. Most of the sample can be considered complete 90% down to $z \simeq 26.0$ and $Ks \simeq 24.0$.

The galaxy colours in the ACS images were estimated using the isophotal magnitudes provided by `Sextractor`. This procedure ensures that the photometry is computed at different wavelengths in the same physical region, defined by the isophotal area in the detection image (z_{850}-band for the MUSIC catalogue). For what concerns the colours between the ACS images and the IR or UV images, which have poorer quality, the colour estimate was done using a PSF-matching software (ConvPhot, De Santis et al. 2007). This algorithm measures colours from two images of different qualities by exploiting the spatial and morphological information contained in the higher resolution image.

Out of the 14999 sources of the GOODS-MUSIC catalogue ∼12% (1888 galaxies) have spectroscopic redshift. For the sources without a spectroscopic redshift a photometric redshift was estimated, through a standard χ^2 minimization. The set of synthetic templates used for photometric redshift estimate has been drawn from the PEGASE 2.0 synthesis models (Fioc & Rocca-Volmerange 1997). A detailed description of the fitting procedure is described in Giallongo et al. (1998) and Fontana et al. (2000). The resulting photometric redshift compared with the spectroscopic sample provides an average absolute scatter $\langle|\Delta z|\rangle = 0.06$ (with $|\Delta z| = |z_{spec} - z_{phot}|/(1 + z_{spec})$). The full multi-wavelength GOODS-MUSIC catalog is publicly available in electronic form at CDS or at the WEB site `http://lbc.mporzio.astro.it/goods` and an exhaustive description of all the procedures adopted to build the catalog can be found in Grazian et al. (2006).

2.2 The magnitude limited *master sample*

In order to have a representative sample of galaxies suited to follow the evolution and the mass assembly history over a wide redshift range, I selected from the GOODS-MUSIC catalogue all the sources having an apparent magnitude $K_s \leq 22$. This magnitude cut allows to have a good spectroscopic redshift coverage (see below), and to perform an accurate morphological classification of galaxies up to z∼2.5. Moreover, the K-band selection collects the light from low-mass stars dominating the baryonic content of galaxies and thus provides a better mass completeness level.

To ensure that the *master sample* was completed at $K_s = 22$, I first verified that the *Ks* number counts (number of galaxies per magnitude bin and square

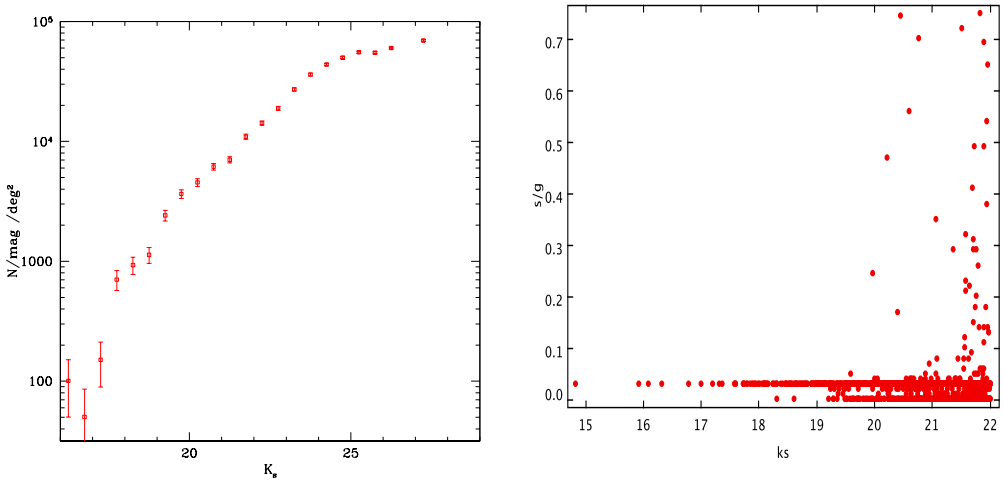

Figure 2.2: *Left:* K_s galaxy counts for the MUSIC catalogue. The counts continue to rise with a power law slope up to $K_s = 24$. *Right:* stellarity index as function of the K_s magnitude. For index greater then 0.8 the sources were classified as stars.

degree [N/mag/deg^2]) of the MUSIC catalogue do not drop for $K_s \leq 22$. The left panel of Fig. 2.2 shows that from the Ks-band galaxy counts no evidence of flattening is inferred below Ks=24. In fact, also numerical simulations performed by Grazian et al. (2006) demonstrated that the 90% completeness level of the MUSIC catalogue is reached at $Ks \simeq 24.0$. It follows that all the sources brighter than Ks=22 are detected, thus the $K_s = 22$ sample is complete.

It was also verified that the magnitude selection at $K_s = 22$ from the MUSIC catalogue provided a good compromise between the number of collected galaxies and the number of sources with a spectroscopic redshift measure. In Table 2.2 the percentages of galaxies with spectroscopic redshift in magnitude limited samples selected within intervals of Δmag=1 are shown. It can be noticed that at increasing magnitude more sources are collected but the spectroscopic coverage appreciably drops at magnitude fainter than 22. We selected galaxies at $K_s \leq 22$ given the sizeable number of galaxies (1302) at this magnitude-limit, the high spectroscopic completeness (988 galaxies, 76%) and the reliability of the morphological classification at this magnitude limit. Moreover, the $K_s = 22$ sample allows to homogeneously cover the redshift interval $z = 0.5 - 2.5$ and assures a good statistic in the entire redshift range.

The selection of the $K_s = 22$ sample has also been combined with a cleaning from stellar objects. I first removed the stars from the samples, relying

K_s selection	Galaxy Number	$\%z_{spec}$
18.0	40	85
19.0	122	83
20.0	363	84
21.0	789	80
22.0	1302	76
23.0	2822	59

Table 2.2: Number of galaxies selected from the MUSIC catalogue with different magnitude cut in the K_s band. The third column reports the percentage of galaxies with spectroscopic redshift measures in each magnitude-limited sample.

on the `Sextractor` (Bertin & Arnouts 1996) star/galaxy (s/g) classifier. This algorithm through a neural network separates galaxies from stars. I defined stars as those sources having a stellarity index larger than 0.8 (right panel of Fig. 2.2) and having a point-source FWHM in all the bands. A visual inspection made on the F850LP band images confirmed the reliability of the classification.

The final *master sample* consists of 1302 galaxies of which 314 (∼24%) and 988 (∼76%) with photometric and spectroscopic redshift respectively. The photometric and spectroscopic redshift have been taken from the MUSIC catalogue. To increase the completeness of the spectroscopic data, the sample was cross-correlated with the last version of the Spectroscopy Master Catalog developed by ESO-ECF (European Coordinating Facility). The redshift distributions for the total and the spectroscopic samples are shown in the right panel of Fig. 2.3; the median value of the two distributions is z∼ 0.74. From the two distributions it can be seen that the sub-sample of galaxies with spectroscopic redshift is representative of the total sample. The distributions of the galaxies as a function of the apparent magnitude in the Ks and z_{850} bands are shown in the left and central panels of Fig. 2.3. The 1302 galaxies have apparent magnitudes in the K_s band in the range $15.0 \lesssim Ks \leq 22.0$ (left panel of Fig. 2.3). The z_{850} distribution is presented since the morphological classification of galaxies was done in this HST-ACS band. The central panel of Fig. 2.3 shows that only ∼ 30 galaxies of the sample are not as bright as F850LP(AB)=24.5, the magnitude at which the morphological classification has been proved to be feasible and reliable (e.g. Mei et al. 2006; Raichoor et al. 2012; 2011; Saracco et al. 2011).

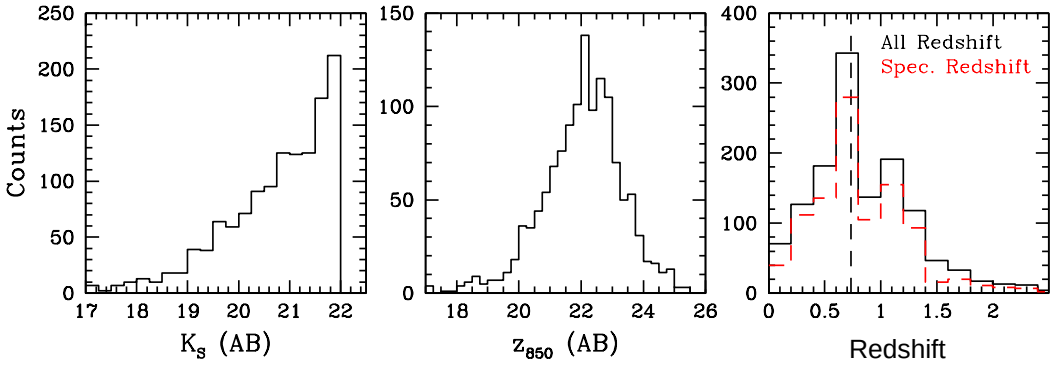

Figure 2.3: *Left and central:* apparent magnitude distributions of the sample of 1302 galaxies in the Ks and z_{850} bands. *Right:* redshift distribution of the Ks$\leq$22 sample. The continuous black line and the dashed one indicate the whole sample and the objects with spectroscopic redshift, respectively. The vertical dotted line at z$\sim$0.74 indicates the median of redshift distribution.

2.3 Physical and structural parameters estimation

In the following sections the methods of analysis used to retrieve information about galaxy properties are shown. I will present the estimation of the structural parameters (e.g. effective radius, axis ratio) derived by studying the surface brightness profile and the estimation of the physical parameters (e.g. stellar mass, mean age of the stellar population, rate of star formation) obtained from the analysis of the observed spectral energy distribution of the galaxies.

2.3.1 The light profile analysis and the estimation of physical parameters

The study of the surface brightness profile allows to derive the main parameters describing the structure of the galaxy. Indeed, the observed light profile of a galaxy describes how the intensity I of the light of a galaxy varies with distance R from its centre. We used the software `GALFIT` to model the galaxy light distribution (v. 3.0.4; Peng et al. 2002); it provides the galaxy structural parameters through a bi-dimensional fitting with analytic functions. In the fitting procedure, the models are convolved with the point spread function (PSF) using Fast Fourier Transform to take into account the diffraction and scattering of the light as it passes through the optical of the telescope. Afterwards, the routine provides the best fitting parameters of the profile,

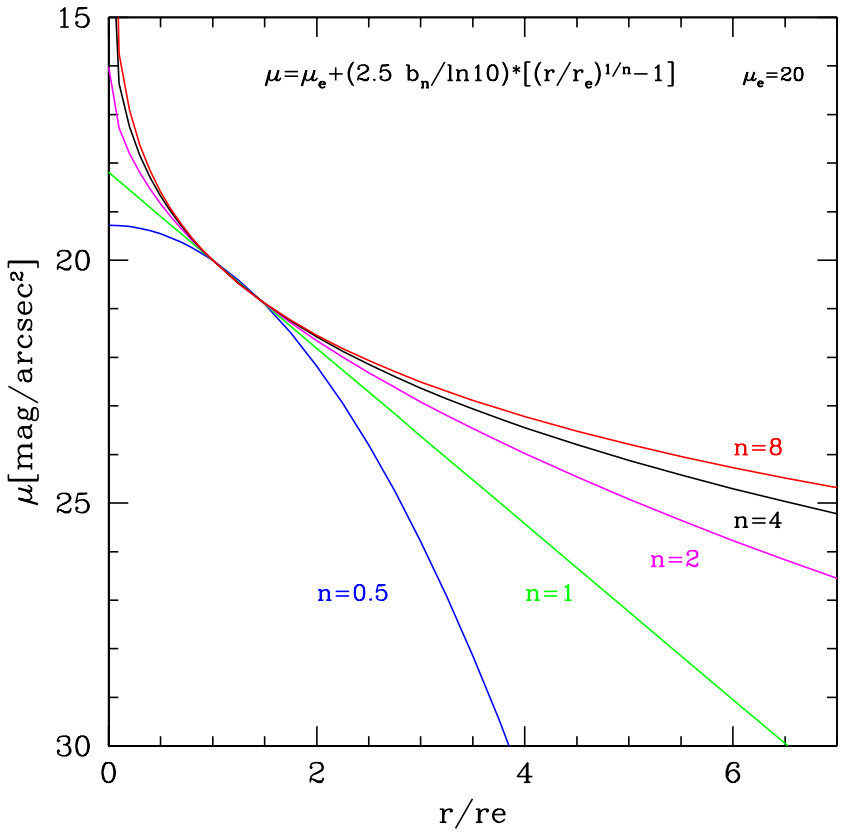

Figure 2.4: The Sérsic profile for different values of n as described in equation 2.1. As the Sérsic index grows the profiles are more comparable.

minimizing the differences (residuals) between the PSF-convolved model and the input galaxy image. In my analysis I adopted a single Sérsic component (Sersic 1968) to fit the intrinsic light distribution of the F850LP images. The F850LP images are characterised by high signal-to-noise ratio, good spatial resolution (FWHM∼0.11" measured on the images) and an excellent sampling of the PSF (pixel size=0.05"). The analytic expression of the adopted profile is,

$$\mu(r) = \mu_e + \frac{2.5 b_n}{ln(10)} \Big[\Big(\frac{r}{r_e} \Big)^{1/n} - 1 \Big], \tag{2.1}$$

where $\mu(r)$ is the surface brightness (SB) measured at distance r from the centre of the galaxy in units of mag arcsec^{-2}, μ_e is the SB at the effective radius r_e that encloses half of the total light from the model, n is the Sérsic index connected with the profile shape and b_n is a parameter depending on n ($b_n \sim 2n - 1/3 + 0.009876/n$, Prugniel & Simien 1997; Ciotti 1991; Graham

et al. 2005).

For large values of n, the profile is steep at small radii and is highly extended in the outer region; for small n, the profile has a flatter core with a sharp truncation at large radii (Fig. 2.4). Fixing $n = 1$ and $n = 4$, the Sérsic profile coincides with the exponential and the de Vaucouleur profiles (de Vaucouleurs 1948) respectively, which are often used to describe profiles of spiral and elliptical galaxies. Thus, the Sérsic index is sometimes used as galaxy shape parameter since it describes the distribution of the stars in the different galaxy regions, however, as shown in Sec. 3.1.1 it cannot be a good morphological classifier.

The other free parameters provided by the `GALFIT` fitting are the semi-major axis a_e of the projected elliptical isophote, containing half of the total light of the profile, the axial ratio b/a, and the total magnitude in the filter F850LP. The effective radius is derived by the equation $r_e = a_e\sqrt{b/a}$.

I avoid to guess initial parameters to fit the galaxies, because as reported in the `GALFIT` Web site, when a single component Sérsic fit is performed, the algorithm is very robust and insensitive to input parameters.

The fitting process was repeated four times for each galaxy using four different PSF of unsaturated and isolated stars, in order to exclude the dependence of the fitting results from the PSF used. It was verified that the PSF had a high signal-to-noise and was better than Nyquist sampled[1], i.e. FWHM sampled with more than 2 pixels. This request is satisfied in the HST-ACS images since the pixel scale is 0.05"/pixel and the PSF FWHM is ∼0.12". As best fitting parameters it has been chosen the one with the minimum chi-squared.

I used as input sigma image, i.e. the image showing pixel-to-pixel flux uncertainty, the rms map produced by `Sextractor` using the standard HST-ACS weighting image. I also generated an internal `GALFIT` sigma image and I verified that the fitting results did not significantly change compared to the results obtained using the rms map produced by `Sextractor`. The fitting was performed over a box of 6 x 6 arcsec (201x201 pixel) centred on the centroid of each galaxy, except for galaxies with highly extended structures for which a larger box has been adopted. The convolution box size and the PSF image size

[1]The Nyquist theorem asses that to completely determine a given analytic function, f(x), one needs to sample it with at least $q/2x_{max}$ points, where x_{max} is the typical scale where the f(x) varies.

were fixed at 3 x 3 arcsec (101x101 pixel). To define the size of the fitting box I applied an iterative technique, consisting in enlarging the box size around the target source until the parameters converge with growing fitting area. This process was repeated also to fix the convolution and the PSF box size and to ensure that the structural parameters obtained with GALFIT were not biased by the choice of these input parameters. Every object close to a target was fitted simultaneously, while more distant and weak sources were masked out using the `Sextractor` segmentation image. These processes prevent the profile of the surrounding galaxies from overlapping the target profile. Bad fitting results, i.e. fits that do not converge or those for which one or more parameters have been forced to a fixed value in `GALFIT`, are around 5%.

After the conclusion of the fitting procedure, a careful analysis object by object of the residual map provided by `GALFIT` was performed. The residual is the image produced subtracting the PSF-convolved model from the observed image and is a visual indicator of the quality of the fit. The rule of thumb to get a good fitting with an appropriate model is that χ^2_ν is of the order of the unity. Nonetheless, even in the case of a good result, it is important to understand which pixels dominate the statistic in the fitting procedure. In fact, `GALFIT` through the sigma image assigns a greater weight to pixels with an high signal than to pixel with fewer counts. In this way, to fit a galaxy profile, the central pixels will have an high weight than the external ones, and sometimes, even though the simple Sérsic-component fitting has a good value of χ^2_ν, the residual map could show structure of the galaxy not considered in the model. Consequently, if the goodness of the fit is considered only on the basis of the χ^2_ν value, a wrong conclusion on the galaxy light distribution could be done. In Fig. 2.5 some examples of good and bad light profile fitting are shown. In each column the upper panel represents the F850LP image of the galaxy, the middle panel shows the best-fitting Sérsic model profile convoluted with the PSF and the lower panel the residual image. The galaxy in the first column of Fig. 2.5 is a clear example of a good fitting with clean residual map and a $\chi^2_\nu = 1.05$, alternatively the other two galaxies have a poor fitting with the presence of symmetric surface brightness arms in the residual maps. However, the fitting result of the right-hand galaxy provides a $\chi^2_\nu = 1.04$ that clearly does not represent the goodness of the fitting.

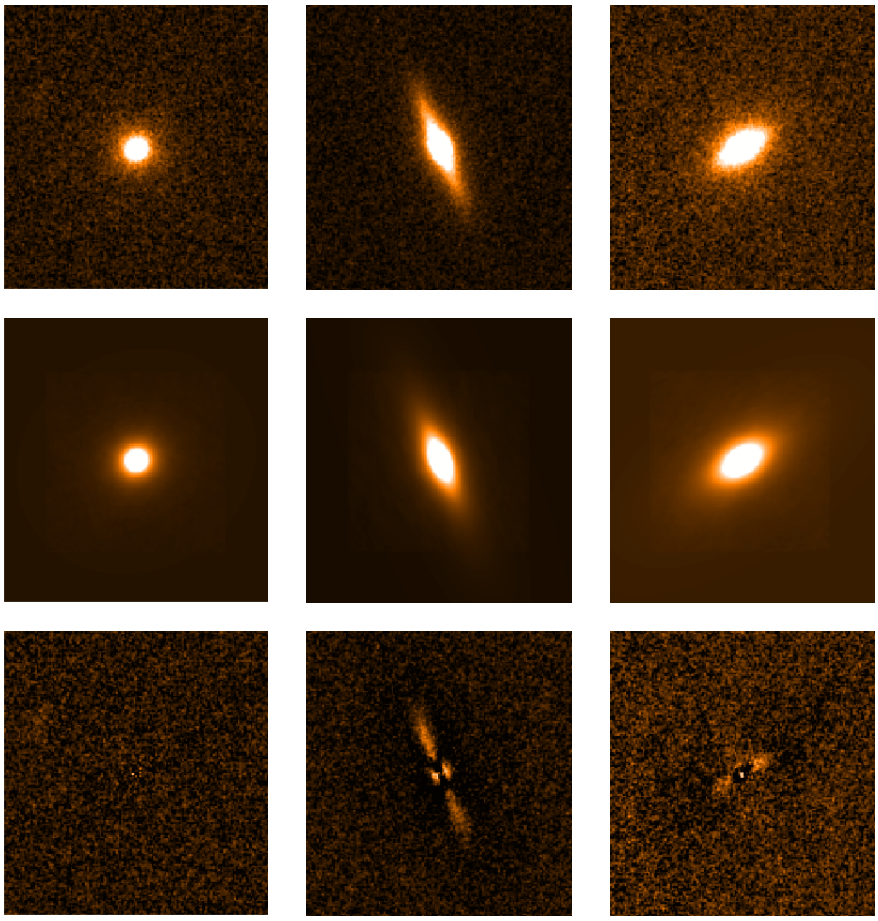

Figure 2.5: Each column shows the GALFIT input and output for three galaxies of the magnitude limited sample. In the upper panels are shown the images of the galaxies in the F850LP filter, in the middle panels the best fitting Sérsic model profiles and in the lower panels the residual images obtaining by subtracting the model from the image.

2.3.2 The stellar population synthesis models

The observable quantities of galaxies are fluxes within different photometric bands, that describe the spectral energy distribution (SED). The galaxy SED traces the emission of the galaxy across the electromagnetic spectrum; it is the result of different stellar and dust contents and allows to derive a large amount of information, such as stellar mass and age of the main stellar component. To derive the galaxy properties both a wide sampling of the SED and a large set of spectrophotometric models, able to analytically reproduce the galaxy SEDs as function of their fundamental parameters, are required. The basic idea of the stellar population synthesis models is that a galactic spectrum can be represented through the sum of the spectra of its stars (Tinsley 1972, Larson & Tinsley 1978). The simplest way to model a stellar population is through the Simple Stellar Population (SSP), which represent a single generation of stars born at the same time (in a burst of star formation activity of negligible duration) and from the same protostellar cloud, thus stars with equal age and metallicity. This is the simplest way to reproduce a stellar system, but in a real situation a galaxy can rarely be featured by SSPs. Indeed, galaxies have different episodes of star formation (SF), prolonged in time and not instantaneous as in the case of the SSPs, that leading to the creation of a composite stellar population (CPS) with a complex star formation history (SFH) and a star formation rate (SFR) function of time. The integrated flux at time t of a composite stellar population with a star formation rate $\psi(t)$ and metal-enrichment law $\xi(t)$ can be written as

$$F_\lambda(t) = \int_0^t \psi(t-t')S_\lambda[t', \xi(t-t')]\,\mathrm{d}t' \tag{2.2}$$

where the function $S_\lambda[t', \xi(t-t')]$ is the sum of the spectra of the stars defining the isochrone of SSP of age t' and metallicity $\xi(t-t')$ (Bruzual & Charlot 2003). Essentially, the spectrophotometric models, given the amount of stars formed (SFR(t)), the stellar initial mass function (IMF) and the chemical composition of the SSPs, produce the synthetic spectra for the diagnostic of observed galaxies. Typically, different laws, parametrizing the SFH of a galaxy, can be used to construct sets of models to reproduce the observed SEDs. The simplest of them is a SFH constant [$\psi(t) \propto$ const], but more complex SFH are available, such as the *delayed* [$\psi(t) \propto \tau^{-2} t\ exp(-t/\tau)$], the *linear declining* [$\psi(t) \propto t^{-1}(1-(t/\tau))$] or the more common *exponentially declining*

SFH [$\psi(t) \propto \tau^{-1} exp(-t/\tau)$]. In this work the latter SFH, the exponentially declining, that have the peak of star formation in the first stage of the galaxy life, is adopted. With the growing of the SF time-scale τ, named *e-folding time*, the star formation is spread over a long time-scale and for $\tau \rightarrow \infty$ it becomes constant over the whole galaxy life's time. Conversely, if τ assumes small values, the star formation is focused on a short time and reproduces the instantaneous burst of a SSP for $\tau \rightarrow 0$. It is worth noting that this is a mathematical parametrization, not necessary reproducing the real star formation history of a galaxy and does not consider any possible secondary bursts.

In this work I made use of the stellar population synthesis models of G. Bruzual & S. Charlot (Bruzual & Charlot 2003, hereafter BC03). The models consists of a matrix of data that at fixed age lists the fluxes for each wavelength available in the spectra. The BC03 models are based on library of observed stellar spectra assembled by Le Borgne et al. (2003), named STELIB, computed in a wavelength range from 3200 to 9500 Å with an high resolution. A wider wavelength range, from 91 Å to 160 μm, was computed at lower resolution with the theoretical spectral library BaSeL.

As mentioned above the fundamental parameters of the spectrophotometric models are the IMF, the age, the SFR and the chemical composition. Namely, knowing the distribution of the number of stars as a function of the mass, of the chemical composition and of the evolutionary stage, is possible to reproduce the galaxy emission at different wavelengths and to derive galaxy physical properties. An important step using the spectrophotometric models is understanding how the combination of the different models ingredients (e.g. age, SFR, metallicity, IMF) leads to the retrieval of the galaxy properties. Indeed in the fitting procedure the combination of different parameters can produce the same spectral energy distribution, thus understanding the degeneracies present in the models it is crucial to correctly interpret the obtained results. In Fig. 2.6 it is shown the comparison between the model SEDs obtained varying the ages of the stellar population and fixing all the other ingredients (τ=0.1 Gyr, Z=$Z_{\odot}$, Salpeter IMF). At increasing age it can be observed the growth of the infrared emission due to the ageing of the stellar populations. Indeed for the most evolved models ($t = 5 - 10$ Gyr) the contribution of the young and massive stars,

that emit mostly in the UV range, respect to the total emission is smaller compared to the younger models. Moreover a stellar population of 2 Gyr has a spectral shape more similar to a 10 Gyr one than to a 0.5 Gyr, since the time elapsed from the star formation epoch for $t = 2$ Gyr is much longer than the star formation time-scale ($t \gg \tau$) than for $t = 0.5$ Gyr. Hence, the stellar component is much more similar to the 10 Gyr population.

The role played by the age and the SF time-scale is also shown in Fig. 2.7, where it is shown the comparison between two models with different SF time-scale at fixed age, metallicity and IMF. If the SF time-scale is of the order of the age of the stellar population ($t = 1$ Gyr and $\tau = 1$ Gyr, cyan line in Fig. 2.7) the contribution of the young massive stars is predominant on the overall spectrum compared to the model with a small τ, since the star formation is still ongoing. On the other hand, the emission coming from the infrared wavelength is comparable in the two models, since both populations have had the same time of 1 Gyr for ageing. From the comparison of the cyan spectrum of Fig. 2.6 ($t = 0.5$ Gyr and $\tau = 0.1$ Gyr) and the cyan spectrum of Fig. 2.7 ($t = 1$ Gyr and $\tau = 1$ Gyr) it can be noticed the degeneracy between the age t and the SF time-scale τ, that produces a similar result. In fact, a tight correlation between these two parameters exists, that can cause best-fitted SEDs almost undistinguishable with different combinations of t and τ.

In Fig. 2.8 the effect of the metallicity variation on the overall spectral shape can be inferred. The metallicity variation does not strongly influence the spectral shape, but a model with an higher metal content (red line, Z=0.04) has a reddened spectrum with infrared emission more pronounced. Comparing the effects of the ageing and of the metallicity on the spectral shape the well-known problem of the age-metallicity degeneracy (e.g. Worthey et al. 1994) can easily noticed. Indeed, both age and metallicity are properties that tend to redden the spectrum of a galaxies. In this work this problem has been avoided assuming always a fixed solar metallicity.

The last parameter adopted in the stellar synthesis models is the stellar initial mass function. The IMF is the mass distribution of stars and provides the relative number of low- and high-mass stars formed in a burst of star formation. The relative number of low- and high-mass stars in a galaxy determines its integrated properties, i.e. chemical enrichment, colour, luminosity, stellar mass and their evolution over cosmic time. It follows

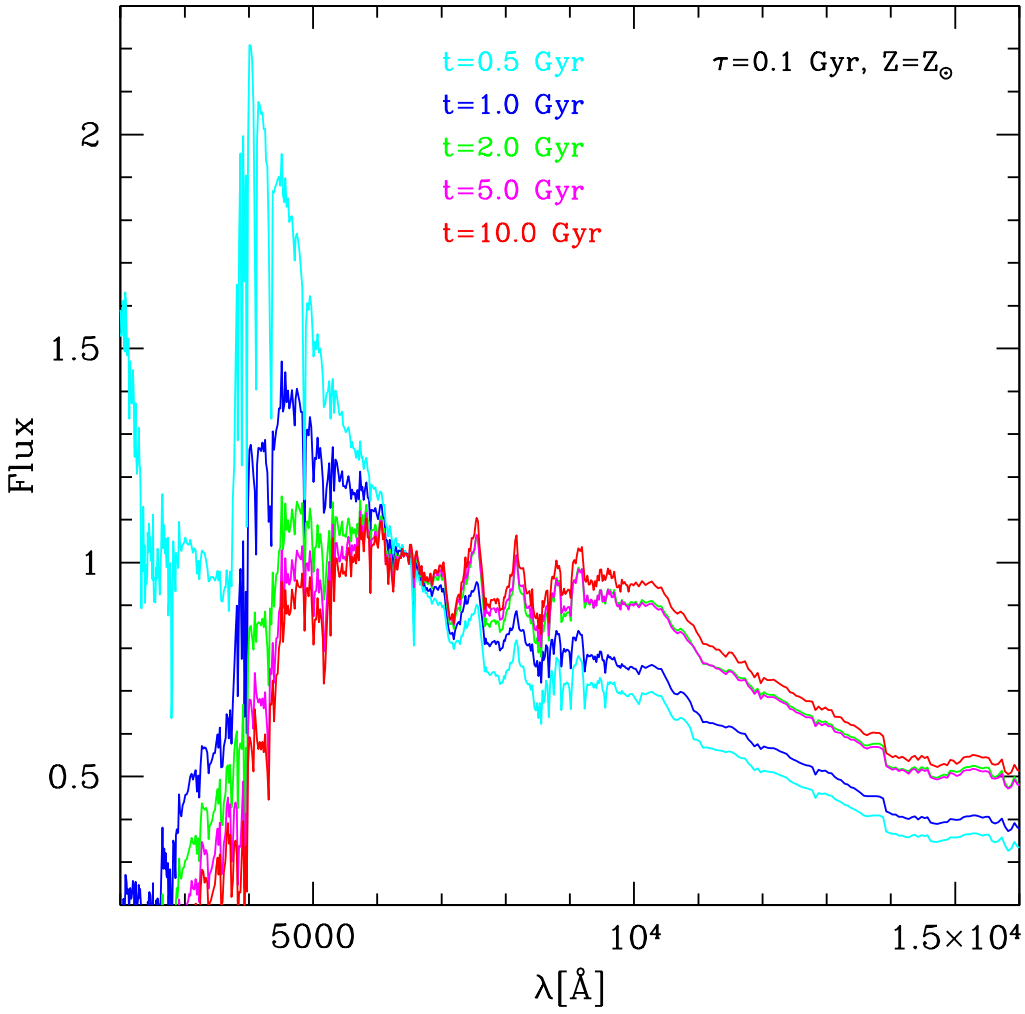

Figure 2.6: BC03 models at different ages with fixed τ=0.1 Gyr, Z=$Z_{\odot}$ and Salpeter IMF. The cyan spectrum is the most younger with a pronounced emission of young stars in the UV range, while the red SED represent an evolved population of stars with an high contribution at the infrared wavelengths. The normalization of the spectra is at $6000 \leq \lambda \leq 7000$ Å.

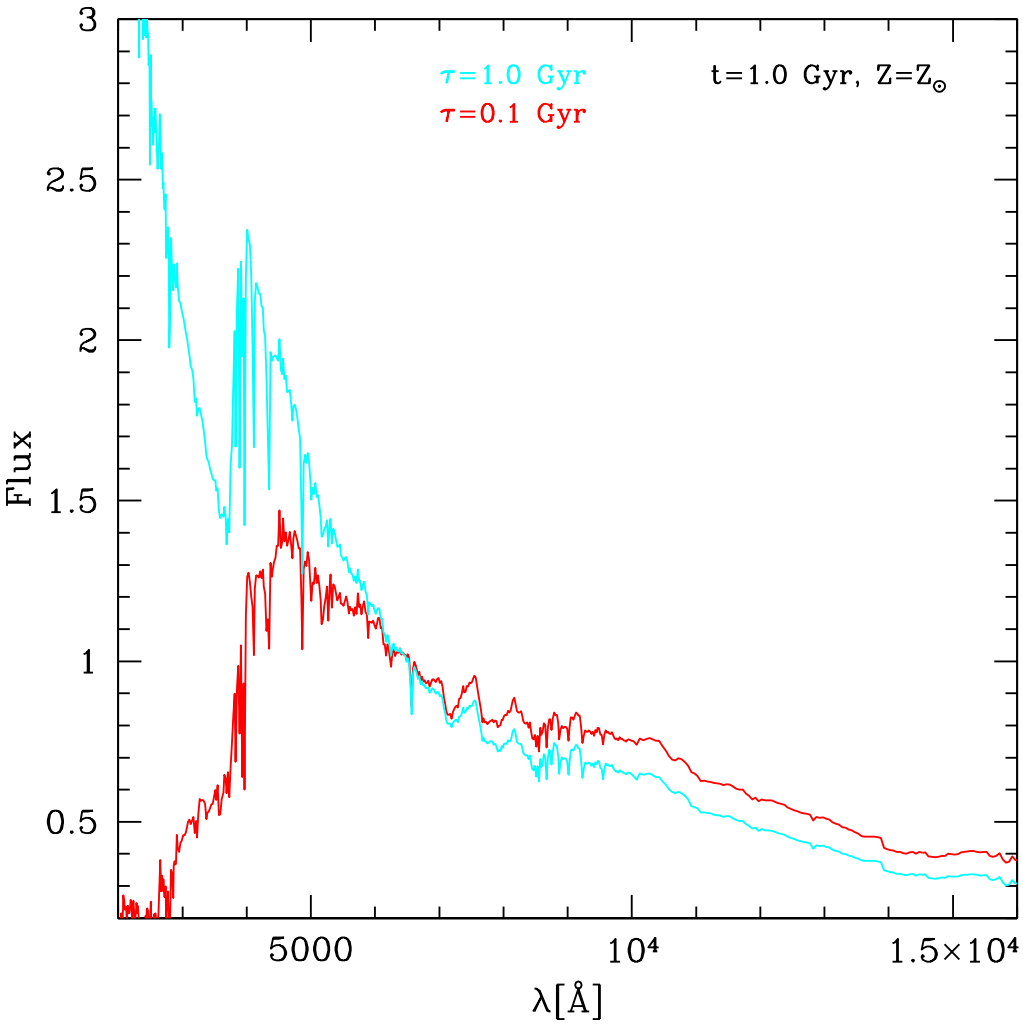

Figure 2.7: Comparison of BC03 models for stellar population with different star formation time-scales (τ = 0.1 Gyr and τ = 1 Gyr) at fixed age, metallicity and IMF. The normalization of the spectra is at $6000 \leq \lambda \leq 7000$ Å.

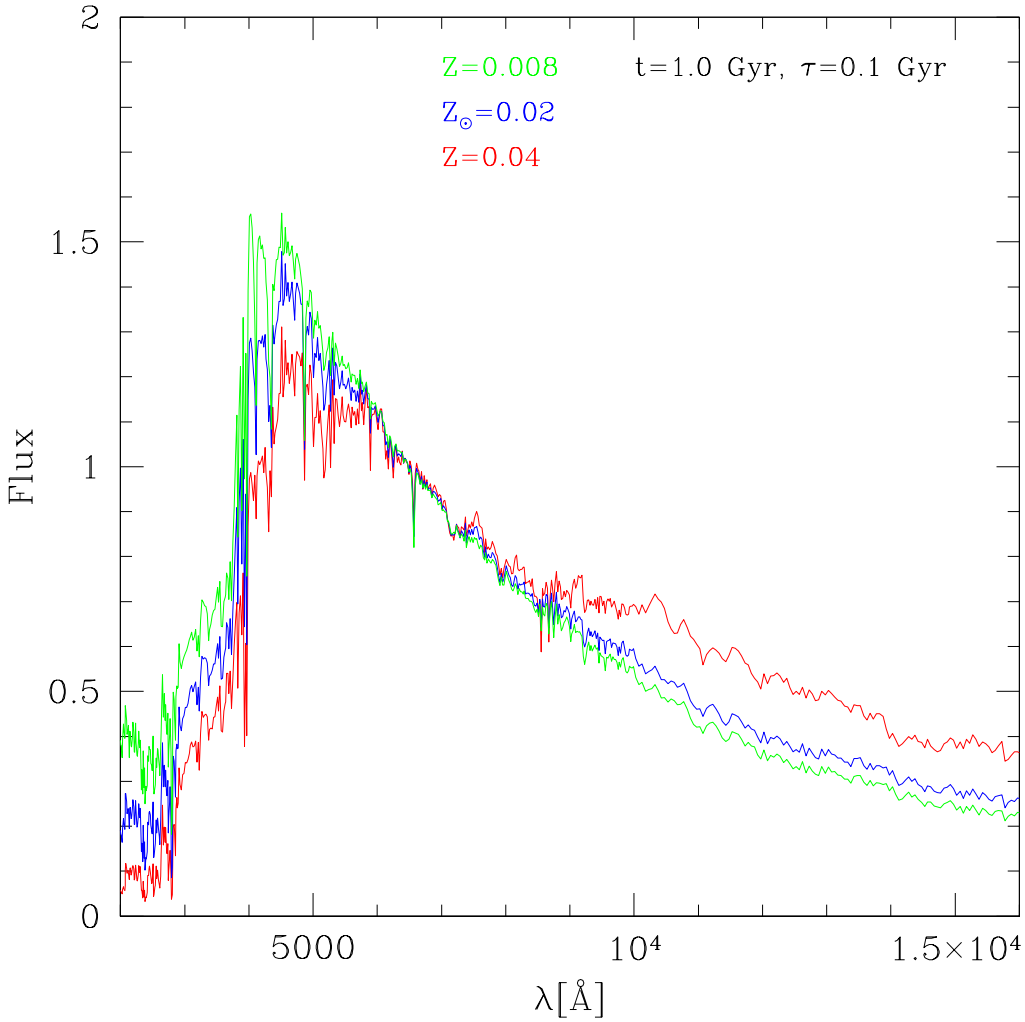

Figure 2.8: Comparison of BC03 models for stellar population with different metallicity at fixed age $t = 1$ Gyr, $\tau = 0.1$ Gyr and Salpeter IMF.

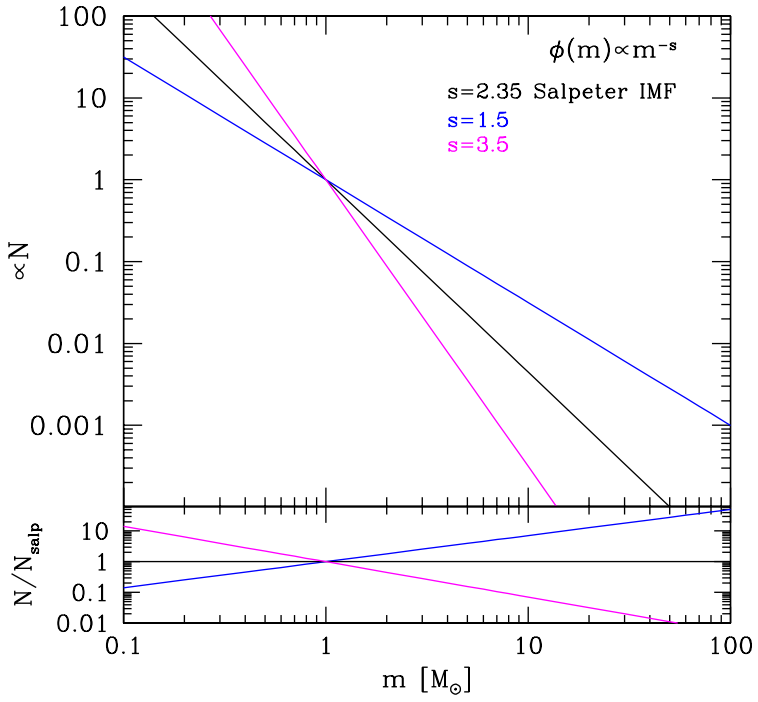

Figure 2.9: Stellar initial mass functions with a different proportion of low-to-high mass stars (m) described by a power-law IMF $\phi(m) \propto m^{-s}$ with slopes s=1.5, 2.35 (Salpeter IMF) and 3.5. Steeper is the slope of the function higher is the contribution of low-mass stars.

that any variation of the relative abundance of low-to-high mass stars would drastically modify the basic properties of a galaxy. Usually, many works based on spectrophotometric models make use of the same fixed IMF, independently on redshift and on any other parameters of a galaxy. As mentioned above (Sec. 1.5) there are several reasons to suppose that the relative abundance of low-to-high mass stars changed across the time. To consider this variation is not convenient to fix a priori an initial mass function. For this reason I performed a best fitting of the spectral energy distribution (SED) of galaxies with stellar population models considering also different IMFs. The model fitting relies on a grid of stellar population models, BC03, reproducing the spectral energy distribution of galaxies for different proportion of low-to-high mass stars. In particular, I adopted 5 different libraries of models to account for 5 different proportion of low-to-high mass stars, according to an IMF analytically described by a power law form ($\phi(m) \propto m^{-s}$) with slopes in the range 1.5-3.5. In Fig. 2.9 the variation of the stellar mass content at changing

of the IMF slope is shown. In magenta is displayed the steeper IMF with slope s=3.5 and an high abundance of low-mass stars, while in blue is presented the flatter IMF with slope s=1.5 and a high ratio of high-to-low mass stars.

In addition to these IMFs, in order to compare with other works, I also considered the classical Salpeter and Chabrier IMFs (Salpeter 1955; Chabrier 2003). In Fig. 2.10 the models for three of the five IMF are shown: in magenta the IMF with an higher ratio of low-to-high mass stars (s=3.5), in green (s=2.5) an IMF with a stellar content similar to a Salpeter IMF and in blue (s=1.5) an IMF with an higher abundance of massive stars. The model SEDs were produced assuming a solar metallicity and an age of 3 Gyr. The SEDs show a difference in the infrared interval, in particular assuming an IMF (s=3.5) with an high abundance of low-mass stars there is an enhancement of the emission at $\lambda = 9000 - 15000$ Å.

2.3.3 The SED-fitting technique

To derive the physical galaxy properties from the stellar population synthesis models, I appeal to the SED fitting technique. The SED fitting procedure consists of analysing and deriving several physical properties of galaxies not directly observable, from fitting synthetic spectral models to an observed SED. To this purpose I used the software `HYPERZMASS`, a modified version of the photometric redshift code `HYPERZ` (Bolzonella et al. 2000), which found the best-fitting SED by minimizing the χ^2 between observed ($f_{obs,i}$) and model fluxes ($f_{temp,i}$), for galaxies at fixed known redshift:

$$\chi^2 = \sum_{i=1}^{N_{filters}} \left[\frac{f_{obs,i} - b \times f_{temp,i}}{\sigma_i} \right]^2 \tag{2.3}$$

the i indicates the filter in which the fit is performed, σ_i represent the flux uncertainty in the i-th filter and b is a normalization constant to multiply by the template fluxes, because all the used SSP model are normalized to a total mass of 1 $M_\odot$. The software after reading the observed magnitudes, with the corresponding errors, transform them in fluxes. Subsequently, it builds up an hypercube, with the model fluxes of the reference templates reddened for an extinction law convolved with the filter response function and shifted at the galaxy redshift. At this point, the program proceeds with the χ^2_ν calculation, finding the best-fit model among a set of models with different masses, ages, SFH, metallicity and dust reddening.

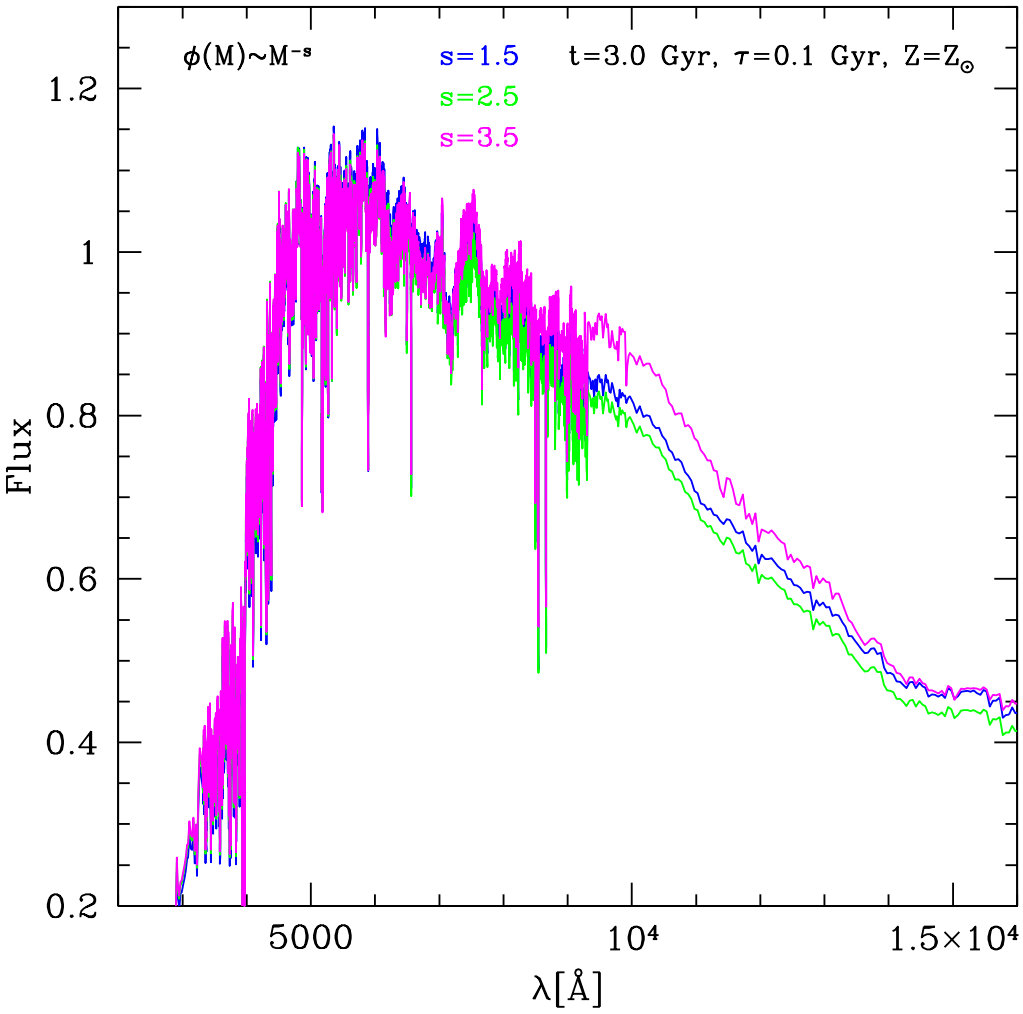

Figure 2.10: Comparison of BC03 models for stellar population with different IMF. In magenta is shown the model with the higher abundance of low-mass stars, alternatively in blue is presented the model with the higher content of young and massive stars.

The SED fitting procedure has been applied to the 1302 galaxies of the magnitude limited sample, in order to get accurate measurements of stellar mass, age and star formation rate (SFR) of the sources. I fitted the observed spectral energy distribution (SED) of our galaxies from the UV to the 24 μm (15 points) to a set of models by Bruzual & Charlot (BC03) at fixed solar metallicity. The set of considered templates includes seven star formation histories described by an exponentially declining star formation rate (SFR$\propto$exp$^{-t/\tau}$) with e-folding time τ=[0.1, 0.3, 0.4, 0.6, 1, 2, 5] Gyr and 221 ages in the range t=[0.001, 20] Gyr. The age of the galaxies at each redshift was not allowed to exceed the age of the Universe at that redshift. I adopted seven different stellar initial mass function (IMF) with lower and upper cut-off of 0.1 and 100 $M_{\odot}$: the classical Salpeter and Chabrier IMF (Salpeter 1955; Chabrier 2003), and other five power law IMF ($\phi(m) \propto m^{-s}$) with slope in the range 1.5-3.5.

The Calzetti law (Calzetti et al. 2000) was applied to describe the dust extinction, and the extinction parameter A_V was fitted in the range $0 \leq A_V \leq$1.8 mag, imposing a prior to allow significant extinction only for galaxies with an high SFR, i.e. $A_V > 0.6$ only if $t/\tau <$4. With this prior, the A_V could not exceed the fixed value $A_V = 0.6$ when the age of the galaxies is four times the SF time-scale τ and, hence almost all the dust should have been sublimated.

Another important parameter that the software `HYPERZMASS` permits to fix during the procedure is the maximum wavelength of the filters to be used during the fitting. This variable enables to choose the number of filters necessary to find the best fitting models of the galaxies. As said before, the observed spectral energy distribution (SED) of the MUSIC catalogue is extended from the UV to the MIR (24 μm) with 15 photometric points. The last five points of the SEDs are Spitzer data affected by errors larger than those formally derived from the electron statistic, since many of the sources are blended in the Spitzer images (especially at $\lambda > 5.8$ μm) due to the large PSF of the instrument (3-5 arcsec). The fitting procedure gives an higher weight to these points and often the χ^2_ν is minimized only fitting this Spitzer data. In this way the overall shape of the SED is not performed. To avoid this inconvenience, I carried out a careful study about the maximum wavelength (WL_{MAX}) of the filters to be considered in the fitting, studying the fitting result at varying of

this parameter. I found that a good fitting is performed for WL_{MAX}=23000 Å using filters with λ_{eff} >WL_{MAX} only when $\lambda_{eff}/(1+z)$ <WL_{MAX}. This means that for galaxies at $0.6 \lesssim z \lesssim 1$ all the filters from 3500 Å to 3.6 μm are considered in the fitting, while for galaxies at $1 \lesssim z \lesssim 1.5$ also the 4.5 μm filter is used and at $1.5 \lesssim z \lesssim 2.5$ the 5.8 μm filter is added.

In Fig. 2.11 the best fitting at fixed redshift to four galaxies of the sample are shown as example. The photometric points (red in Fig. 2.11) sample the observed SED uniformly from the U_{35} band to the 24 μm Spitzer band. The observed SEDs of the galaxies in the top panels is reproduced by a model with an age and a star formation time-scale of $t = 1.3$ Gyr and $\tau = 0.1$ Gyr for the galaxies in the left panel, and of $t = 0.9$ Gyr and $\tau = 0.1$ Gyr for the galaxies in the right panel; hence the SFHs ($\propto e^{-t/\tau}$) have declined by a factor of $\sim 10^{-4}$ for the galaxies with $t = 0.9$ Gyr and $\tau = 0.1$ Gyr and by a factor of $\sim 10^{-6}$ for the galaxies with $t = 1.3$ Gyr and $\tau = 0.1$ Gyr. As a consequence the very massive stars, that mainly emit in the blue wavelengths, are evolved, hence their contribution in the galaxy spectrum is negligible, compared to the emission of the low massive stars at redder wavelengths.

On the other hand, the two galaxies in the bottom panels have the emission in the UV band very pronounced, they are best-fitted by model with ages comparable with the SF time-scales, however while for the galaxies in the left-panel the emission of the young stellar component dominates the entire SED, for the galaxies in the right-panel the emission of the older component is still pronounced; this is due to the fact that in 2 Gyr (the galaxy age) the stellar components have had enough time to ageing, simultaneously the younger stellar populations continue to emit due to the prolonged SF time-scale $\tau = 2$ Gyr.

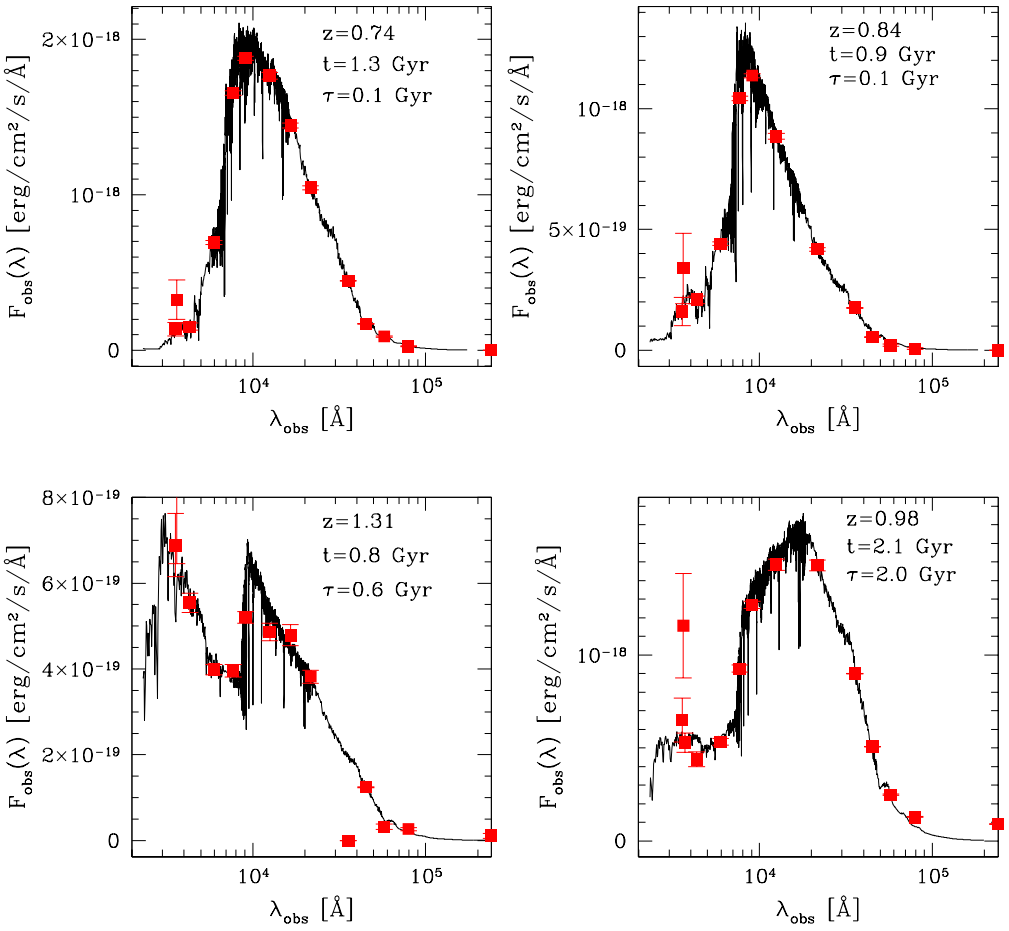

Figure 2.11: Examples of the SED fitting performed on the observed SED of four galaxies of the K22 sample. Filled red points are the fluxes measured through the 15 photometric bands U_{35}, U_{38}, U_{VIMOS}, $F435W$, $F606W$, $F775W$, $F850LP$, J, H, K_S, 3.6, 4.5, 5.8, 8.0, and 24 μm. The solid line is the best-fitting template to the observed SED.

Chapter 3

Definitions, selection and comparison of samples of ETGs and passive galaxies

Galaxies have been historically classified in the local Universe according to their visual morphology that enables to place them in a well defined sequence (the Hubble Tuning Fork, Hubble (1926), Sec. 1.2) consisting of two main types of galaxies: ellipticals and spirals. Despite the progress made in the study of the properties of these two major classes of galaxies (e.g. stellar populations, correlations among observed quantities, etc.), the physical processes involved in the formation and evolution of early-type galaxies (ETGs, i.e. elliptical and spheroidal galaxies) and discs are still unclear (Sec. 1.3), and many attempts have been done to solve this issue starting from the analysis of the galaxy morphology.

In fact, the different morphologies of galaxies testify the different processes with which their stellar mass has been assembled. If visual morphological classification at low redshift does not demand challenging efforts, at higher redshift it was not always feasible due to observational limits. However, the morphological analysis has made significant progress in the last 15 years thanks to the Hubble Space Telescope and its several "Deep Field" campaigns, that enable to identify thousands of galaxies up to $z > 2$. At the same time, the increasing size of galaxy samples has favoured the development and the use of classification methods faster than the visual one and often based on the photometric properties of local galaxies (Sec. 1.6). However, since there is not a one to one correspondence between the photometric properties of a galaxy and its shape, all these methods may fail in distinguishing the morphology

of galaxies producing mixed samples of ETGs and discs. Moreover, the photometric properties observed in the local Universe not necessarily are those characterizing the galaxies at high-z.

In this chapter I address whether a morphological classification of ETGs corresponds to a classification based on a property of the galaxy stellar component. In particular, I select a sample of early-type galaxies classified on the basis of the morphology and a sample of passive galaxies classified on the basis of their specific star formation rate (sSFR), i.e SFR/M_* the star formation rate (SFR) normalised for the stellar mass (M_*). The aim of the analysis is to understand whether the two selection criteria select approximately the same galaxies, i.e. elliptical and spheroidal galaxies, and hence they can be used interchangeably or instead they produce samples of galaxies significantly different whose properties cannot be compared. Moreover, it will be tested the dependence of the selection criterion based on the sSFR on the different model assumptions, in particular on the choice of the stellar Initial Mass Function (IMF).

3.1 The morphological classification

To select samples of early-type galaxies many criteria have been developed: the standard method of classification by eyes, photometric criteria that appeal to the colour or automatic procedures that analyse the light distribution of the objects to recover the morphological type of the galaxies. However, no automatic or visual classification is perfect and a certain level of contamination can persist. If on one hand the visual classification allows to examine carefully and individually each galaxies, especially at high redshift a certain level of subjectivity can occur. On the other hand, the automatic morphological classification can be applicable to very large galaxy samples but the results are not directly verifiable.

In this work I build up a sample of morphological ETGs, separated from all the remaining morphological types, adopting a combination of two methods. I combine a pure visual classification and a visual inspection of the residual images, obtained by fitting the galaxy surface brightness profiles with a Sérsic model (Sec. 2.3.1).

The visual morphological classification was independently performed on the high resolution HST/ACS F850LP images ($72928 \lesssim t_{exp} \lesssim 197000$ s)

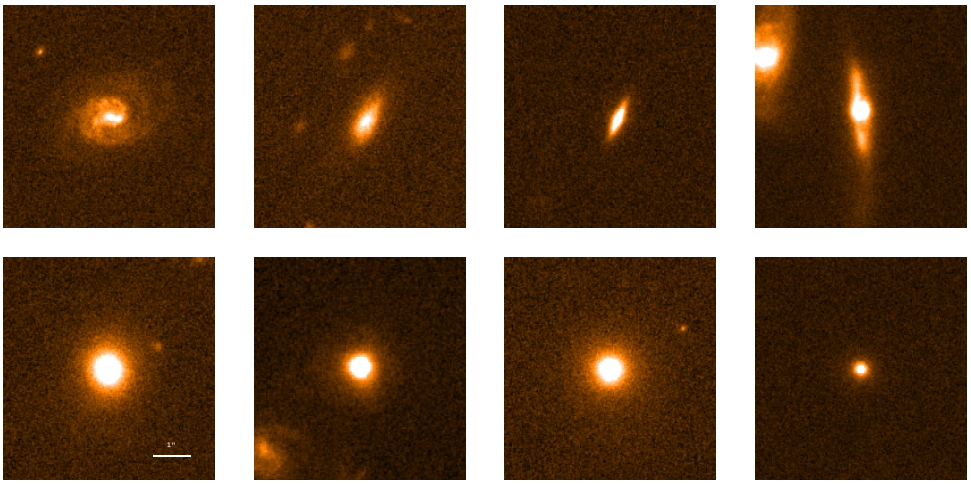

Figure 3.1: Examples of galaxies that fall into our late-type (*top panels*) and early-type (*bottom panels*) classification. The snapshots are taken from the F850LP-band images of the GOODS-S survey.

of the 1302 galaxies of the magnitude limited sample (see Sec. 2.2). The ACS-F850LP images provide high signal-to-noise ratio, good spatial resolution (FWHM∼0.11" measured on the images), a good sampling of the PSF (pixel size=0.05"), and the possibility to do reliable morphological classification up to $z = 2.5$.

Two morphological classes were defined: 1) early-type galaxies, i.e. ellipticals (E) and transition E/S0 galaxies, which include those centrally concentrated galaxies that look spheroid or ellipsoid with a regular shape and no hint of disc; 2) late-type galaxies, i.e. spirals (S), irregulars (Irr), and merging galaxies, i.e. galaxies with a clear disc and/or irregular structures or with a hint of an ongoing merger process. The first step of the morphological classification was to identify galaxies with a clear presence of a disc and those with irregular shape, immediately classified as LTGs (e.g. Fig. 3.1, top row). For the remaining galaxies I analysed both the images and the residual maps, the latter obtained by best fitting the HST-ACS/F850LP images with a 2D-PSF convoluted Sérsic model by means of the `GALFIT` software (see Sec. 2.3.1).

Finally, I classified as ETGs those galaxies with a regular shape, no signs of disc in the F850LP images, and no irregular or structured residuals resulting from the fitting (e.g. Fig. 3.1, bottom row). Galaxies having a clear sign of structures in the residual maps were categorized as late-type galaxies.

It is worth to note that the limiting surface brightness of the ACS images in the F850LP filter (~ 27.5 mag/arcsec^{-2}) is at least 2.5 magnitude fainter than

the faintest effective surface brightness ($\mu_e \sim 25$ mag/arcsec^{-2}) measured for the ETGs of the sample. Hence, the depth of the images gives us an accurate sampling of the profile of the galaxies well beyond 2 R_e for all the galaxies.

As said before, the morphological classification of galaxies has been done on the F850LP images for all the galaxies of the sample, that cover a wide redshift range between $z = 0.1$ and $z = 2.5$. In this redshift interval the F850LP filter does not sample the same wavelengths in the rest frame of the galaxies, but it varies between $2400 \lesssim \lambda \lesssim 7700$ Å, covering the galaxy emission from different stellar populations. Hence, I wondered whether the morphological classification may be affect by this effect. For galaxies at $z \gtrsim 1.2$ the F850LP filter matches the U-band rest frame ($\lambda < 4000$ Å), where the galaxy emission is mainly dominated by the light coming from the same young stellar component. On the contrary, for $z < 1$ the F850LP band samples the rest frame at $\lambda > 4000$ Å, dominated by the emission of the older stellar component, hence a different stellar population compared to the galaxies at $z \gtrsim 1$. To assure the sampling of the same stellar component, for the lower redshift galaxies at $0.6 \leq z \leq 1$ (the minimum redshift I used for the studies on galaxies evolution is z=0.6) I also performed the morphological classification in the F606W filter, that at $z < 1$ samples the U-band rest frame. I found that out of the almost 400 galaxies at $0.6 < z < 1$, only 2.5 per cent have a different morphology in the two filters; for the other galaxies the morphological classification in the F606W and F850LP filters is the same. In Fig. 3.2 some examples of galaxies at $z < 1$ observed in the F850LP (left column) and F606W (right column) images are shown. The galaxies' shape appears the same in both the filters or sometimes the morphological differences are negligible in the way to not affect the visual classification. From the figures, it can be noticed that the galaxies morphologically classified as ETGs (first two lines) have a more pronounced emission in the F850LP band, that samples the emission of the older stellar component. On the other hand, the two LTGs (third and fourth lines) have the bulge emission more dominant in the F850LP band than in F606W band, in agreement with the general knowledge that the spiral bulges are populated by older stars; instead, the spiral arms and the other structures appear more detailed in the F606W images.

From the morphological analysis 247 out of 1302 galaxies have been classified as early-type galaxies in a redshift range $0.1 \lesssim z \lesssim 2.5$. The remaining

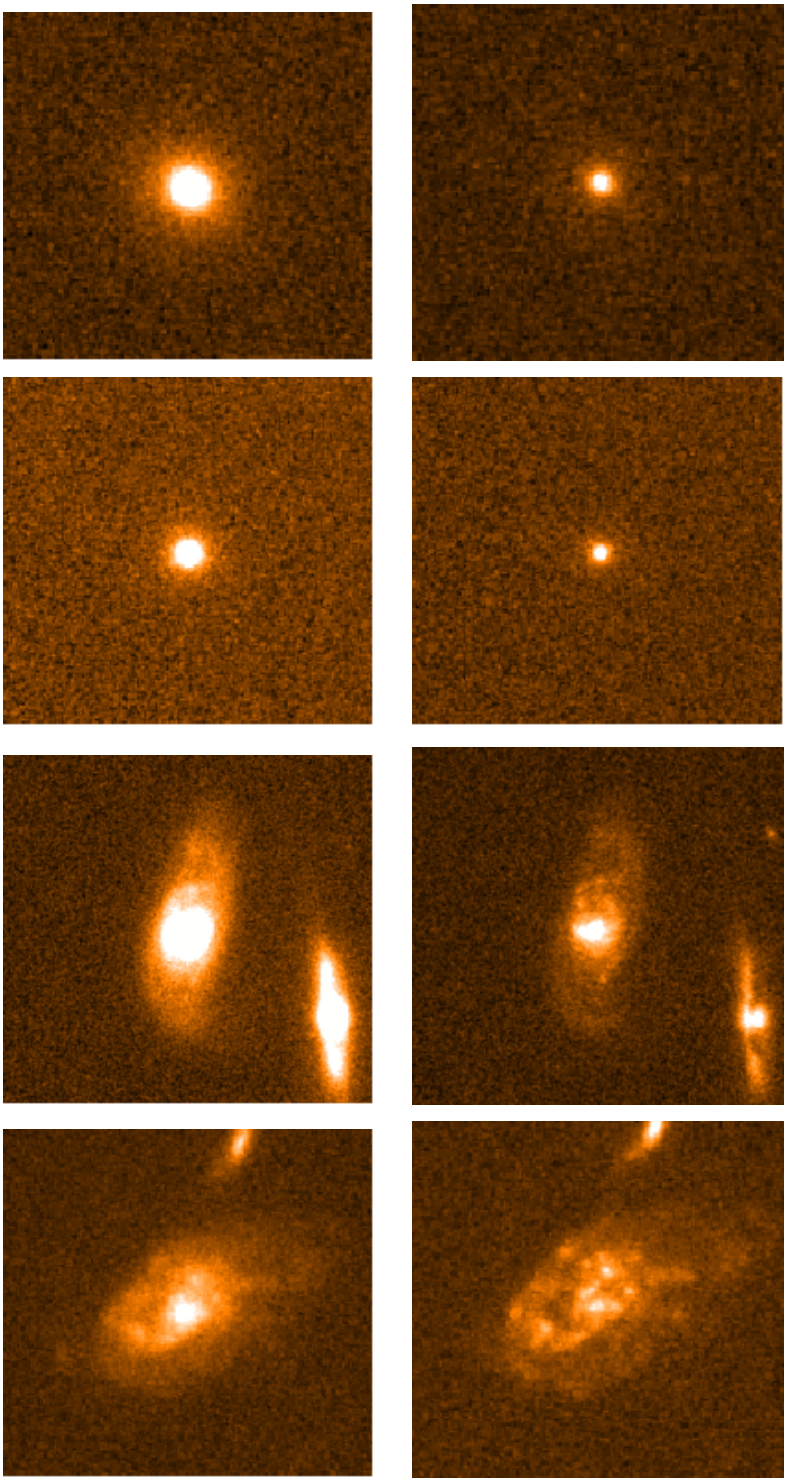

Figure 3.2: Examples of galaxies with redshift $0.6 < z < 1$ moorphologically classified both in the F850LP band (*left panels*) and in the F606W band (*right panels*) of the GOODS-S survey.

galaxies have been classified as LTGs.

3.1.1 Morphological misclassification from the use of the Sérsic index

The morphological classification of galaxies is often based on several parameters connected with the galaxy shape but not directly observable. One of these methods is the parametric analysis that retrieves the physical properties of the galaxy by fitting an analytic model to the galaxy observed light distribution. Several morphological classification have been proposed on the basis of these physical and structural parameters. Ravindranath et al. (2004) and Barden et al. (2005), for example, proposed a classification based only on the Sérsic index, distinguishing between spheroidal types with $n > 2.5$ and late-type galaxies with $n < 2.5$. As seen in Sec. 2.3.1 the Sérsic profile (Eq. 2.1) is a flexible parametric description of the surface brightness distribution of the galaxies and contains the exponential ($n = 1$) and de Vaucouleurs (n=4) models as particular cases, generally associated to the description of a light profile of a disc and of an elliptical respectively. However, there are important deviations from this simple picture. For example, there are many elliptical galaxies with low Sérsic indexes, and there are many late-type galaxies with high Sérsic indexes.

For this reason, in our morphological classification no selection criterion based on the Sérsic index has been adopted, in the ETGs or in the LTGs identification. This choice was made after a careful analysis of the residual maps. Indeed, for a significant number of cases the fitting results, despite their goodness, provided a high value of n (n >2.5 generally related to an elliptical profile) for clearly disc-shaped galaxies and conversely a low value of n (n <2.5) for pure spheroidal galaxies. Some examples of clear misclassification that would have been made if we had selected ETGs by making a blind cut with $n > 2.5$ are shown in the first two columns of Fig. 3.3. In the last column of the same figure an example of a pure elliptical that would have been excluded from the ETGs sample having a low Sérsic index (n <2.5) is shown. In each column the upper panel represents the F850LP image of the galaxy, the middle panel shows the best-fitting Sérsic model profile convoluted with the PSF, and the lower panel the residual image. The presence of symmetric low surface brightness arms in the residual maps is clearly visible in the first two columns, indicating the spiral morphology of the galaxies despite the high value of the

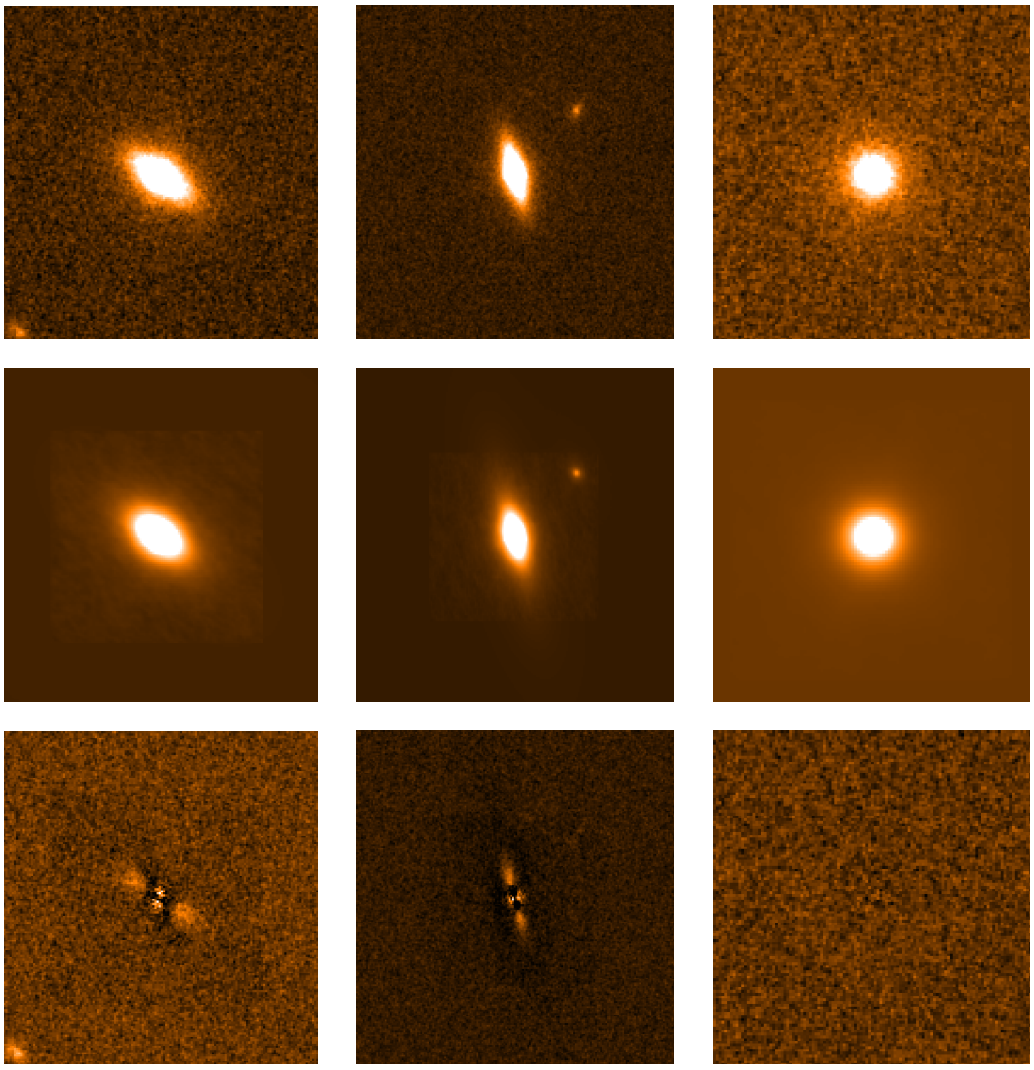

Figure 3.3: Each column shows the GALFIT input and output for three galaxies of the magnitude limited sample. In the upper panels are shown the images of the galaxies in the F850LP filter, in the middle panels the best fitting Sérsic model profiles, and in the lower panels the residual images obtaining by subtracting the model from the image. The first two columns illustrate an example of late morphology galaxies with a best fitting Sérsic index $n > 2.5$, while the last column displays an elliptical galaxy with $n < 2.5$.

Sérsic index. In the left panel the fitting result provides values of $n = 3.3$ and $\chi^2_\nu = 1.17$, while the central galaxy has $n = 4.5$ and a bad $\chi^2_\nu = 1.80$; in this last case if we had not analysed the residual or the chi squared we would have arrived at the wrong morphological classification. Thus, the Sérsic based criterion would not have allowed the separation between early- and late-type population. The choice to exclude this selection criterion is also in agreement with Mei et al. (2012). The authors, analysing a sample of morphologically classified ETGs in clusters and groups, found that if they classify ETGs using n >2.5 as classification method then the ETG sample would be composed of $\sim 40\%$ of late-type galaxies.

3.2 Selection of passive galaxies

One of the most fundamental correlation between the properties of galaxies in the local Universe involves the morphology, the colour and the star formation rate. The galaxy population may be divided into an actively, star forming, blue family and a principally passive and red family, depending on their colour and their global star formation rate per unit stellar mass (i.e. sSFR), which indicates the relative importance of ongoing star formation in the overall integrated light distribution of the galaxy. Historically, in the local Universe, after the morphological separation of spheroids from discs, it was noticed that the spheroids were mostly passive. From this finding, it followed the idea that selecting passive galaxies corresponded to select elliptical galaxies (not considering that especially at $z = 0$ many spirals are passive; e.g. the Milky Way).

This characteristic of local galaxies were then adopted also at high redshift to select elliptical and spiral galaxies, however the photometric properties of a morphological class observed in the local Universe not necessarily are those characterizing the same class at high-z. For this reason I am interested in studying whether exists a one to one correspondence between passive galaxies and ETGs at redshift greater than zero.

I defined passive galaxies those galaxies with specific star formation rate sSFR$\leq 10^{-11}$ yr^{-1}. The applied cut in sSFR selects galaxies which are increasing their mass at rate less than 1/100th of their present mass. This arbitrary threshold of sSFR allows to compare my results with previous works, most of which use the same criterion to select passive galaxies (e.g. Cassata

et al. 2011). However, I will present in a following section the dependence of the passive galaxies samples on the choice of the sSFR threshold and on the spectrophotometric models.

The sSFR is the ratio between the galaxy star formation rate (SFR) and its stellar mass (M_*), both derived by best fitting the observed spectral energy distribution (SED) with stellar population synthesis models. In particular, to measure these parameters I fitted the observed SED of the 1302 galaxies over 15 photometric bands (from 0.35 μm to 24 μm) with the stellar population synthesis models of Bruzual & Charlot (Bruzual & Charlot 2003, hereafter BC03) at fixed solar metallicity. The set of templates considered includes seven star formation histories described by an exponentially declining star formation rate (SFR$\propto$exp$^{-t/\tau}$) with e-folding time τ=[0.1, 0.3, 0.4, 0.6, 1, 2, 5] Gyr and 221 ages in the range t=[0.001,20] Gyr. For each of the 1302 galaxies of the sample, the fitting process was repeated assuming the seven different stellar Initial Mass Function (IMF) described in Sec. 2.3.2: the classical Salpeter (Salpeter 1955) and Chabrier IMFs (Chabrier 2003) and other five power law IMFs ($\phi(m) \propto m^{-s}$) with slope s=1.5, 2.0, 2.5, 3.0, 3.5. From the SED fitting analysis I derived for each galaxy its stellar mass M_*, the mean age of its stellar population and its star formation rate. The stellar mass adopted is the mass associated to the best fitting template considering only the mass contained into stars, including stellar remnants (white dwarf, neutron stars, etc.). An accurate description of the SED fitting procedure can be found in Sec. 2.3.3.

From now on, unless otherwise specified, I refer to passive galaxies derived using a Salpeter IMF for the comparison with the morphologically selected sample. In Sec. 3.4 I will discuss how a passive galaxy selection depends on the different IMFs adopted in the spectrophotometric models.

Applying the sSFR selection (sSFR$\leq 10^{-11}$ yr^{-1}) and assuming in the models a Salpeter IMF, a sample of 281 passive galaxies has been selected.

3.3 How a sample of passive galaxies differs from a sample of ETGs

The selection of passive galaxies produced a sample of 281 galaxies, while the morphological selection led to a sample of 247 ETGs. Actually, the mismatch between these numbers is not the most important difference between the two selection criteria. Indeed, of the 247 visually classified ETGs, 182 are passive

galaxies while 65 ETGs do not satisfy the passivity criterion. Instead out of the 281 passive galaxies 99 have a disc-like/irregular morphology. This means that ∼35 % of passive galaxies are not ETGs and that the selection criterion based on the passivity of the galaxies misses 26 per cent of spheroids. Thus the two different criteria do not select the same sources, i.e. the sample of ETGs does not coincide with that of passive galaxies and the passive sample does not include all the pure ETGs contained in the original magnitude limited sample.

On the basis of these differences, I wondered whether the two samples share the same physical properties. The distributions of physical and structural parameters are shown in the 4 top panels of Fig. 3.4, where red and black represent ETGs and passive galaxies respectively. I found that from the analysis of stellar masses, star formation rates and mean ages of the stellar populations no significant differences are detected. Similarly, the distributions of the effective radii are almost indistinguishable for the two samples. This may be due to the 182 galaxies in common between the two samples; therefore, the possible differences resulting from the unshared objects are diluted in the global distributions.

For this reason I analysed the galaxies not in common between the passive and the ETGs samples (i.e. 65 non-passive ETGs and 99 passive LTGs), searching for any peculiarities that make them different from the 182 galaxies present in both samples.

With regard to the 65 pure-ETGs that fall outside the passivity criterion, I verified that ∼70 per cent of them have a sSFR$< 5 \times 10^{-11}$ yr^{-1}, which is slightly higher than the chosen threshold. Also the axial ratio distributions of the active and quiescent ellipticals are indistinguishable, both peaking around $b/a \simeq 0.8$. Hence these galaxies are basically equal to the other ETGs, but due to the sSFR threshold they have been excluded from the selection.

For the 99 passive LTGs I compared their stellar mass, SFR, age of their stellar populations, and their effective radius with those of passive ETGs (bottom 4 panels of Fig. 3.4). I found that the stellar masses of passive LTGs do not show measurable differences compared to the stellar masses of the passive ETGs. This is not surprising if the galaxy luminosity function is consider (e.g. Salimbeni et al. 2008), indeed the ETGs at higher mass are numerically more abundant, but the mass distribution is spread over the same range between LTGs and ETGs, thus the stellar mass distribution of the

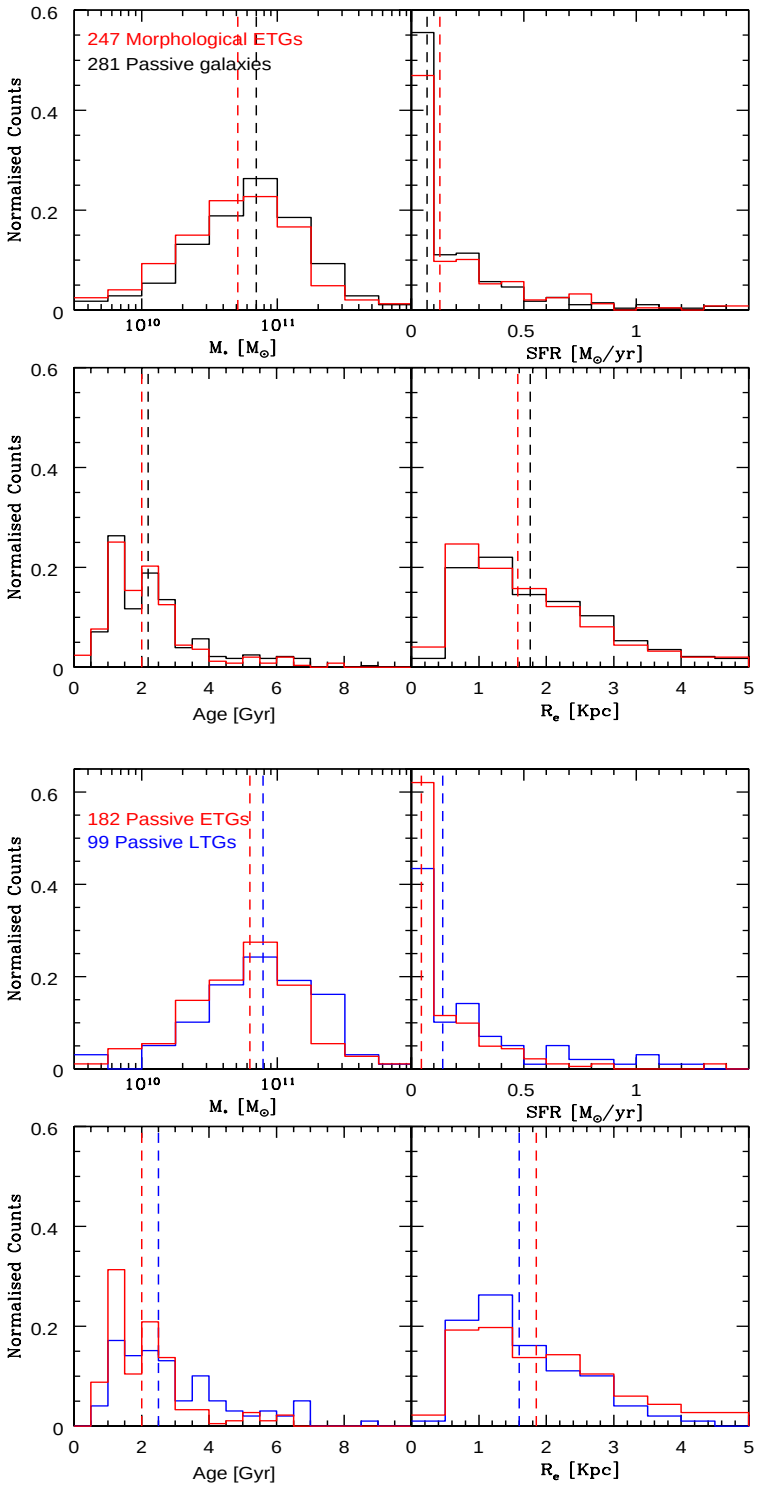

Figure 3.4: **-Top panels-** *First line from left to right*: stellar mass and star formation rate distributions of passive (black) and morphological early-type galaxies. *Second line from left to right*: mean age of stellar populations and effective radius of passive (black), and morphological early-type galaxies (red). Vertical lines are the median values. **-Bottom panels-** *First line from left to right*: stellar mass and star formation rate distributions of passive LTGs (blue), and passive early-type galaxies (red). *Second line from left to right*: mean age of stellar populations and effective radius of passive LTG (blue), and passive early-type galaxies (red). Vertical lines are the median values. The distributions are normalized by the total number of galaxies in each sample.

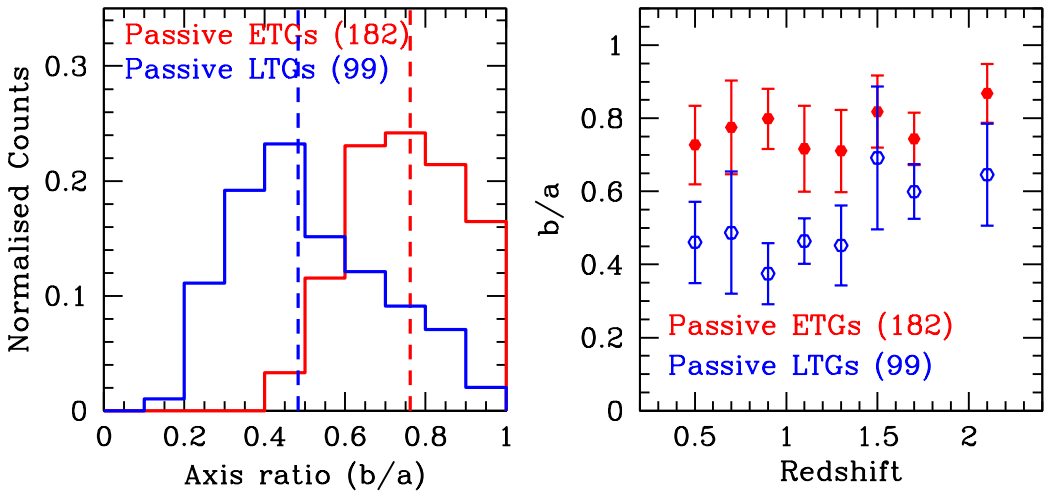

Figure 3.5: *Left)* Axis ratio distribution of passive ETGs (red) and passive LTGs (blue). *Right)* Median axis ratio evolution as a function of redshift for passive ETGs (red) and passive LTGs (blue).

passive galaxies has no dependence on the galaxy morphology.

In addition the distributions of the effective radii of discs and spheroids are very similar; for the passive late-type population, 50% of the emitted total light is concentrated in a median radius $r_e \sim 1.6$ kpc compared to the median value $r_e \sim 1.8$ kpc of passive ETGs. To determine whether this analogy of the effective radii was expected, I calculated the effective radii of two galaxies assumed to have the same stellar mass and surface brightness profiles described by a pure disc profile (n=1) in one case and by a de Vaucouleurs profile (n=4) in the other. I found that the effective radii differ by a factor of 1.26, in agreement with the observed r_e differences. This means that from an analytical point of view the effective radius of a Sérsic profile generally associated with a disc ($n = 1$) does not show substantial differences compared to the r_e of a profile generally associated with spheroidal object.

Moreover, the samples of passive ETGs and LTGs have almost the same age distribution, with median a age of 2 Gyr and 2.5 Gyr for ETGs and LTGs, respectively. Again, this is not surprising because all the passive galaxies, both late- and early-type, were selected according to the same criterion of passivity, hence their SED is fitted by similar spectrophotometric templates that provide comparable age measures (see Fig. 3.11). The only differences between passive ETGs and passive LTGs have been found in their axis ratios,

a parameter directly related to the shape and dynamic of the galaxy. From the left panel of Fig. 3.5 it is clear that the two populations have different axis ratio values, where the visually classified ETGs typically have $b/a = 0.76$, while the galaxies classified as discs have a median $b/a = 0.48$. The result is consistent with previous studies at low redshift (Padilla & Strauss 2008) and at high redshift (Buitrago et al. 2013); in particular in the latter case, a visually classified sample of massive galaxies at redshift $0 < z < 3$ has been analysed and axis ratio values are in agreement with our median results for both early- and late-type populations. Also van der Wel et al. (2011) analysed a sample of passive galaxies and found that a fraction of quiescent galaxies had small axis ratio values; they claimed that these measurements were probably tracers of a disc population among the quiescent galaxies, but they did not obtain the morphological information for these objects. Our analysis confirms this clue and also provides the percentage of contamination of disc-like objects in a sample of passive galaxies. In the left panel of Fig. 3.5 the presence of an overlapping region between the axis ratios of ETGs and LTGs, with a fraction of discs populating the tail at greater axis ratios can also be seen. This overlapping region led us to investigate if the higher b/a values of LTGs were due to a systematic loss of the low surface brightness structures at increasing redshift, since at high redshift the profile fitting may be biased by the low signal-to-noise ratio of the images (Mancini et al. 2010), because the surface brightness scales as $(1+z)^4$. The result shown in the right panel of Fig. 3.5 suggests that this may affect the measurement of the axis ratios of passive LTGs that tend to be greater at higher redshift, however a possible physical evolution of the galaxy shapes cannot be excluded.

The analysis of the axis ratios provides additional and independent information on the morphology of the galaxies and confirms that the passive sample is composed of morphologically different galaxies, which cannot be handled as a homogeneous population of objects.

I verified whether the presence of passive discs in the sample of passive galaxies had a dependence on the redshift and on the stellar mass. In Fig. 3.6 the fractions of passive LTGs as function of redshift and mass are shown. As can be inferred from the left panel of Fig. 3.6 the fraction of discs in the passive sample is almost constant at $\sim 35 - 40$ % up to $z \sim 2$, and then it increases till a value of ~ 60 %. However, since in the highest redshift bin

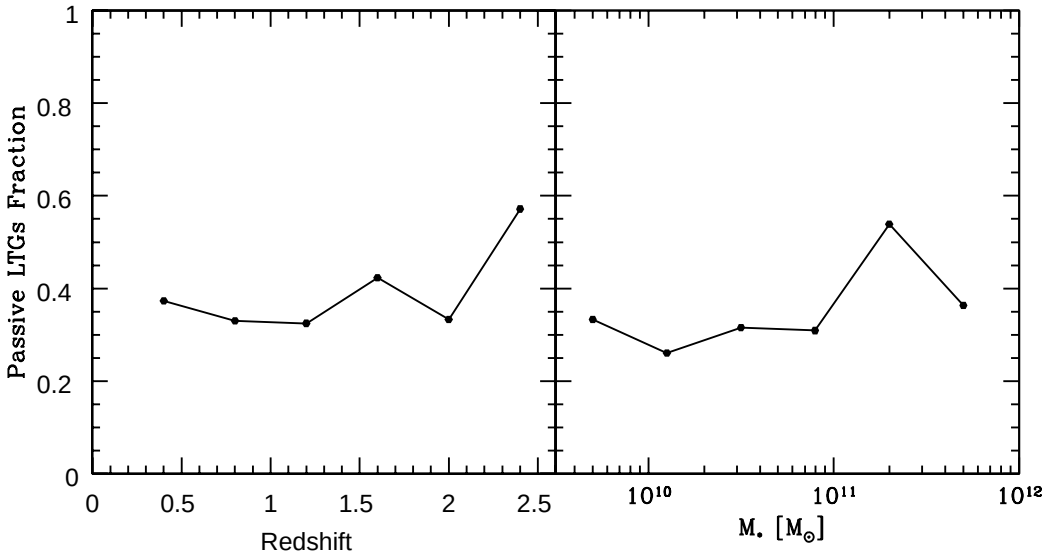

Figure 3.6: Fraction of passive late-type galaxies as function of redshift (left) and stellar mass (right)

there are only 7 galaxies (4 with a disc morphology and 3 with a spheroidal shape), and since at those redshift only the very massive galaxies are visible, due to the mass selection function (see Sec. 4.1), no evolutionary effect can be inferred. A same constant trend is observed also for the fraction of passive LTGs as function of mass, indeed up to $M_* = 10^{11}$ $M_\odot$ the fraction of this population is nearly constant at 30-35 per cent, even though a peak at 2×10^{11} $M_\odot$ is observed. In conclusion, from this analysis it has been found that the disc-shaped galaxies enter in the passive selection at any redshift and, that the passivity of a spiral galaxy does not seem correlated to its mass.

3.4 Dependence of the passivity of galaxies on the IMF

The definition of passive galaxies rests on a selection criterion based on a fixed threshold of the specific star formation rate (sSFR$\leq 10^{-11}$ yr^{-1}). The sSFR is a model-dependent quantity, that results from the ratio between the star formation rate and the stellar mass. We have seen in Sec. 2.3.2 that the properties of galaxies (e.g. stellar mass, SFR, mean age of stellar population, etc.) are derived from the comparison of the observational multiwavelength photometry with stellar population models. In the SED-fitting process several parameters, such as the IMF, must be fixed, with the consequence that the retrieved physical properties can be influenced by these assumptions. The

IMF Type	Passive Galaxies	ETGs fraction	LTGs fraction
Salpeter	281	182 (64.8 %)	99 (35.2 %)
Chabrier	272	177 (65.1 %)	95 (34.9 %)
s=1.5	403	209 (51.9 %)	194 (48.1 %)
s=2.0	312	194 (62.2 %)	118 (37.8 %)
s=2.5	256	172 (67.2 %)	84 (32.8 %)
s=3.0	195	133 (68.2 %)	62 (31.8 %)
s=3.5	146	103 (70.6 %)	43 (29.4 %)

Table 3.1: Number of passive galaxies and relative morphological fractions of samples of passive galaxies selected assuming different IMFs in the models.

fixed IMF affects the SED fitting in the way that the shape and normalization of the continuum emission depend on the relative abundance of low-to-high mass stars, hence also the stellar mass, the SFR and the sSFR can change if the IMF varies.

Here, I investigate how the samples of passive galaxies and their morphological mix change, at fixed sSFR threshold and for different IMFs adopted in the models. Indeed, often in literature the same threshold of sSFR is adopted with different IMFs, not considering that the variation of the relative abundance of low-to-high mass stars changes the stellar mass and the SFR with which the sSFR is estimated. Thus, I wondered how the sSFR of a galaxy depends on the assumed IMF and how the same definition of passivity (i.e. sSFR$\leq 10^{-11}$ yr^{-1}) affects the selection of samples of passive galaxies.

To this end, from the original magnitude limited sample of 1302 galaxies I selected five samples of passive galaxies, one for each of the five power-law slopes (s=1.5, 2.0, 2.5, 3.0, 3.5) of the considered IMF (see Sec. 2.3.3), according to the selection criterion sSFR$\leq 10^{-11}$ yr^{-1}.

The results of the selection are shown in Tab. 3.1, where in the first column the number of galaxies classified passive on the basis of sSFR using different IMFs in the models is reported. A clear trend is visible: the higher the abundance of low-mass stars in the IMF, the lower the number of objects classified as passive galaxies, from 146 objects for the bottom-heavy IMF (s=3.5) to 403 for the top-heavy IMF (s=1.5). This trend could be due to a balance of the best fitting parameters: to fit a given observed SED, the intrinsically redder colour of the models with steeper IMF must be counterbalanced by younger ages and/or longer SFHs. As a consequence, a higher value of sSFR than the above selection criterion will be assigned to

the galaxy. Since the galaxies collected in the various samples are different, I analysed how the morphological composition of these samples changes as a function of the IMF. In the second and third columns of Tab. 3.1 the number of ETGs and LTGs included in each of the five samples of passive galaxies are reported. From the analysis of these numbers, it follows that the selection of passive galaxies never includes only and all the spheroidal galaxies. In all the considered cases a remarkable fraction of passive galaxies have a late-type morphology irrespective of the assumed IMF. In particular, for increasing abundance of low-mass stars, the selected ETGs move from $\sim$ 85% (i.e. 209/247 for s=1.5) to $\sim$ 41.7% (i.e. 103/247 for s=3.5), when compared to the 247 ETGs of the morphological sample. However, although the samples with steeper IMF select a smaller number of ETGs, they have a lower contamination of discs; indeed, the fraction of LTGs passes from 48% in the sample with $\mathrm{IMF}_{s=1.5}$ to a 29% regarding the sample obtained with $\mathrm{IMF}_{s=3.5}$. Hence, keeping the sSFR threshold fixed and varying the IMF, the selected samples of passive galaxies considerably differ both in the number of selected galaxies and in the morphological composition.

To understand how the modification of the IMF affected the physical properties derived by the SED fitting I compared the distributions of the stellar mass, the SFR, the sSFR and the mean age of the two passive samples with $\mathrm{IMF}_{1.5}$ and $\mathrm{IMF}_{3.5}$ with that of the passive sample obtained assuming a Salpeter IMF. The results presented in Fig. 3.7 show that the parameter most affected by the IMF is the stellar mass. This is not surprising if we consider that the IMF describes the relative abundance of low-to-high mass star in a burst of star formation. On the other hand, the star formation rate have a similar distribution irrespective of the chosen IMF, while the mean age have a median value slightly lower for the passive galaxies with a steeper IMF.

Until now I compared the physical parameters of passive samples made by different galaxies, finding that, except for the stellar mass, the main distributions are not very different. However, to study the dependence of the passive properties on the IMF, the analysis must be focused on the passive galaxies in common to the various samples, to distinguish the eventual trend lost in the global distributions. Thus, I use the properties derived by the SED fitting processes to study the dependence with IMF of the age, of the stellar mass and of the star formation rate attributed to the same galaxies. For this

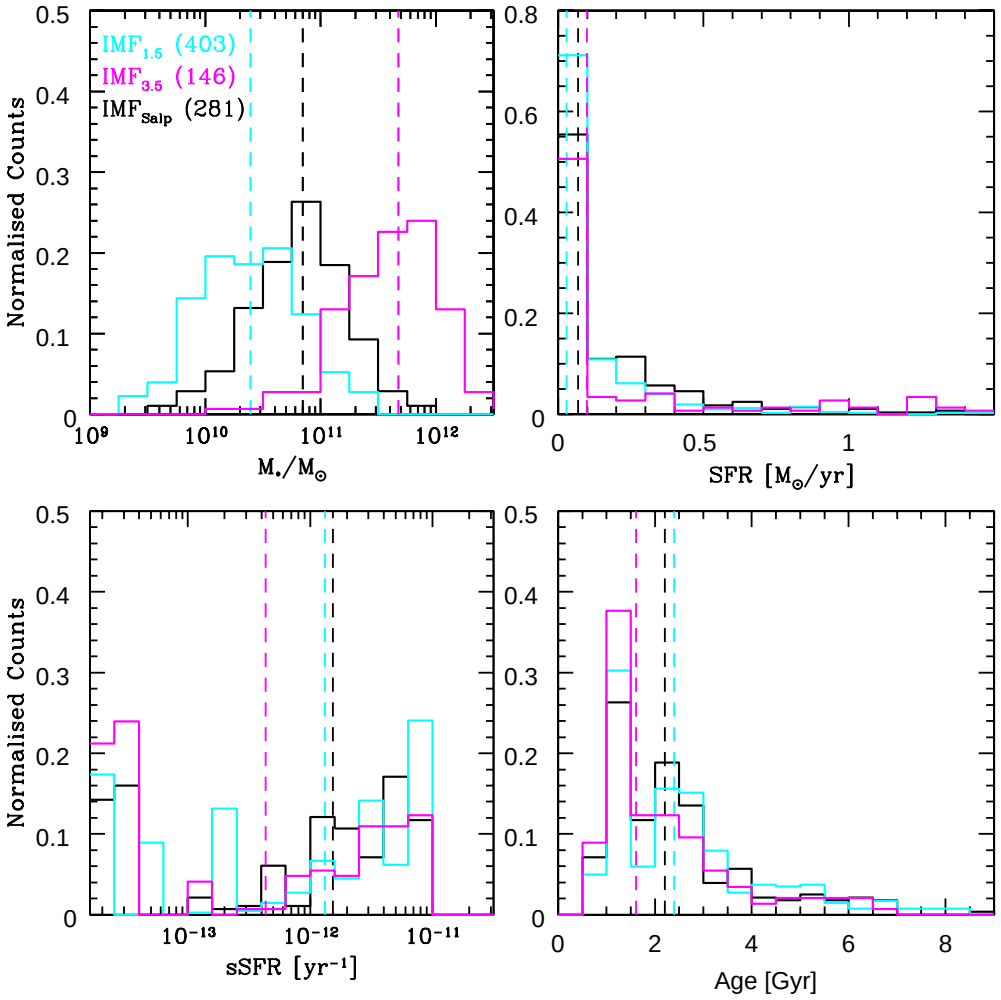

Figure 3.7: *Top line*: stellar mass and star formation rate distributions; *bottom line*: sSFR and mean age of the stellar populations distributions for three samples of passive galaxies selected adopting in the models different initial mass function: $IMF_{1.5}$ (cyan), $IMF_{3.5}$ (magenta), Salpeter IMF (black). Vertical lines are the median values. The distributions are normalized by the total number of galaxies in each sample.

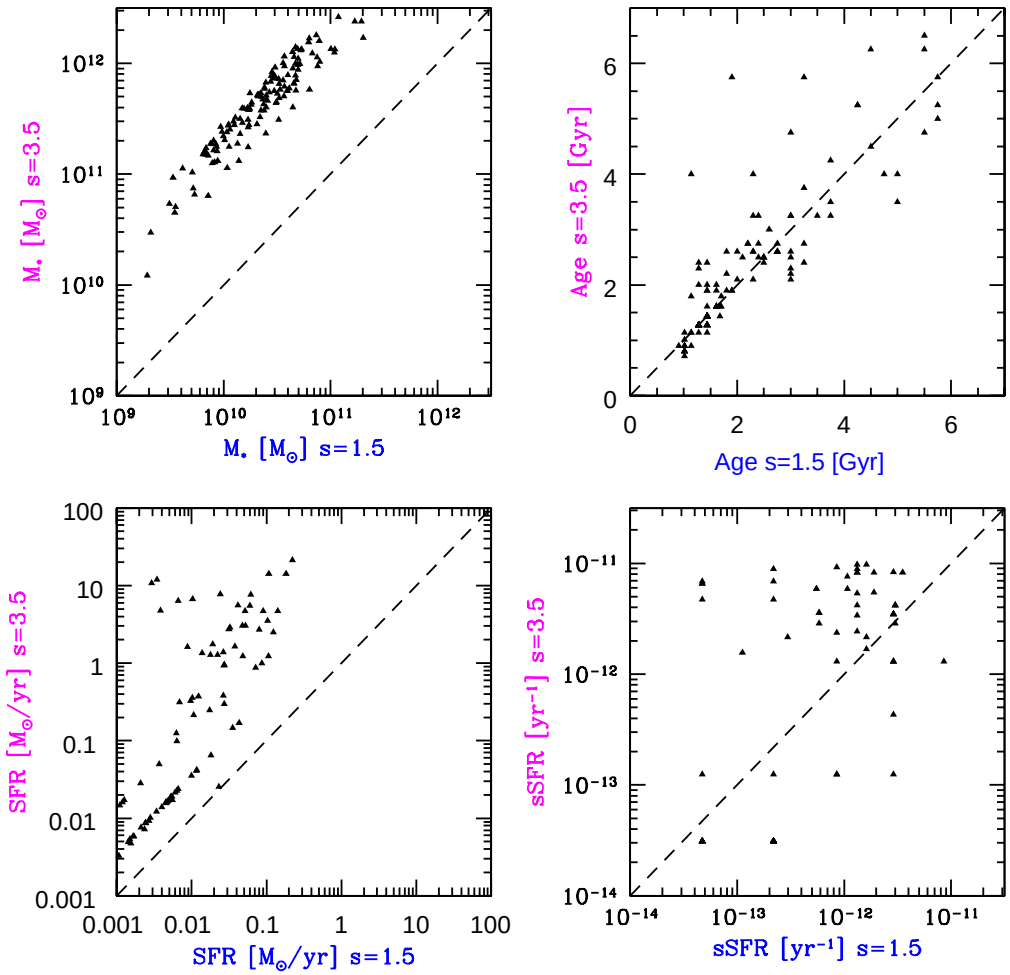

Figure 3.8: Comparison between stellar mass, age, SFR, sSFR estimated adopting an IMF with slope s=3.5/s=1.5, i.e. considering an higher/lower abundance of low-mass stars.

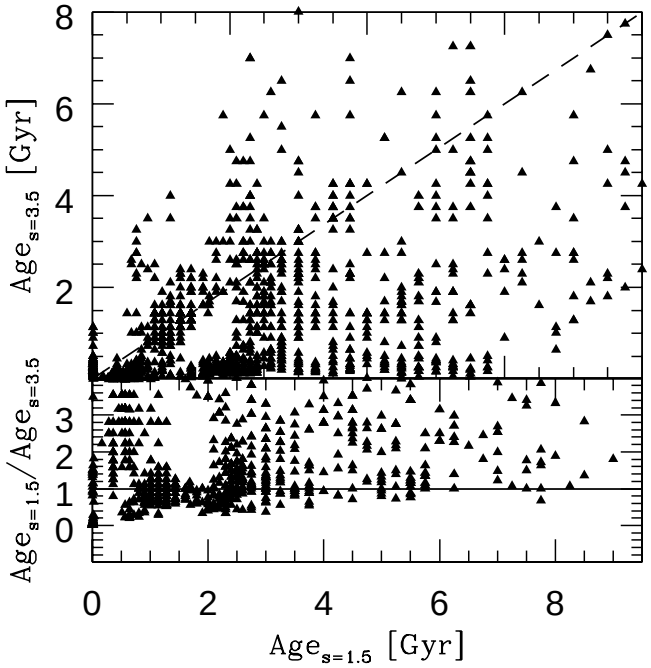

Figure 3.9: Comparison of the ages derived with IMF$_{s=1.5}$ and IMF$_{s=3.5}$ for the original sample of 1302 galaxies. The solid line represent the relation Age$_{s=1.5}$=Age$_{s=3.5}$.

purpose I selected all the galaxies in common to the two samples with opposite IMF (s=1.5 and s=3.5), and I analysed the properties obtained for the same galaxies as a function of the different IMF. The objects in common are 144 passive galaxies. In Fig. 3.8 the stellar mass (M$_*$), the age, the SFR and, the sSFR associated to each galaxy with the two IMFs are shown. As expected for the stellar mass there is a clear offset of more than an order of magnitude due to the fact that the larger fraction of low-mass stars implies higher galaxy mass. Also the star formation rates derived with the steeper IMF are higher than the one obtained with flatter IMF. For what concerns the ages of this 144 passive galaxies they do not depend on the IMF adopted in the models. It is worth to note that this result is valid for passive galaxies and cannot be extended to the whole sample, i.e. to the no-passive galaxies; indeed comparing the ages of the 1302 galaxies of the original sample (Fig. 3.9) we found that different IMFs produce a different estimate of the ages of the stellar component. In particular, if we assume the IMF$_{s=1.5}$ the bulk of the galaxies has an higher value of age than that derived assuming the IMF$_{s=3.5}$.

IMF Type	sSFR threshold $[yr^{-1}]$	Passive Galaxies	ETGs fraction	LTGs fraction
Salpeter	$\leq 1.0 \times 10^{-11}$	281	182	99
Chabrier	$\leq 1.2 \times 10^{-11}$	295	184	111
s=1.5	$\leq 5.7 \times 10^{-12}$	319	181	138
s=2.0	$\leq 7.7 \times 10^{-12}$	313	193	120
s=2.5	$\leq 1.4 \times 10^{-11}$	283	182	101
s=3.0	$\leq 3.1 \times 10^{-11}$	280	179	101
s=3.5	$\leq 7.1 \times 10^{-11}$	286	182	104

Table 3.2: Samples of passive galaxies with relative morphological compositions, selected using different sSFR thresholds, according to the different IMFs adopted in the population synthesis models.

3.4.1 Rescaling the sSFR threshold for different IMFs

We have seen how the passive samples change keeping fixed the sSFR threshold and varying the stellar initial mass function. It has also been verified that different IMFs imply different values of stellar mass and star formation rate, hence different sSFR.

For this reason, as the IMF changes new sSFR thresholds should be applied in order to select and compare samples of passive galaxies. In particular, to be consistent, the sSFR threshold should be rescaled according to the used IMF.

I performed this exercise by adopting as reference the sSFR derived assuming a Salpeter IMF and I redefined the sSFR thresholds for the other IMFs. In particular, for each IMF I derived a scale factor as the median value of the ratio $sSFR_{IMF}/sSFR_{Salp}$ obtained for each of the 1302 galaxy.

The resulting sSFR thresholds are $\mathrm{sSFR}_{s=1.5} \leq 5.7 \times 10^{-12}$ yr^{-1}, $\mathrm{sSFR}_{s=2.0} \leq 7.7{\times}10^{-12}$ yr^{-1}, $\mathrm{sSFR}_{s=2.5} \leq 1.35{\times}10^{-11}$ yr^{-1}, $\mathrm{sSFR}_{s=3.0} \leq 3.11{\times}10^{-11}$ yr^{-1}, $\mathrm{sSFR}_{s=3.5} \leq 7.13{\times}10^{-11}$ yr^{-1} and, $\mathrm{sSFR}_{Chabrier} \leq 1.17{\times}10^{-11}$ yr^{-1}. With this new sSFR thresholds we repeated the selection of the passive samples and we found that the number of passive galaxies varies from a minimum of 280 with an $\mathrm{IMF}_{3.0}$ to a maximum of 319 with an $\mathrm{IMF}_{1.5}$ (Col. 3 in Tab. 3.2). However, also in this case none of these selection of passive galaxies allow us to collect all the ETGs regardless of the IMF assumed in the models and all the samples contain a considerable fraction ($\sim$36-43 %) of late-type populations. In conclusion, a significant number of LTGs is included in the passive population, whatever the IMF assumed in the models, and this should be accounted for when studying the evolution of the properties of the ETGs population, that

cannot be successfully selected adopting the passivity criterion.

3.5 The galaxy colours of the morphological and passive samples

Here, I investigated how the morphologically classified galaxies are located on the colour-colour diagram to understand the connection between the morphology of a galaxy and the stars contained in it. Indeed, it is well known that the colour of a galaxy is tightly related to the stellar populations and brings a track of the age, the star-formation time scale, the metallicity and the presence of dust of the galaxy. For this reason the galaxy colours have been often used to separate different type of galaxies (red/quiescent versus blue/active, Strateva et al. 2001, Baldry et al. 2004), however few attention has been given to the reverse path, i.e. understanding if a given morphology implies a given stellar population.

To this aim I considered the colour-colour plot $(U-V)_{rest}$ versus $(V-J)_{rest}$ (hereafter UVJ diagram). This colour-colour plot has been widely adopted to segregate actively star-forming galaxies from their quiescent counterpart (e.g. Labbé et al. 2005, Wuyts et al. 2007, Williams et al. 2009, Muzzin et al. 2013), since break the colour degeneracy between red quiescent galaxies and dust-obscured red star-forming galaxies. The rest frame U-V colour samples the amplitude of the 4000 Å break in the galaxy SED, that reflects the absorption from ionized metals in the atmospheres of late-type stars ($M_* > 1\ M_\odot$). It is an indicator of the galaxy stellar population age and it is more pronounced in old stellar population in which the level of star formation has been negligible for more than 1 Gyr. The rest frame V-J colour measures the slope of the galaxy SED between 5500-12500 Å. At these red wavelengths the galaxy emission is mostly dominated by old stellar populations with mass $M_* < 1\ M_\odot$, hence if the contribution to the emission of these stars is low, the V-J will be bluer.

In the top panels of Fig. 3.10 I show the rest frame UVJ diagram for the morphologically classified galaxies of the magnitude limited sample ($K_s \leq 22$) in six bin of redshift. The absolute magnitude, for a given photometric band and a given galaxy redshift, was obtained with the software `Hyperzmass` (Bolzonella et al. 2000) from the apparent magnitude of the filter that most closely matches the rest-frame one. The applied k-correction takes into account the difference between these two photometric bands.

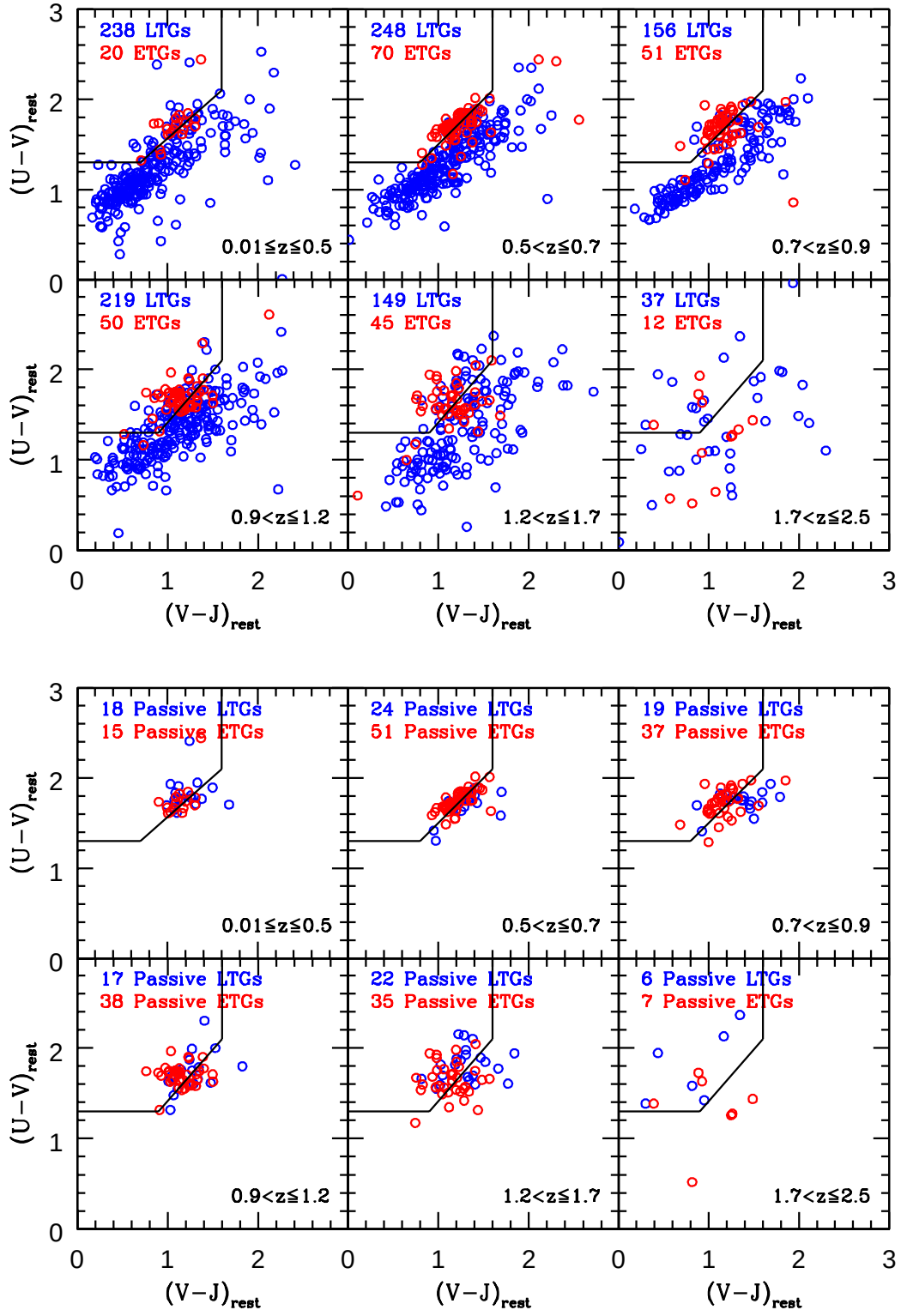

Figure 3.10: *Top:* Rest frame U-V vs. V-J colours of $K_s \leq 22$ galaxies at various redshift. The red points represent the ETGs and the blue points refer to the LTGs, both the population were morphologically selected as described in Sec.3.1. The black lines enclose the "passive region" as defined in Williams et al. (2009). *Bottom:* Rest frame U-V vs. V-J colours of the passive galaxies selected adopting a Salpeter IMF.

A clear trend is visible in Fig. 3.10: early-type galaxies are placed in a localized clump that spans a narrow colours range, both for the U-V ($1.4 \lesssim$U-V$\lesssim 2.0$) and for the V-J ($0.8 \lesssim$V-J$\lesssim 1.6$) colours; on the other hand, the LTGs occupy a diagonal track that extends from the bluer U-V vs V-J colours to the redder portion of the UVJ plane. The observed bimodal distribution of ETGs and LTGs is clearly seen up to $z \sim 1.7$, although the scatter increases at higher redshift. In the last redshift bin ($1.7 < z \leq 2.5$) the two distinct populations are not visible any more, probably due to the weaker observed fluxes and the low statistics. As the redshift increases the galaxies in the UVJ diagram are progressively more scattered, independently of galaxy morphology. This spread cannot only be due to the photometric errors that increases as the redshift increases, since these errors can account at most for a spread of 0.2 mag, while the observed scatter is almost ~ 1 mag. This effect, present for both the morphological classes, can be a consequence of the gradual approaching to the time at which galaxies have formed their star formation, hence is tightly related to the stellar population properties. At these epochs, close to the SF events, the colours are highly variable, and the ages of the stellar populations are comparable with the star formation time-scales. As shown in Sec. 2.3.2 when the t/τ ratio is close to 1, hence a short time is passed from the star formation, the galaxy SEDs highly vary their shape, and the galaxy colours assume more spread values.

Beyond the observed bimodality, the trends observed in Fig. 3.10 show that the spheroidal morphology implies a particular stellar population with given colours, the same is not true for the late-type population. Hence, starting from the analysis of the stellar colours is not obvious going back to the morphology.

Since the UVJ has been used in many studies to separate quiescent and star-forming galaxies, following Williams et al. (2009) I identified the so-called "passive region" defined as:

- U-V$>$ 1.3, V-J$<$ 1.5 [all redshift];
- U-V$>$V-J$\times$0.88+0.69 [$0 < z < 0.5$];
- U-V$>$V-J$\times$0.88+0.59 [$0.5 < z < 1.0$];
- U-V$>$V-J$\times$0.88+0.49 [$1.0 < z < 2.5$].

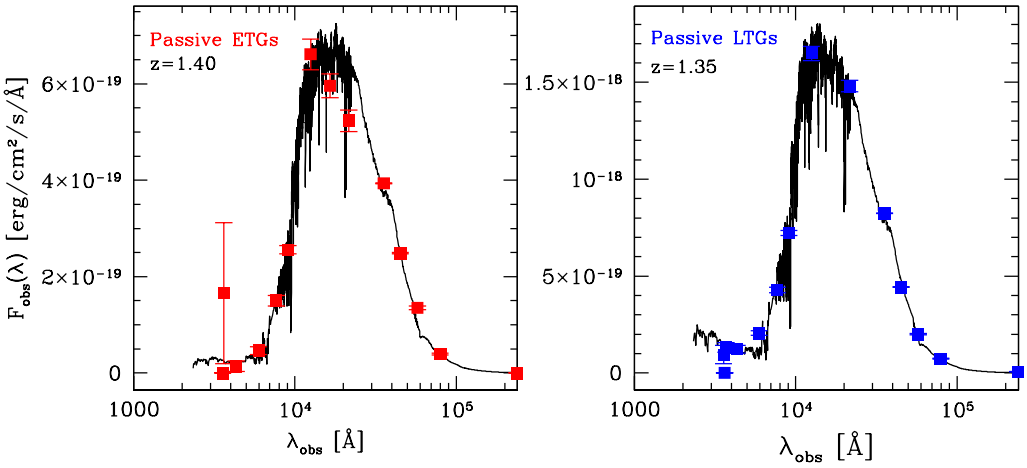

Figure 3.11: Observed SEDs with their best fitting models (black) of a passive ETG (red) and a passive LTG (blue).

The boxes were defined by Williams et al. (2009) with the aim to maximize the differences in sSFR based on the UV/K and 24μm/K flux ratios for their sample of galaxies. The black wedges in Fig. 3.10 represent the above selection. It can be seen that these boxes do not select efficiently the spheroidal galaxies and included also galaxies with a late-type morphology. Indeed, a not negligible fraction of early-type galaxies do not fit perfectly the passive UVJ region, behaviour in agreement with Moresco et al. (2013) that found only a 63% of their morphological ETGs overlapping the passive region of the UVJ diagram.

Since the above selection were applied to select quiescent galaxies, I show in the bottom panels of Fig. 3.10 how the passive sample is placed on the colour-colour diagram. The passive galaxies were selected assuming a Salpeter IMF and were divided by morphology (red for passive ETGs, blue for passive LTGs). Also in this case the above colour selections are not able to select passive galaxies. Moreover, as showed in Sec. 3.3 not all the passive galaxies have a spheroidal morphology, this means that also in a colour-colour diagram the passive discs are located in the same region of the passive spheroids. This colours similarity is not surprising if we consider that a galaxy to be classified as "passive" should necessarily have a particular shape of the observed SED. Indeed as shown in Fig. 3.11 the SED of a passive ETG is almost equal to the SED of a passive LTG.

In conclusion the UVJ selection criterion neither selects samples of strictly

defined ETGs nor sample of passive galaxies with only spheroidal morphology, introducing a clear mix of spirals and spheroids.

3.6 Summary and Discussion

In this chapter it has been performed a morphological classification of a magnitude limited sample of 1302 galaxies of the GOODS-South field with the aim to select a sample of ETGs and to perform a comparison with a sample of passive galaxies, selected according to their specific star formation rate. The evidences collected in the previous sections suggest that a visual classification of ETGs cannot be replaced by a classification of passive galaxies. Indeed even though in the local Universe the ETGs often host an old stellar population and have a negligible rate of star formation for mass unit, I found that also a significant fraction of LTGs (> 30 %) contain a similar stellar component, hence the classification method based on the sSFR is not able to separate properly ellipticals from discs. Moreover, I found that also several ETGs (~ 26 %) can fall outside the definition of passive galaxies, since the sharp cut on the sSFR cannot considered the outliers even if their sSFR is close to the fixed threshold.

I then performed an accurate study on the physical properties of the galaxies contained in each sample (i.e. the morphological and the passive ones) to understand how the different morphological composition of the passive sample would reflect on the general properties with respect to the morphological sample. This analysis shows that a passive sample cannot be distinguish by a morphological sample of ETGs from the study of the physical and structural parameters, such as the stellar mass, the mean age of the stellar population and the effective radius. However even if the properties of the two samples can be interchangeably their morphological composition is different and to study the evolutionary path over cosmic time of the early and late population this difference can be crucial.

Subsequently, I presented a discussion on the dependence of the passive sample both on a parameter adopted in the population synthesis models, i.e. the IMF, and on the threshold of sSFR used to select passive galaxies with different IMFs. I demonstrated that the composition of passive samples is highly dependent on the IMF used in the models, since the IMF acts on the measurement of the stellar mass and of the SFR used to retrieve the

sSFR. The realized analysis suggests that the selection of galaxies through the passivity criterion is strongly dependent on model and on the definition of passive galaxies. These dependence does not enable a fair comparison between different literature works and always produces mixed sample of early and late-type galaxies.

Finally I performed a study on the rest-frame colour-colour diagram both for the morphological sample and for the passive sample. The analysis has pointed out how also this selection does not enable to collect galaxies with only a spheroidal morphology but it has underlined how the colour of the ETGs are confined in a narrow range, constant at different redshift.

Chapter 4

Following the evolution of ETGs and LTGs through their main properties

In the previous chapters, we have seen that morphology and passivity are not equivalent: a selection of passive galaxies is highly dependent on the assumed IMF, produces samples with a high fraction of LTGs, and misses a significant fraction of ETGs. Hence, samples of passive galaxies cannot be used to study the evolution with redshift of a particular morphological class. In fact, to disentangle the evolutionary phases of spheroids and/or discs it is necessary to not mix these two morphological classes in the same sample, since their different dynamic suggests a different formation history. In this chapter the morphological sample obtained on the basis of the visual classification (Sec. 3.1) and composed of 1055 late-type objects and 247 strictly defined ETGs will be used to study the evolution with redshift of this two morphological types of galaxies.

4.1 Stellar masses and mass completeness

From the morphological analysis it has been found that 247 out of 1302 galaxies of the magnitude limited sample has been classified as early-type galaxies (i.e. ellipticals (E) and transition E/S0 galaxies) in a redshift range $0.1 \lesssim z \lesssim 2.5$. The remaining 1055 galaxies have been classified as LTGs.

The derived masses for the Ks=22 sample are shown in Fig. 4.1 as a function of redshift. The stellar masses for all these galaxies were estimated by fitting their Spectral Energy Distribution (SED), as sampled by the GOODS-MUSIC multi-band photometry, with a library of stellar population models

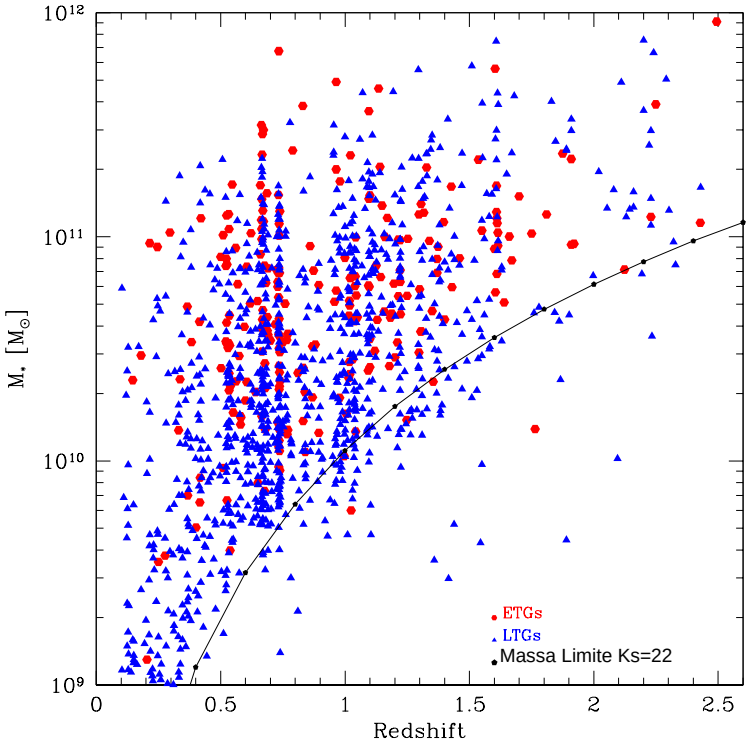

Figure 4.1: The stellar masses as function of redshift for all galaxies in the Ks=22 magnitude limited sample. The red dots are for the ETGs, the blue triangles indicates the LTGs. The black curve indicate the mass completeness in each redshift bin.

based on Bruzual & Charlot (2003, see Sec. 2.3.3 for more details) adopting a Salpeter IMF. No evident differences in the stellar mass between the two morphological types of galaxies are inferred. From Fig. 4.1 it is clear that the very massive galaxies, in the range $10^{11} \leq M_* \leq 10^{12}$ M$_\odot$, are detected all the way to z=2.5, however at $z \lesssim 0.5$ the massive galaxies are not well sampled, due to the small solid angle subtended by the GOODS-S survey.

Conversely, the magnitude limit in the Ks band translates at different redshift into different minimum luminosity, and hence different mass limit. In Fig. 4.1 it can be seen that as redshift increases only the more massive galaxies are detected. If not treated appropriately, this behaviour introduces a bias against high mass-to-light ratio galaxies, i.e. objects that would enter the sample if this were purely mass selected, but that are excluded simply because they are too faint to fulfil the apparent magnitude limit.

To derive the limiting stellar mass (M$_{lim}$, black curve in Fig. 4.1) at

which the sample is approximately complete, I calculated the mass a galaxy would have at its redshift if its apparent magnitude was equal to the limiting magnitude of the sample (i.e. Ks=22.0). In a magnitude-limited sample, the minimum stellar mass for which observations were completed depends on both the redshift and the stellar mass-to-light ratio M/L. This latter quantity depends on the stellar populations and on galaxy colours. For simplicity to estimate the limiting stellar mass I fixed the mass-to-light ratio $M/L = 1$. Our sample is therefore approximately incomplete below this curve.

From Fig. 4.1 it is clearly visible that the stellar mass at which the sample is complete over the whole redshift range is $M_* \geq 10^{11}$ $M_\odot$. However, the small field of view of the GOODS-S survey subtends a small solid angle that prevents to sample properly massive galaxies at low redshift. This effect can be seen in Fig. 4.1 where at $z < 0.6$ the number of massive galaxies drastically falls with respect to higher redshift. For this reason, a mass-complete sample of galaxies with $M_* \geq 10^{11}$ $M_\odot$ was extracted in the redshift range $0.6 \leq z \leq 2.5$. The mass-complete sample is composed by 187 galaxies of which 54 ETGs and 133 LTGs. To be conservative, the redshift cut in the range $0.6 \leq z \leq 2.5$ was then extended to the low-intermediate mass galaxies.

The Ks=22.0 magnitude-limited sample resulting after the redshift cut at $0.6 \leq z \leq 2.5$ is composed of 196 ETGs and 723 LTGs, for a total of 919 galaxies.

4.2 The evolution of the relative fraction of early- and late-type galaxies

The evolution of the galaxy morphology with redshift is now addressed, studying how the visual appearance of the galaxies has evolved over the redshift range $0.6 \leq z \leq 2.5$. Two mass ranges have been considered in this analysis: $M_* \geq 10^{11}$ $M_\odot$, for which the sample is complete over the whole redshift range (hereinafter we refer to this sample as the massive galaxies sample), and $M_* < 10^{11}$ $M_\odot$, the range of low-intermediate mass where the completeness threshold of M_* is different at different redshift, as shown in Fig. 4.1.

In Fig. 4.2 the fraction of the two morphological classes is shown as a function of redshift for the whole sample (panel A), the low-intermediate mass range sample ($M_* < 10^{11}$ $M_\odot$, panel B) and the massive galaxies sample ($M_* \geq 10^{11}$ $M_\odot$, panel C). The data are given in Table 4.1. The most evident

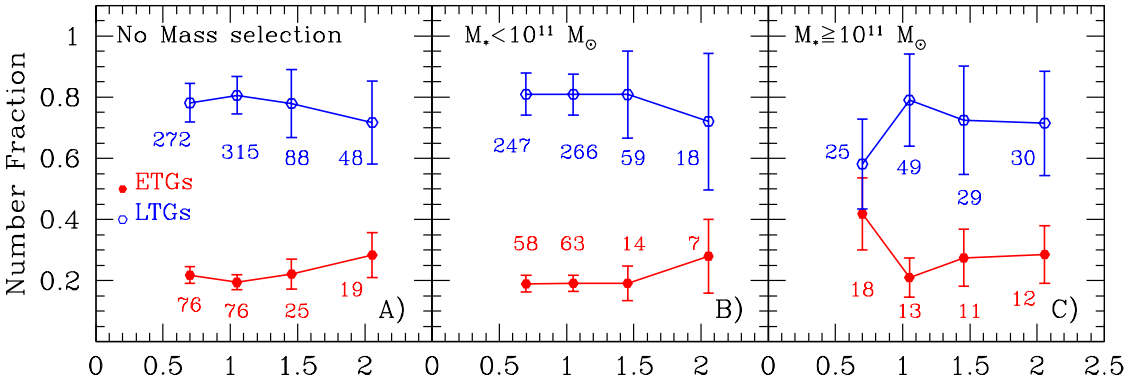

Figure 4.2: Evolution of the morphological fraction of ETGs (red) and LTGs (blue) for the entire morphological sample A), for the low-intermediate mass sample B) and for the massive sample C). The number of galaxies in each redshift bin is given.

Redshift	ETGs fraction $M_* < 10^{11}$ $M_\odot$	LTGs fraction $M_* < 10^{11}$ $M_\odot$	ETGs fraction $M_* \geq 10^{11}$ $M_\odot$	LTGs fraction $M_* \geq 10^{11}$ $M_\odot$
$0.6 \leq z \leq 0.8$	0.19 ± 0.03	0.81 ± 0.07	0.42 ± 0.12	0.58 ± 0.15
$0.8 < z \leq 1.3$	0.19 ± 0.03	0.81 ± 0.07	0.21 ± 0.06	0.79 ± 0.15
$1.3 < z \leq 1.6$	0.19 ± 0.06	0.81 ± 0.14	0.27 ± 0.09	0.73 ± 0.18
$1.6 < z \leq 2.5$	0.28 ± 0.12	0.72 ± 0.22	0.29 ± 0.09	0.71 ± 0.17

Table 4.1: Number fraction of ETGs and LTGs in the low ($M_* < 10^{11}$ $M_\odot$) and high mass ($M_* \geq 10^{11}$ $M_\odot$) regimes for four redshift bins.

result from Fig. 4.2 A) and B) is that the fraction of ETGs and LTGs is nearly constant over the whole redshift range considered. In particular the late-type objects are the dominant population at all redshift, being more than 70 per cent of the entire population, while the spheroidal fraction remains constant at about 20-30 per cent.

This result is in agreement with that of Cassata et al. (2005), based on a morphologically selected sample in a small portion of the GOODS-S field, as shown in the left panel of Fig. 4.3. This agreement provides evidence of the reproducibility and hence of the reliability of the visual classification since the data refer to the same survey but the classification is independent.

I also compared the result with Mortlock et al. (2013); the authors use a sample of galaxies at $1 \leq z \leq 3$ with $M_* \geq 10^{10} M_\odot$ in the CANDELS/UDS field to investigate the formation of the Hubble sequence. As can be seen from the right panel of Fig. 4.3, Mortlock et al. (2013) find that the two classes of galaxies are almost equivalently populated in disagreement with our findings. This inconsistency may be due to two effects. On one hand the band

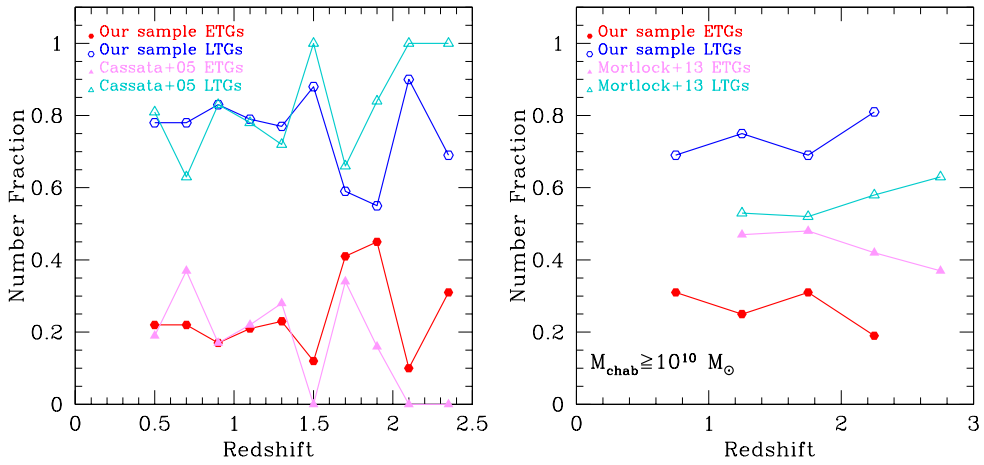

Figure 4.3: Comparison of the morphological fractions of our morphological sample (ETGs in red, LTGs in blue) with the ones derived by Cassata et al. (2005) (left panel) and Mortlock et al. (2013) (right panel). ETGs and LTGs of the other authors are shown in pink and cyan, respectively. The redshift binning is chosen in order to best reproduce the other works intervals.

used by the authors for the visual classification: the H_{160}-band, a redder band compared to the F850LP band used in this work; hence the emission from a galaxy observed for example at $z \sim 1.5$ will come from a younger/older stellar component when the F850LP/H_{160}-band are respectively used. On the other hand, the WFC3 camera with which the H_{160} observations were performed has a double pixel size compared to the ACS camera. This implies a worse sampling of the galaxy images, that can produce the loss of structures more visible in the F850LP images.

Looking at the sample of massive galaxies shown in the right panel of Fig. 4.2, it is visible a deviation from the constant trend of the morphological fraction in the lowest redshift bin, with massive ETGs that increase their fraction from $\sim$ 20 per cent at high z to more than 40 per cent at $z < 1$. This is in agreement with the evidence found in the local Universe, where the present-day mass function is dominated at greater mass ($M_* \geq 10^{11} M_\odot$) by early-type galaxies (Baldry et al. 2004, Conselice 2006).

The relative increase of the fraction of massive ETGs appears qualitatively consistent with the findings of Buitrago et al. (2013) which can rely on a sample of about 700 galaxies in the range of redshift $0.6 < z < 2$. They reported that the fraction of ETGs (defined in their work as elliptical and lenticulars) have little or no evolution in the redshift range $1 \lesssim z \lesssim 2.5$ as we found, while at

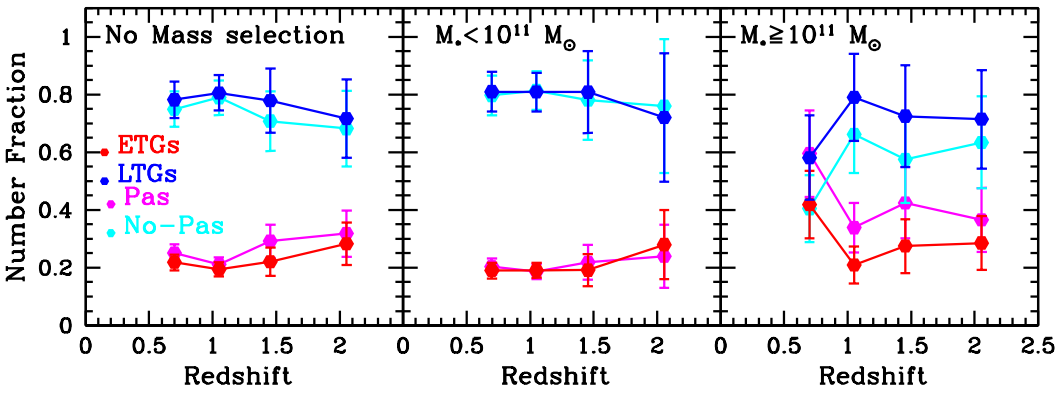

Figure 4.4: Fraction of galaxies selected by morphological classification (ETGs in red, LTGs in blue) and by sSFR selection (passive galaxies in magenta, no-passive galaxies in cyan) as function of redshift for three bins of stellar mass. In panel A) the entire sample without mass selection is shown, in panel B) and C) the $M_* < 10^{11}$ $M_\odot$ and the $M_* \geq 10^{11}$ $M_\odot$ galaxies are respectively displayed.

$z \lesssim 1$ the ETGs strongly increase, becoming the predominant morphological class of massive galaxies. At $z \lesssim 1$ Buitrago et al. (2013) detected higher fraction of ETGs compared to this work, but this can be due to their inclusion of lenticular galaxies in their ETGs sample.

Since in literature the galaxy sample are often selected on the basis of the stellar population properties, for further information, I re-calculated the numerical fraction using the sample of passive and the no-passive galaxies obtained, with the Salpeter IMF. The aim of this work was to investigate how the evolution of the fraction of galaxies would changed if we had adopted galaxies selected on the basis of their sSFR and to facilitate the comparison with different categorisations in the literature. The results, presented in Fig. 4.4, show that the major difference respect to the morphological classification are observed in the range of massive galaxies, with the fraction of passive galaxies more abundant of the fraction of ETGs. In the range of low intermediate mass the overall trend is similar for both classification even if the galaxies composing the two samples are different.

4.3 The evolution of the number density of ETGs and LTGs

To trace the rate of growth of the two populations of galaxies and to quantify their evolution along the cosmic time, the comoving number densities of ETGs and LTGs were estimated. The same mass ranges and redshift bins of Fig.

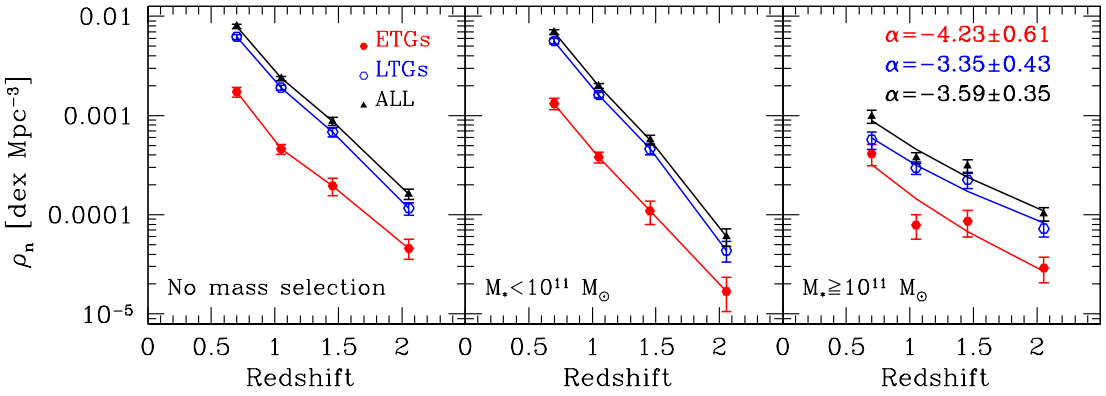

Figure 4.5: Cosmological evolution of the ETG (red) and LTG (blue) number density as a function of redshift in three mass ranges: no mass selection (left panel), low-intermediate mass sample $M_* < 10^{11}$ $M_\odot$ (central panel) and, for the massive sample $M_* \geq 10^{11}$ $M_\odot$ (right panel). Black line represents the number density for all the galaxies in the samples.

4.2 have been considered. The comoving number density of galaxies in a given redshift bin $[z_1, z_2]$ is defined as,

$$\rho(N) = \frac{N(z_1, z_2)}{V(z_1, z_2)}, \tag{4.1}$$

where N is the number of galaxies and,

$$V = \frac{\omega}{4\pi} \int_{z_1}^{z_2} \frac{dV}{dz} dz \tag{4.2}$$

is the comoving volume in the same redshift interval, and $\omega = 1.2 \times 10^{-5}$ sr is the solid angle subtended by the 143 arcmin^2 of the GOODS-South field.

The results in Fig. 4.5 show the number density for the total sample of 1302 galaxies (black) and for the two morphological samples of early- (red) and late-type galaxies (blue). The number density of the global population increases with decreasing redshift for all the mass ranges considered, reflecting the rapid growth of the two morphological classes. For the massive galaxies sample, complete in stellar mass, I computed the rate of growth of the number density fitting the data (Table 4.2) with a power law of the form $\rho_n = \rho_0 \times (1+z)^\alpha$. The fit (solid lines of the right panel) confirms the significant growth of the total galaxy population, that numerically increases by a factor of 8 from $z = 2.5$ to $z = 0.6$. The growth is steeper for massive ETGs ($\alpha_{ETGs} = -4.23 \pm 0.61$) than for massive LTGs ($\alpha_{LTGs} = -3.35 \pm 0.43$). Indeed, the massive ETGs at $z \sim 0.6$ are a factor of $\sim$ 12 more numerous

than at $z \sim 2 - 2.5$, to be compared with a factor of ~ 7 for the massive LTGs; the steepening of the ρ_n is more pronounced in the lowest redshift bin, at $z < 1$, where the two morphological classes became approximately equal in number. The effect of the rapid growth of the ETGs number density for $z < 1$ could be explained by several processes including the formation of new massive ellipticals through the merging of less massive galaxies or by the morphological evolution of some massive discs towards elliptical morphologies.

These results show that the number density of massive galaxies has significantly increased since $z \sim 2.5$, in agreement with many other studies (e.g. Mortlock et al. 2011, Conselice et al. 2011, Brammer et al. 2011, Ilbert et al. 2013, Muzzin et al. 2013). In particular, Muzzin et al. (2013) studying the number density evolution of the massive quiescent and star-forming galaxies in the COSMOS-UltraVISTA field (1.62 deg, $K_s < 23.4$, 90% completeness), found that they increase by a factor 12 and 4 respectively in in the redshift interval $0.6 \lesssim z \lesssim 2.5$. The growing they found for the quiescent galaxies is in agreement with our result, while their star-forming population grows slower than our LTGs (a factor of ~ 4 compared to a factor of ~ 7). Buitrago et al. (2013) with an analysis of a sample of morphologically classified galaxies in the POWIR/DEEP2 (Bundy et al. 2006, Conselice et al. 2007) and GNS (Conselice et al. 2011) found an increase in the number density of massive ETGs and LTGs similar to our results. On the other hand, Brammer et al. (2011) found a growth of the number density of massive quiescent galaxies of the order of 10, in agreement with our findings, but a decrease in the ρ_n of a factor ~ 5 for the star forming population. All these comparisons, however, rely on galaxy samples highly different, with galaxies selected in different ways by means of their colours, passivity or morphological classification. Hence, the similarity and the differences of the results should be considered in the light of the different selection criteria.

As for the numerical fraction I repeated the estimate of the number density also for galaxies selected according to their sSFR. The results presented in Fig. 4.6 shows that the trend of growth of the number density is very similar between the two samples of galaxies selected by morphology or by sSFR. However, the evolution of ρ_n for galaxies of a given shape and dynamic cannot be inferred looking at the passive and no-passive galaxies, since in this sample different population of galaxies are mixed together.

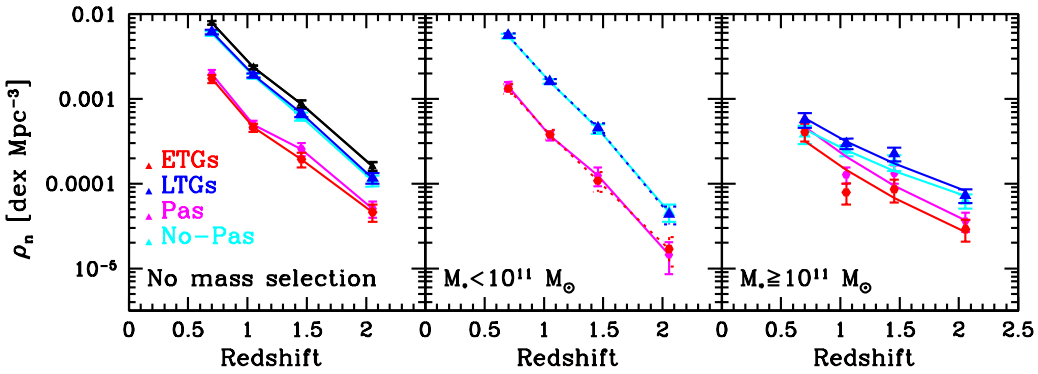

Figure 4.6: Number density of galaxies selected by morphological classification (ETGs in red, LTGs in blue) and by sSFR selection (passive galaxies in magenta, no-passive galaxies in cyan) as function of redshift for three bins of stellar mass. In panel A) the entire sample without mass selection is shown, in panel B) and C) the $M_* < 10^{11}$ $M_\odot$ and the $M_* \geq 10^{11}$ $M_\odot$ galaxies are respectively displayed.

Redshift	N_{gal}	ρ_n(tot) Mpc^{-3}	ρ_n(ETGs) Mpc^{-3}	ρ_n(LTGs) Mpc^{-3}	ρ_*(tot) $M_\odot$ Mpc^{-3}	ρ_*(ETGs) $M_\odot$ Mpc^{-3}	ρ_*(LTGs) $M_\odot$ Mpc^{-3}
$0.6 \leq z \leq 0.8$	43	98.0 ± 15.0	41.0 ± 9.7	57.0 ± 11.4	16.4 ± 1.0	8.2 ± 0.8	8.2 ± 0.6
$0.8 < z \leq 1.3$	62	37.6 ± 4.8	7.9 ± 2.2	29.7 ± 4.2	7.5 ± 0.3	1.9 ± 0.2	5.5 ± 0.3
$1.3 < z \leq 1.6$	40	31.1 ± 4.9	8.6 ± 2.6	22.5 ± 4.2	7.0 ± 0.4	1.6 ± 0.2	5.4 ± 0.4
$1.6 < z \leq 2.5$	42	10.2 ± 1.6	2.9 ± 0.8	7.3 ± 1.3	2.7 ± 0.2	0.7 ± 0.1	2.1 ± 0.1

Table 4.2: Comoving number densities (in 10^{-5} dex Mpc^{-3} units) and mass densities (in 10^7 $M_\odot$ Mpc^{-3} units) for the complete sample of 187 massive galaxies ($M_* \geq 10^{11}$ $M_\odot$) at $0.6 \leq z \leq 2.5$.

The main implication of my findings for galaxies more massive than $10^{11} M_\odot$ is that irrespective of their morphology the majority of the massive galaxies are not yet in place until $z \sim 0.6$. For redshift lower than z=0.8-1 several authors (Cimatti et al. 2006, Ilbert et al. 2013, Buitrago et al. 2013) reported that the number density of massive ETGs is nearly constant and that no new massive ETGs formed within that redshift interval. However, we cannot exclude the eventuality that the trend of growth of the ρ_n found up to z=0.6 could tend to become constant at lower redshift, although in the lowest range of redshift (z=0.6-0.8) of my data no sign of flattening is observed.

4.4 The stellar mass content of different morphological types

In this section the study of the mass fraction and of the stellar mass density over the 5 Gyr of time that occurred in the redshift range $0.6 \leq z \leq 2.5$ are presented.

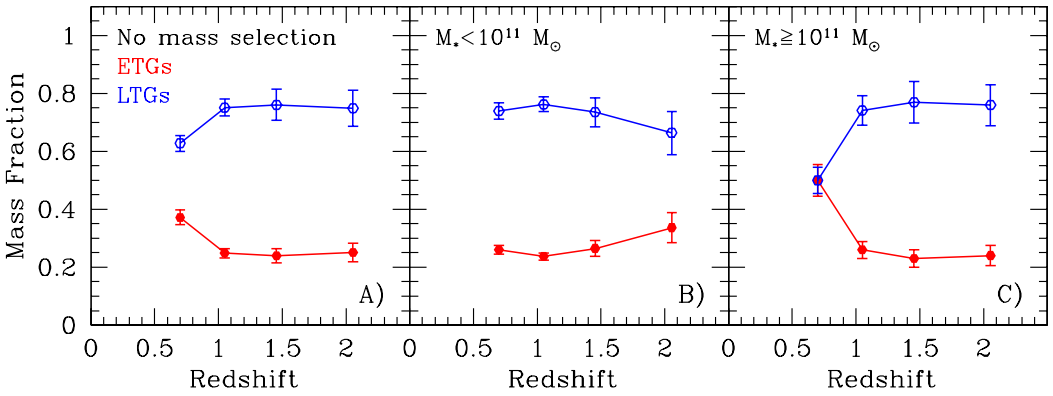

Figure 4.7: Fraction of stellar mass in galaxies of different morphological type (ETGs in red, LTGs in blue) as a function of redshift for three bins of stellar mass. In panel A) the entire sample without mass selection is shown, in panels B) and C) the $M_* < 10^{11}$ $M_\odot$ and the $M_* \geq 10^{11}$ $M_\odot$ galaxies.

The stellar masses adopted in this analysis were estimated assuming a Salpeter IMF; an alternative choice of the IMF would cause a shift in the derived values of stellar masses without affecting the trends of our results. For instance, masses obtained assuming a Salpeter IMF can be converted into those with Chabrier IMF dividing the former by a factor of 1.8 (Longhetti & Saracco 2009), the same applies to the other IMFs discussed in this paper. As characteristic uncertainty on the stellar masses, we assume a typical error of 30 per cent.

The stellar mass fraction as a function of redshift is shown in Fig. 4.7. It can be noticed that the stellar mass fraction held in spheroidal galaxies tend to increase at $z < 1$ (Fig. 4.7 A). This growth disappears for the low-intermediate mass galaxies ($M_* < 10^{11}$ $M_\odot$, Fig. 4.7 B), for which the same constant trend found for the number fraction (Fig. 4.2 B) has been retrieved. Considering the massive galaxies (Fig. 4.7 C), it was found that the stellar mass contained in ETGs is constant at $1 < z < 2.5$, while it increases from $\sim 25\%$ to $\sim 50\%$ at $z < 1$, reflecting roughly the number fraction. At $z \sim 0.6$ the fraction of stellar mass locked in the massive spheroidal population is similar to that in massive disc-like and irregular galaxies. Hence, the increase in the mass fraction of ETGs observed at $z < 1$ in the total sample (Fig. 4.7 A) seems to be due to a decrease in the mass locked in massive late-type galaxies, rather than to a real mass increase of massive ETGs. Indeed, looking at Fig. 4.8 the mean stellar mass contained in massive LTGs decreases with decreasing redshift. On the

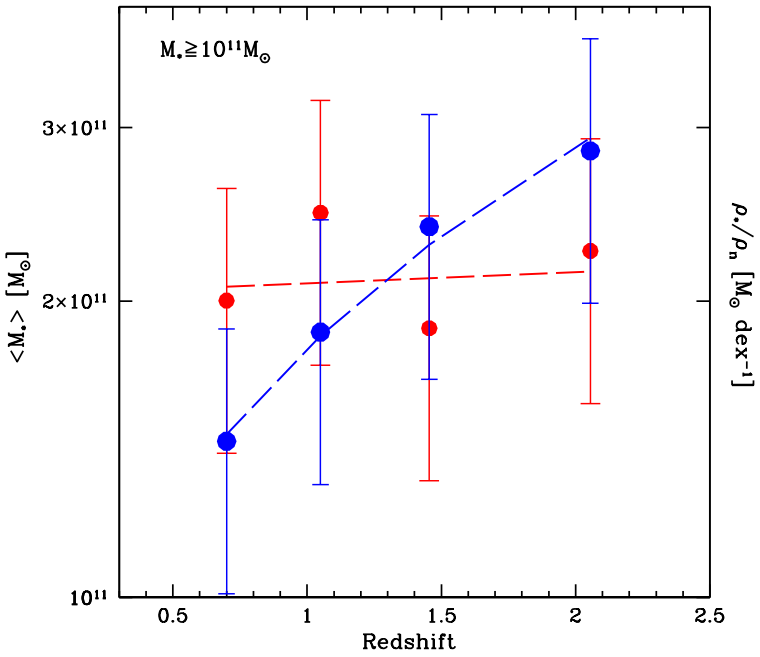

Figure 4.8: Mean stellar mass as a function of redshift for the sample of galaxies more massive than $M_* \geq 10^{11}$ $M_\odot$. Red and blue refer to the morphological classes of early- and late-type galaxies. The dotted lines represent a weighted least squares fit to the points. Errors bars represent the typical uncertainty (30 per cent) we assumed on the stellar masses. The average stellar mass corresponds to the ratio of the stellar mass density and the number density (ρ_*/ρ_n), as indicated in the right label of the y-axis.

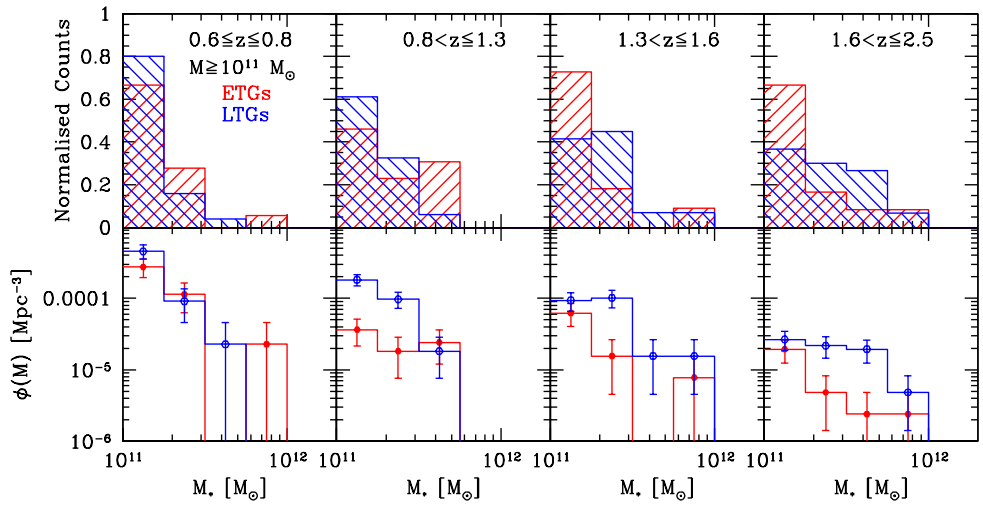

Figure 4.9: Stellar mass (top panels) distributions and mass function distributions (bottom panels) of massive ($M_* \geq 10^{11}$ $M_\odot$) ETGs (red) and massive LTGs (blue). The samples are split in the same redshift intervals adopted in Fig. 4.2 and Fig. 4.7. The binning in stellar mass is not linear, it is performed between $log(\frac{M_*}{M_\odot}) = 11$ and $log(\frac{M_*}{M_\odot}) = 12$ with a step of 0.25.

other hand, the mass contained in the massive ETGs tends on average to be constant with cosmic time. The error bars in Fig. 4.8 represent the typical uncertainty (30 per cent) we assumed on the stellar masses.

In the top row of Fig. 4.9 the normalised stellar mass distributions in four redshift bins for the $M_* \geq 10^{11}$ $M_\odot$ sample are shown. It can be seen that as the redshift decreases the distributions of the late-type populations become more populated at the lower mass-end ($M\sim 10^{11}$ $M_\odot$), while for the massive ETGs the distributions do not change significantly over the redshift range covered by our sample. A similar trend is found in the $\phi(M)$, i.e. the number density of galaxies as a function of the stellar mass (Fig. 4.9 bottom row), that represents the stellar mass function of galaxies more massive than 10^{11} $M_\odot$. The stellar mass function of galaxies $\phi(M)$ in a given redshift bin is defined as,

$$\phi(M)dM = \sum_i \frac{1}{V_i} dM \tag{4.3}$$

where the comoving volume was estimated as in the Eq. 4.2. For the late-type morphology as the redshift decreases it was observed a clear trend to largely populate the low-mass end of the mass function. Furthermore, the LTGs tend to steadily populate the extremely-massive regime at every redshift or even

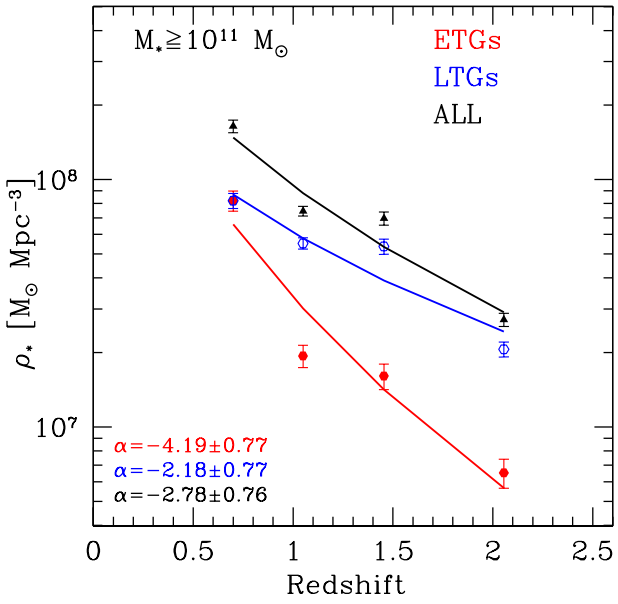

Figure 4.10: Stellar mass density as a function of redshift, split by morphology, and with a mass cut of $M_* \geq 10^{11}$ $M_\odot$. The solid lines illustrate power-law fits of the form $\rho_* = \rho_{*,0} \times (1+z)^{\alpha}$.

to disappear in the highest mass bin at $z < 0.8$. On the other hand, the early-type population (54 ETGs) shows extremely-massive galaxies both at high and at low redshift and the same tendency of LTGs to replenishment the low-mass end distribution. Despite low statistics, the data show that the extremely-massive galaxies ($M_* > 3-4 \times 10^{11}$ $M_\odot$) were already in place at $z \sim 2$ and that their number did not increase substantially, otherwise I should observe some growth at lower redshift as it happens for the less massive galaxies ($10^{11} \leq M_*/M_\odot \leq 3 \times 10^{11}$). Hence the population of extremely massive galaxies formed at $z > 2.5-3$.

If it is real and not due to statistical fluctuation, the lack of new extremely-massive LTGs at $z < 1.3$ seen in Fig. 4.9 could be evidence of a morphological transformation of these galaxies into more massive spheroids. However, the extremely massive LTGs tend to have high values of specific star formation rate and early formation epochs $z_{form} > 5$. Thus, a mechanism capable of shutting off their star formation and of removing the disc so that the morphological transformation occurs, should take place in this hypothesis.

In Fig. 4.10 the comoving stellar mass density as a function of redshift for the two samples of massive ETGs and LTGs is shown (data in Table 4.2). An

overall increase in the mass density was observed, although the evolution for the massive LTGs is more modest compared to the one observed for massive ETGs. Fitting our data with a power law form $\rho_* = \rho_{*,0} \times (1+z)^{\alpha}$, a significant difference between the slope of the ETG and LTG mass density with $\alpha_{ETGs} = -4.01 \pm 0.77$ and $\alpha_{LTGs} = -2.19 \pm 0.77$ was found. This difference is mainly due to the steepening observed for spheroidal galaxies between $z \sim 1$ and $z \sim 0.6$. By comparing the number and the mass density (Fig.4.5 right panel, and, Fig. 4.10) of the massive galaxies from $z \sim 2$ to $z \sim 0.6$, it can be noticed that both the number and the mass density of ETGs increase by an order of magnitude ($\sim 11-12$), in agreement with Brammer et al. (2011). On the contrary, the late-type population increases its number by a factor of ~ 7 while its mass by a factor of ~ 3.5. This implies that the new massive late-type objects are progressively added with smaller masses; indeed, as shown before in Fig. 4.8, the average mass (i.e. the ratio between the mass and number density) of LTGs declines by a factor of 2 since $z \sim 2.5$.

These results are also consistent with the UltraVISTA measurements (Muzzin et al. 2013), that found a general faster growth of the stellar mass density of the quiescent galaxies compared to the star-forming one, with growing factors strictly in agreement with our finding for both the galaxy classes.

4.5 Dating the stellar mass content of massive galaxies

In this section I investigate when the stellar mass content of the massive galaxies formed. Indeed, although the current knowledge of galaxy formation tends to associate to the LTGs a younger stellar component while to the ETGs an older one, dating the age of the stars that form the galaxies is not easy, mainly at high redshift where the stellar populations are unresolved. For what concerns the spheroidal galaxies, it has been proposed that they may host a small fraction of younger stars, accounting for a few percent of galaxy mass at $z \sim 0$, superimposed to an old base population (e.g. Thomas et al. 2010). The presence of two stellar components with different ages clearly emerges from very recent studies conducted on ETGs at $z > 1$, when the Universe was younger than 4.5 Gyr. The comparison of the two age dependent spectral indices H+K(CaII) and D4000 in ETGs at $z \sim 1$ (Lonoce et al. 2014) show the presence of a small mass fraction (< 5 %) significantly younger than the

bulk of the stellar mass. Furthermore, significant colour gradients have been detected in high redshift ($z \sim 1.3$) ETGs (e.g. Gargiulo et al. 2012), probably due to the age variation of the stellar component. Hence, the presence of a young component and its spatial location within ETGs is still debated, and represent another key point to understand the accretion history of the ETGs.

For this reason, I analysed the stellar ages, derived by means of SED fitting process, for the sample of massive galaxies that are spread in a wide redshift range. This can help to have an overall view of the galaxy ages at different epochs.

The epoch t_{form} at which the bulk of the stellar mass was formed, has been estimated for each galaxy with $M_* \geq 10^{11}$ $M_\odot$,

$$t_{form} = Age_{Univ}(z_{gal}) - Age_{star}(z_{gal}), \tag{4.4}$$

where $Age_{Univ}(z_{gal})$ is the age of the Universe at the redshift of the galaxy and $Age_{star}(z_{gal})$ is the mean age of the galaxy stellar population at its redshift.

The age of the stellar population was derived by best fitting the galaxy SED with stellar population synthesis model as described in Sec. 2.3.3 , hence it corresponds to the model age obtained assuming an exponentially declining star formation history. It represents the age of the stars dominating the overall galaxy emission and includes the contribution of stellar remnants.

In the left panels of Fig. 4.11 the normalised distributions of the formation epoch t_{form} for early- (red) and late-type (blue) galaxies in four different redshift bins are shown. It is clearly visible that the formation redshift $z_{form} = z(t_{form})$ of the stellar population of massive galaxies are spread over a wide cosmic time that varies between $z_{form} \sim 1$ and $z_{form} \sim 10$, without a preferred time for the formation of the bulk of the stars. The distributions suggest that the majority of galaxies apparently formed their stars at an epoch decreasing with decreasing redshift, with the bulk of stellar mass produced within a few Gyrs of the observation redshift. This result is not surprising if we consider how the number density of massive galaxies evolves (Fig. 4.5, bottom right). Indeed it has been seen that new massive galaxies are progressively added as redshift decreases, thus only a small fraction of galaxies observed in the lower redshift bins were already assembled at higher redshift. In each redshift bin a tail of galaxies with stellar populations formed at earlier epochs was observed. However, the bulk of the stars in each redshift bin was created when the Universe was a few Gyrs younger than the time at which they were

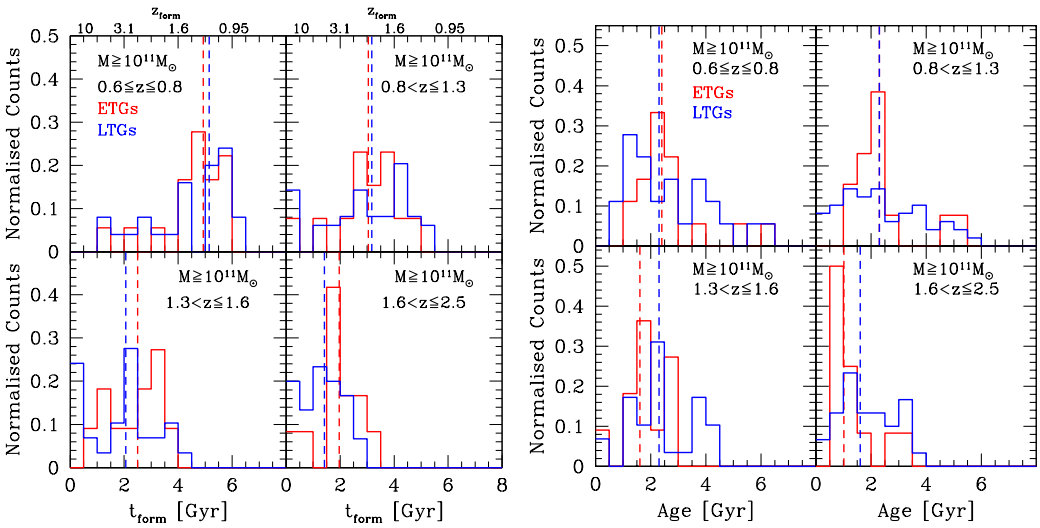

Figure 4.11: Distributions of formation epochs (left panels) and ages (right panel) of the stellar component of massive galaxies ($M_* \geq 10^{11}$ $M_\odot$) split into four redshift bins. Red and blue represent the ETGs and LTGs classes. Dotted vertical lines represent the median values. In the left panels the formation redshift z_{form} ($z_{form} = z(t_{form})$ is indicated on the top x-axis.

observed. In the right panels of Fig. 4.11 the distributions of the mean ages of stars contained in massive galaxies are shown; the same wide spread observed for the formation epochs can be evinced, with median ages of the stellar components of about 2 Gyr for every redshift bin and morphological type.

Summarizing, the galaxy number density grows with decreasing redshift, thus new massive galaxies are formed as the cosmic time passes. Moreover, the age of the stellar component of these galaxies in each redshift bin is generally 1-2 Gyr older than the time at which the galaxies were observed. Thus, the epoch at which stars have been formed and the time at which the galaxy has been assembled could not be temporally distant.

Alternatively massive ETGs, at least some of them, after a primary initial episode of star formation have increased their mass through further star formation events that lower the mean age of the resulting stellar population. Another possibility could be the merging between subunits with a younger stellar population occurred at different times or a star formation feeding by cold streams and minor mergers (Birnboim & Dekel 2003, Kereš et al. 2005, Ceverino et al. 2012) that still shift the formation epoch to a more recent time.

I emphasize that for the age of the stellar populations of our galaxies, the

mean age of the best fitting model was used. This averaged age cannot keep track of the presence of a more complex composition of the stellar populations inside the galaxies. For instance, Lonoce et al. (2014) through the analysis of spectroscopic indices of a sample of 15 ETGs at $0.7 < z < 1.1$ have found that the main component ages tend to be older than the ages derived by the standard SED fitting.

As known, the optical blue and UV ranges of a galaxy SED are typically dominated by very luminous young stellar populations even when they represent a small percentage of the total stellar content of the galaxies. Since our sample covers the range from z=0.6 to z=2.5, at low redshift we do not have the same good sampling of the far-UV wavelengths (rest frame) as happens for higher redshift. Thus, the ages measured in the range z=0.6-0.8 are affected by a poor SED coverage in the far-UV range. With the aim to asses the dependence of age estimates on the rest-frame wavelength coverage, the SED-fitting process was repeated to ensure that all the galaxies had the same rest frame photometric coverage. A new SED-fitting was performed, eliminating from the fitting process those filters bluer than the outermost UV_{rest} filter at z=0.6 ($\lambda_{r.f.} \sim 2250$ $\mathring{A}$). I found that shortening the UV_{rest} coverage implies slightly younger ages. Therefore, if we had in the bin $z = 0.6 - 0.8$ all the coverage available at higher redshift we would probably have obtained even younger ages. This result guarantees that the recent formation epochs found for the bulk of the stellar populations at $0.6 \leq z \leq 0.8$ are not due to the filter choice and that the found behaviour would not change with different wavelength coverage.

4.6 Variation of the ages and star-formation time-scales with stellar mass

In the previous section we have seen how the mean age of the galaxy stellar components evolves as a function of redshift for the different morphological classes. Here, we probe the possible dependence of the age and of the SF time-scale on the stellar mass of the galaxies, and if this dependence is influenced by the galaxy morphology.

Since our sample of galaxies is spread over a wide redshift interval, we considered galaxies in two narrow redshift bin to minimize the evolutionary effects within each bin. The chosen redshift intervals are $0.6 \leq z \leq 0.8$ and

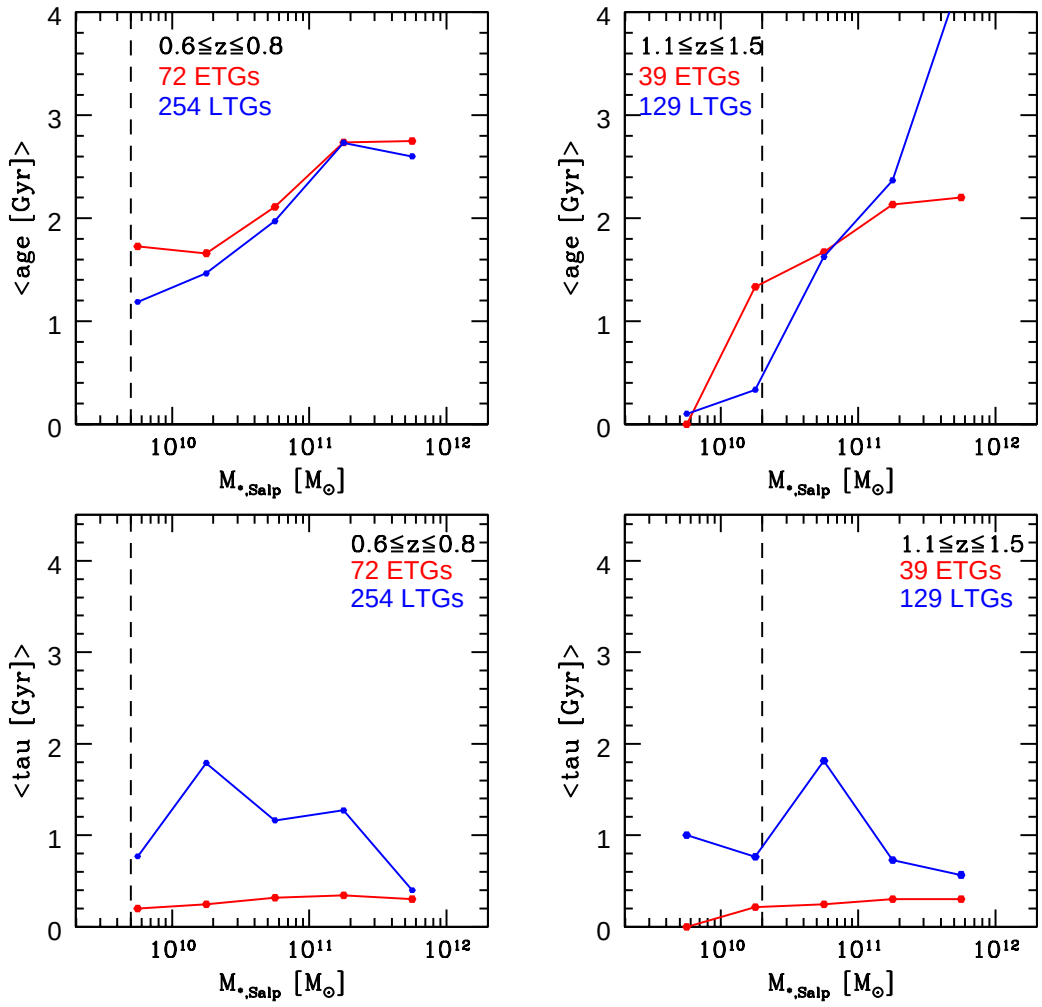

Figure 4.12: *Top:* mean age as a function of the galaxy stellar mass for ETGs and LTGs. *Bottom:* star formation time-scale as a function of the galaxy stellar mass. The dotted vertical lines represent the limit in mass completeness: $M_* > 5\times10^9$ $M_\odot$ for the interval $0.6 \leq z \leq 0.8$ and, $M_* > 2\times10^{10}$ $M_\odot$ for the interval $1.1 \leq z \leq 1.5$.

$1.1 \leq z \leq 1.5$, that both enclose about 1 Gyr of cosmic time.

In the top panels of Fig. 4.12 the evolution of the mean age with stellar mass in the two redshift bins is shown. The dotted vertical lines represent the limit in mass completeness: $M_* > 5 \times 10^9$ $M_\odot$ for the interval $0.6 \leq z \leq 0.8$ and, $M_* > 2 \times 10^{10}$ $M_\odot$ for the interval $1.1 \leq z \leq 1.5$.

From Fig. 4.12 (top panels), it is clearly visible the increasing of the mean age as the mass grows for both the morphological classes. This means that galaxies with greater mass have stellar population older than their counterpart with lower mass. This evolution reproduces the expectation of the downsizing scenario (Sec. 1.3, Cowie et al. 1996), where the more massive galaxies are the

first to form stars and populate the galaxy mass function. Hence, the galaxies have a mass-dependent assembly history, with most massive systems ending their SF and their assembly first and, less massive systems that have prolonged SF extended to later epochs.

In the bottom panels of Fig. 4.12, the evolution of the star formation time-scale, τ, as a function of the stellar mass (derived with a Salpeter IMF) is shown. The same redshift ranges adopted for the mean ages are used. In each redshift bin, the SF time-scales of the ETGs are relatively short whatever the galaxy mass. Indeed they are included in a small range of $0.2 \leq \tau \leq 1$ Gyr. The constant trend of the τ_{ETG} in the entire mass range is a direct indication of the uniformity of the stellar component of spheroidal galaxies. The same constant trend is not verified for the late-type galaxies that have values of τ more scattered as a function of the stellar mass. However, the LTGs have on average longer SF time-scale ($\tau > 1$ Gyr) compared to the ETGs, in agreement with the downsizing scenario discussed above.

Thus, selecting ETGs and LTGs on the basis of their morphology, instead of using model-dependent methods (e.g. sSFR) or methods based on stellar population properties (e.g. colours), I found that the star formation time-scales of the two morphological classes are different. Indeed, the star formation time scales of the two galaxy types never overlap, testifying the differences in terms of average stellar properties of ETGs and LTGs.

From the top panels of Fig. 4.12 it can be also noticed that at $0.6 \leq z \leq 0.8$ the mean ages of the spheroids are almost comparable with the disc-shaped ones, confirming that at low redshift the stellar populations of ETG and LTG are almost coeval, independently on the galaxy mass. At higher redshift the trend is less sharp, with higher stellar ages for low mass ETGs compared to low mass LTGs, and with an opposite trend at greater masses. Probably, the low mass ETGs at redshift $1.1 \leq z \leq 1.5$ have aged stellar population with respect to the less massive LTGs that could have still ongoing star formation.

Chapter 5

Probing the possible variation of the stellar initial mass function

In this chapter I present an analysis aimed at investigating whether any significant variation of the relative number of low-to-high mass stars in galaxies occurred in the last 9 Gyr, i.e. whether the IMF has changed across the time.

The IMF is the mass distribution of a stellar generation at birth and provides the relative number of different mass stars in a burst of star formation. This relative number is one of the main ingredients determining the properties of the stellar population, i.e. its SED, mass-to-light ratio, chemical enrichment and how these properties change with time. It follows that any variation of the relative abundance of low-to-high mass stars would drastically modify the basic properties of a galaxy and its evolution.

Our knowledge of the IMF is based on the relative abundance of stars observed in the solar neighbourhood and on the properties observed in local galaxies, from which the IMF is described by one (Salpeter 1955) or two declining power laws (e.g. Kroupa 2001, Chabrier 2003) with slope $s \simeq 2.35$ for $M \gtrsim 1$ $M_{\odot}$ and flatter slope for lower masses.

Efforts to model the formation and evolution of galaxies have generally assumed that the IMF is an universal function, that does not vary with time, but it has long been recognized that the predictions of such models would be importantly altered if the IMF would vary. The implicit assumption is that the relative number of low-to-high mass stars has been always and anywhere the same, at any epoch.

Nonetheless, theoretical arguments spread doubts on IMF universality (for a complete review see Bastian et al. 2010, Kroupa et al. 2013). Indeed there are theoretical evidences that the mass spectrum of the stars formed in a burst

of star formation is deeply connected with the physical properties of the gas cloud in which these stars originated (Padoan & Nordlund 2002, Hennebelle & Chabrier 2008, Hopkins 2013), fact that rise doubts about the validity of the current IMF universality assumption. Moreover, observational studies of spectral features, known to be sensitive to the presence of low-mass stars (e.g. the Na I doublet and the Ca II triplet) in massive ETGs, found that these features vary with ETG velocity dispersion and Mg/Fe ratio in the direction of progressively bottom-heavier IMF with the increase of these two parameters (Conroy & van Dokkum 2012, Spiniello et al. 2012, Ferreras et al. 2013, La Barbera et al. 2013). Furthermore, the validity of the local IMF also at high redshift does not seem a robust assumption, due to the unknown long mass assembly history of local galaxies, and also because several studies suggested at high-z an IMF more dominated by massive stars, contrary to the local IMF, since the first stars are expected to contain no heavy elements (e.g. Abel et al. 2002, Bromm et al. 2002).

To tackle the issue of a possible variation of the IMF, I define a method to constrain the IMF which pass trough the comparison between the observed properties of galaxies in a wide redshift range ($0.1 \lesssim z \lesssim 2.5$), and a suited set of stellar population models able to reproduce the observed SED (15 photometric points, 0.35-24 μm) of galaxies for different proportion of low-to-high mass stars, according to an IMF analytically described by a power law form. The galaxies were selected according to the same criteria in the entire redshift interval and were characterized by the same set of observations, that allow to perform the same comparison between observations and models both at high-z and low-z. Furthermore, the power law form is the most simple and direct functional form, that allows to straightforwardly probe if any variation of the relative number of low-to-high mass stars occurs.

5.1 The best fitting IMF in the K22 sample

To each galaxy of the K22 sample (Sec. 2.2) I associated the best IMF (IMF_{BEST}), defined as the IMF associated to the best-fitting with the lowest χ^2_ν (hereinafter $\chi^2_{\nu;BEST}$), among the fitting obtained with the five power-law IMF (Sec. 2.3.2). In this way, each galaxy has its best fitting IMF and, the relative values of stellar mass, age of the stellar population, star-formation time-scale derived from the SED fitting.

However, the $\chi^2_{\nu;BEST}$ could be statistically indistinguishable from the other χ^2_ν derived by adopting other IMFs. For this reason, I checked if each galaxy would have a range of stellar initial mass functions that are statistically indifferent compared with the best IMF. This estimate has been done by calculating, with the statistic F-test, the probability that the χ^2_ν are different, fixing a probability threshold at 1-σ level. The results of this analysis have shown that:

- $\sim$ 3 % of the galaxies in the K22 sample have a unique IMF$_{BEST}$, significantly different from those obtained with the other IMFs;
- $\sim$ 27 % of the galaxies have an IMF$_{BEST}$ statistically indistinguishable from the other IMFs; namely for these galaxies all the five power-law IMF are statistically considerable;
- $\sim$ 70 % of the galaxies reject at least one of the five IMFs and accept the others. In particular, the galaxies best-fitted with one of the bottom-heavier IMF (i.e. $2.5 < s < 3.5$) generally allow the other IMFs in the range $s = 2.5 - 3.5$. Instead, the galaxies best-fitted with the IMF$_{1.5}$ or the IMF$_{2.0}$ usually cannot accept the extremely IMF$_{3.5}$.

From these results it follows that, for the bulk ($\sim$ 70 %) of the galaxies in the K22 sample, the SED can be reproduced by at least more than one IMF with slope close to the IMF$_{BEST}$.

Up to now, many works in the literature adopt as stellar IMF to reproduce most observable properties of the stellar populations, the Salpeter one (Salpeter 1955), described by a declining power-law with slope $s = 2.35$. For this reason, I verified whether the Salpeter IMF, even if does not represent the IMF$_{BEST}$, can be adopted to reproduce the SED of the galaxies in the K22 sample. From the comparison, through the F-test, between the χ^2_ν derived with the Salpeter and the best IMF of each galaxy, it has been found that the Salpeter IMF produces a good fitting for the $\sim$ 85 % of the sample with respect to the IMF$_{BEST}$, even though, the mean index of the IMF$_{BEST}$ is steeper than the Salpeter one (s=2.35) as shown in Fig. 5.1 (black line). This would suggest that, these galaxies have on average a greater abundance of low mass stars independently of redshift. On the other hand, the 15 % of the galaxies that statistically reject the Salpeter IMF (blue line in Fig. 5.1), have at $z < 1$ a higher mean index (i.e. their observed SED is best reproduced

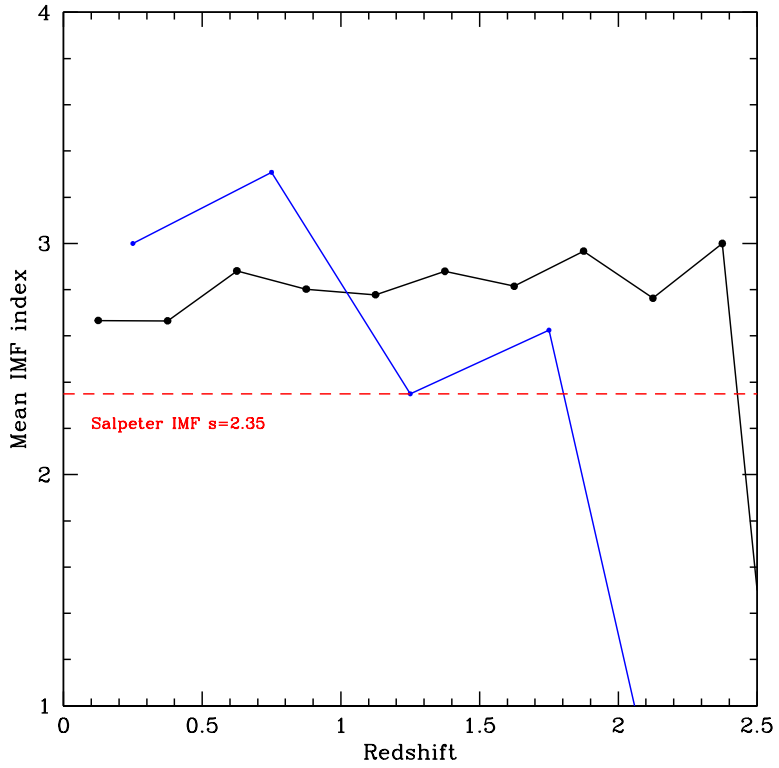

Figure 5.1: Evolution with redshift of the mean IMF index for galaxies whose best IMF is statistically indistinguishable from a Salpeter IMF (black) and for galaxies that statistically reject the Salpeter IMF compared to their IMF$_{BEST}$ (blue).

adopting the bottom-heaviest IMF), while at $z > 1$ have a lower mean index, i.e. they are well reproduced by IMFs with a greater abundance of high mass stars.

To investigate the possible variation of the relative abundance of low-to-high mass stars, according to the distribution of the $\chi^2_{\nu;BEST}$ shown in Fig. 5.2, I selected the 90 % of the galaxies with lower $\chi^2_{\nu;BEST}$. The selection resulted in a sample of 1170 galaxies of which 215 (18.4 %) are ETGs and 955 (81.6 %) are LTGs, with $\chi^2_{\nu;BEST} < 5.6$ and a median value $\chi^2_{\nu;BEST} \sim 1.5$.

I used this sample to estimate the frequency of best fitting for each IMF and to probe whether a tendency of a morphological class to prefer a particular IMF exists. In Table 5.1 the number of galaxies with their best fitting IMF are reported. It can be seen that there is a clear trend to favour stellar initial mass functions with a greater abundance of low-mass stars compared to the flatter IMF, indeed the $\sim$ 85 % of the sample is best-fitted by an IMF with slope $2.5 \leq s \leq 3.5$. This trend is valid for both the two morphological

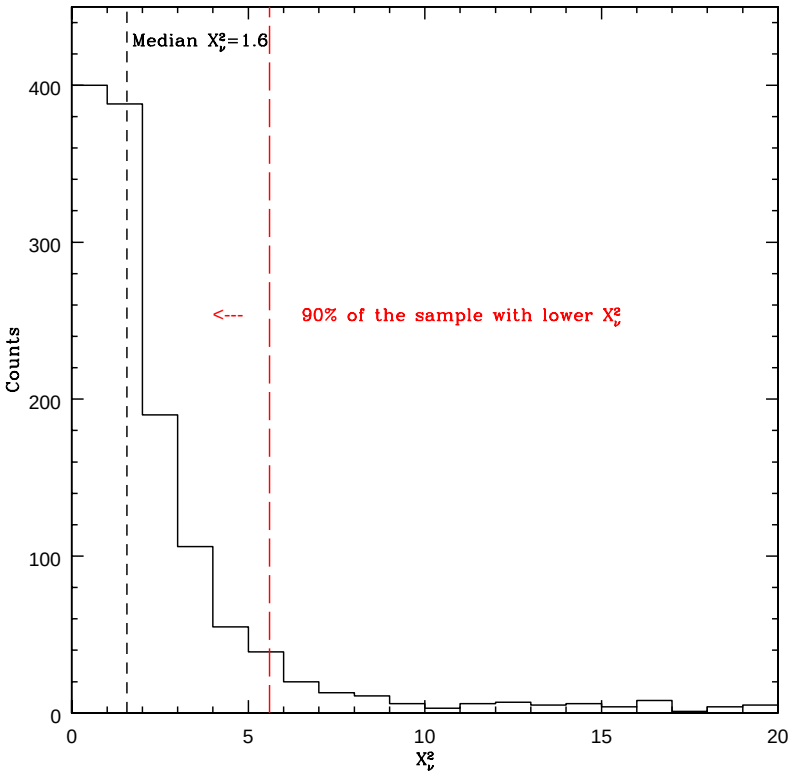

Figure 5.2: Chi squared distribution of the galaxy sample selected adopting for each galaxy its best-fitting IMF. The red vertical line indicates the selection of the 90 % of the sample with lower $\chi^2_{\nu;BEST}$. The black vertical line shows the median value of the distribution, $\chi^2_{\nu;BEST} \sim 1.5$.

Best IMF	N_{gal}	N_{ETGs}	N_{LTGs}
$IMF_{1.5}$	82 (7.0 %)	39 (47.6 %)	43 (52.4 %)
$IMF_{2.0}$	90 (7.7 %)	33 (36.7 %)	57 (63.3 %)
$IMF_{2.5}$	271 (23.2 %)	29 (10.7 %)	242 (89.3 %)
$IMF_{3.0}$	358 (30.6 %)	34 (9.5 %)	324 (90.5 %)
$IMF_{3.5}$	369 (31.5 %)	80 (21.7 %)	289 (78.5 %)

Table 5.1: Number of galaxies best-fitted with different IMF slope ($1.5 < s < 3.5$) and relative morphological content.

classes, with ETGs mainly best-fitted by the bottom-heaviest IMF ($IMF_{3.5}$, 80 ETGs), and LTGs that have a great incidence of IMF with slope between $s = 2.5$ and $s = 3.5$. Hence, an high percentage of galaxy, independently of their morphology, prefers an IMF with a great abundance of low mass stars with respect to the high mass stars.

5.2 Probing the variation of the IMF with redshift

As discussed in the introduction, our knowledge of the IMF is based on the relative abundance of stars of different mass observed in the solar neighbourhood and on the properties observed in the local galaxies. However, galaxies in the local Universe have behind 13 Gyr to form and assemble their stellar content, and their stars can be formed through subsequent episodes of star formation and/or merging. Moreover, galaxies formed at earlier epochs may have a different distribution of stars with respect to galaxies formed later, and many mechanisms may affect the resulting stellar mass function, changing the relative fraction of low-to-high mass stars. For these reasons, adopting an universal IMF, is an extremely strong assumption.

With the aim to investigate this issue, I studied the evolution of the best IMF of the K22 sample as a function of redshift. The fraction of galaxies with their different IMF_{BEST} as a function of redshift is shown in the left panels of Fig. 5.3, for the total sample of 1170 galaxies (top panel), the sample of 215 ETGs (central panel) and the sample of 955 LTGs (bottom panel). From these figures it can be noticed a similar trend in the evolution of the total sample and of the LTGs due to fact that the two samples have in common more than the 80 % of the galaxies. In these two samples it is visible a clear trend of the bottom-heavier IMFs to dominate the whole redshift range from $z = 0.5$ up to $z = 2.5$, conversely the $IMF_{1.5}$ and $IMF_{2.0}$ have negligible fraction of less than 10 per cent over the entire redshift interval. Thus, the SEDs of late-type galaxies are well reproduced adopting IMFs with an equal or greater abundance of low mass stars with respect to a Salpeter IMF and, this behaviour has no dependence on the redshift.

On the other hand, the early-type galaxies for $z < 0.5$ are best fitted by IMFs with slope $2.0 \leq s \leq 3.0$, while from $z > 0.5$ the IMF with the highest percentage of low mass stars ($s = 3.5$) has the highest probability to reproduce the ETG SED (40-50 % of the ETGs at $0.5 < z < 2.5$). In the same redshift

range ($0.5 < z < 2.5$) the LTGs have a lower percentage of galaxy with an high abundance of low-mass stars ($\mathrm{IMF}_{3.5}$), but a greater incidence of galaxies with $\mathrm{IMF}_{2.0}$ and $\mathrm{IMF}_{2.5}$.

To allow a more homogeneous description of the variation of the low-to-high mass stars ratio as a function of redshift, in the right panels of Fig. 5.3 were reported the average IMF_{BEST} index in bin of redshift. For each redshift bin the average IMF_{BEST} index was calculated as $< s >= \sum_{i=1}^{N} s_{best,i}/N$. Looking at the central and bottom panels, it can be noticed that the mean index of the ETGs and LTGs does not present strong variation with redshift, in particular a constant trend to prefer IMFs with a greater abundance of low mass stars ($2.7 \lesssim \bar{s} \lesssim 3.2$) is found in the almost 10 Gyr of time covered by the galaxies in the sample.

These results point to favour a scenario in which the main event of star formation is dominated by low-mass stars ($M < 1$ $\mathrm{M}_{\odot}$) at every redshift. Hence, also at high redshift the ratio between low and high mass stars is strongly skewed toward the low mass stars. This founding should be reconciled with the knowledge derived from the theory of the stellar evolution, in which the early Universe has to be populated by a sufficient number of high-mass stars ($M > 8$ $\mathrm{M}_{\odot}$), necessary to provide the rate of supernovae explosions, that caused the observed metal enrichment of the Universe in the different cosmic epochs (Abel et al. 2002, Bromm et al. 2002). Moreover, on average, the expected IMF should explain the observed galaxy masses, hence the ratio between low and high mass stars should be consistent with the measurements of the galaxy stellar mass.

A further consideration concerns the spectro-photometric models, that may suffer from incomplete spectral libraries (especially for low mass stars, high metallicity and non solar abundance ratios), as well as poorly calibrated mass loss in advanced stellar stages, such as the asymptotic giant branch (AGB, Maraston 2005, Renzini 2006, Maraston et al. 2006). These deficit in the models can be reflected in reproducing the stellar emission of low mass stars ($M < 0.5$ $\mathrm{M}_{\odot}$). It follows that our result of an IMF_{BEST} with a great fraction of low mass stars at any redshift, can be influenced by the uncertainties of the models in the description of the stars that mainly contribute to the steeper IMF.

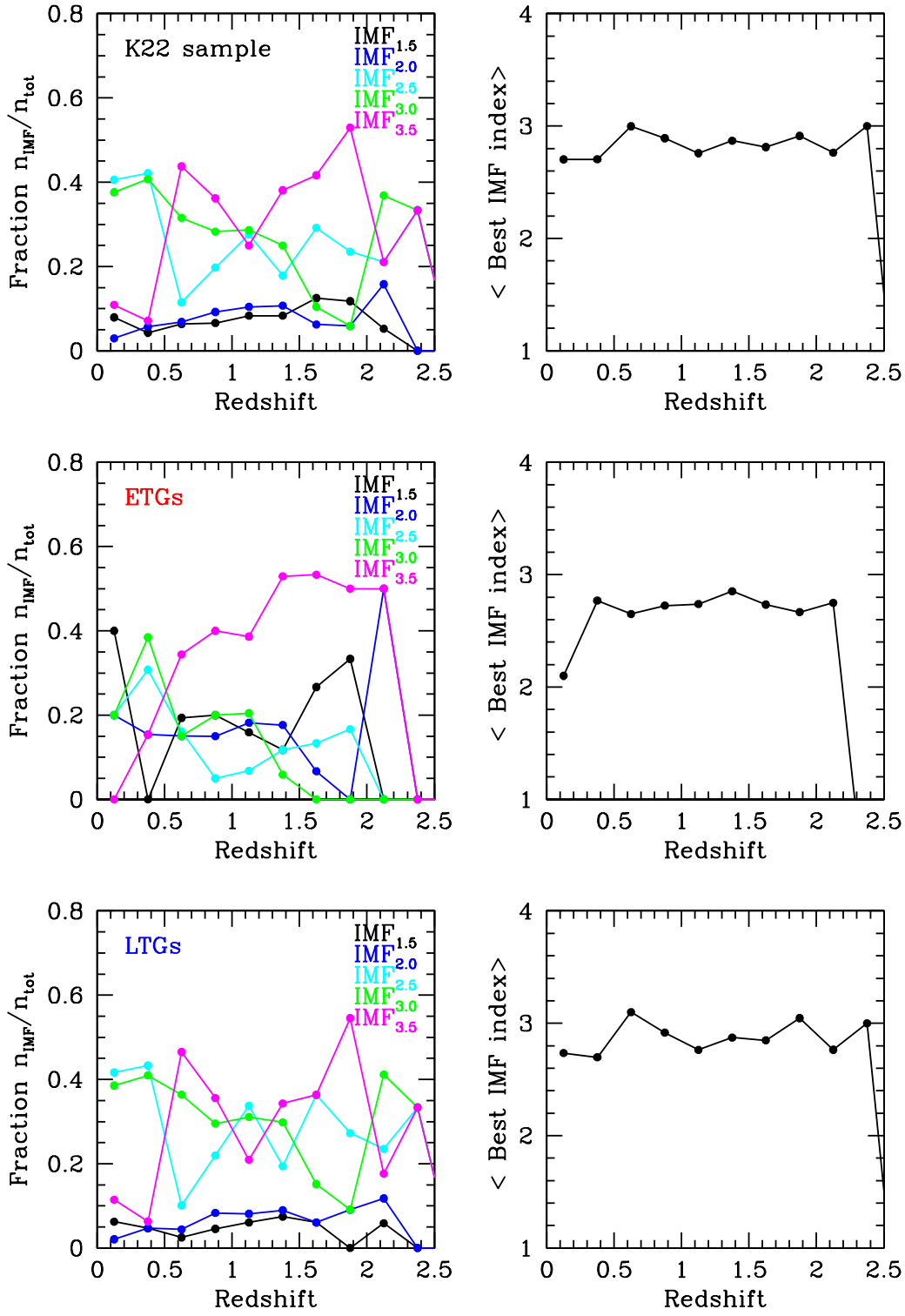

Figure 5.3: Evolution of the IMF_{BEST} fraction as a function of redshift (left) and of the average IMF index (right, $< s >= \sum_{i=1}^{N} s_{best,i}/N$) for the whole K22 sample (top), ETGs (central) and LTGs (bottom).

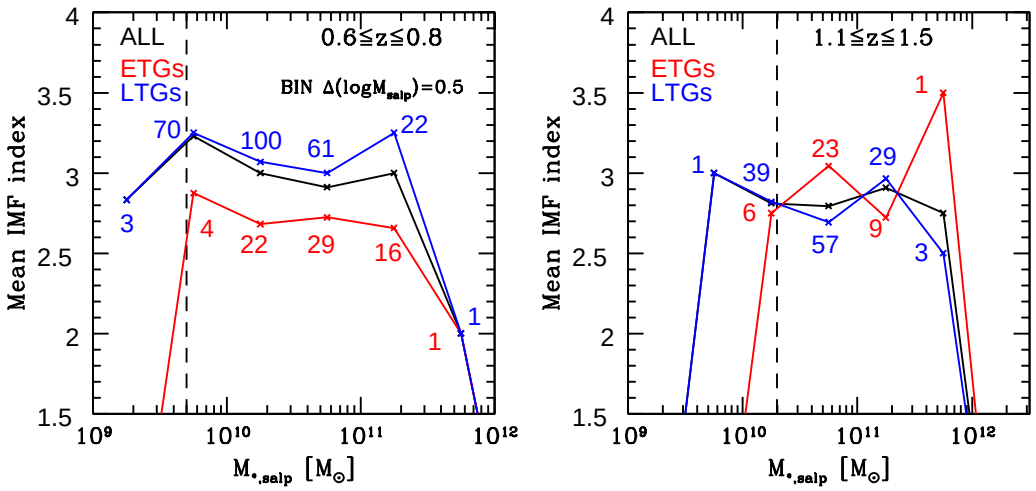

Figure 5.4: Mean IMF index as a function of the galaxy stellar mass, derived adopting the Salpeter IMF in the models. The left and right panels refer to the two redshift intervals $0.6 \leq z \leq 0.8$ and $1.1 \leq z \leq 1.5$. The vertical dotted lines represent the limit in mass completeness: $M_* > 5 \times 10^9$ $M_\odot$ for the interval $0.6 \leq z \leq 0.8$ and, $M_* > 2 \times 10^{10}$ $M_\odot$ for the interval $1.1 \leq z \leq 1.5$.

5.3 Variation of the relative abundance of low-to-high mass stars as a function of the stellar mass

In this section it will be analysed if there is a dependence with the galaxy stellar mass in preferring a particular IMF, since galaxies with different mass could have had a different histories of star formation that could have influenced their IMF. To this aim, two narrow redshift bins were selected to eliminate the possible redshift evolution, since the galaxy sample is spread over a wide redshift range. The chosen redshift intervals are $0.6 \leq z \leq 0.8$ and $1.1 \leq z \leq 1.5$, that both enclose about 1 Gyr of cosmic time. The possible IMF variation with the galaxy mass were investigated analysing the variation of the mean IMF index as a function of M_*. The stellar masses derived assuming a Salpeter IMF were adopted, to break the degeneracies between the best mean index and the stellar mass, otherwise the galaxies would have different M_* each derived with its best fitting IMF. The results, presented in Fig. 5.4, show that the average index of best-fitting is approximately constant on the whole stellar mass range, independently on the galaxy morphology. In particular the galaxies in each mass interval have a relative abundance of low-mass stars higher than that associated to a Salpeter IMF. In the left panel of Fig. 5.4, it

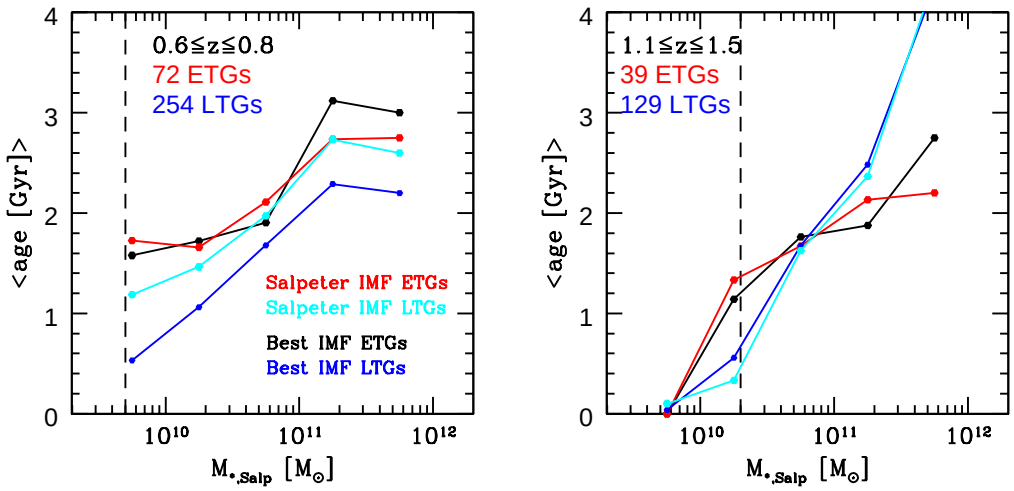

Figure 5.5: Mean age as a function of the galaxy stellar mass; the latter is derived adopting the Salpeter IMF in the models. The ages are derived both with the best-fitting IMF (blue and black lines) and assuming a Salpeter IMF (red and cyan lines). The left and right panels refer to the two redshift intervals $0.6 \leq z \leq 0.8$ and $1.1 \leq z \leq 1.5$. The vertical dotted lines represent the limit in mass completeness: $M_* > 5 \times 10^9$ $M_\odot$ for the interval $0.6 \leq z \leq 0.8$ and, $M_* > 2 \times 10^{10}$ $M_\odot$ for the interval $1.1 \leq z \leq 1.5$.

can be seen that the mean index of the ETGs, although have a constant trend with mass, represents on average an IMF with a lower relative abundance of low-mass stars compared to the LTGs and to the ETGs in the higher redshift bin. This trend is due to the selected redshift range, $0.6 \leq z \leq 0.8$, that presents a slightly deceases on the average IMF index for the ETGs, as can be noticed in the bottom-right panel of Fig. 5.3. In conclusion, no particular indication on the variation of the relative abundance of low and high mass stars, has been found as a function of the stellar mass of the galaxies.

Let's see now the dependence of the age of the stellar population (t) and of the SF time-scale (τ) on the IMF.

To this end, I investigated how the t and τ, derived from the SED fitting, vary adopting a fixed Salpeter IMF or using for each galaxy its best IMF. In Fig. 5.5 the mean ages of the stellar component as a function of the masses derived with a Salpeter IMF are shown. In both the analysed redshift intervals, the ages derived with the IMF$_{BEST}$ do not present strong differences compared to the ages derived with the Salpeter IMFs. This trend is retrieved independently from the mass, the morphology and, the redshift of the galaxies. Hence, keeping free the IMF to change no clear differences are detected with

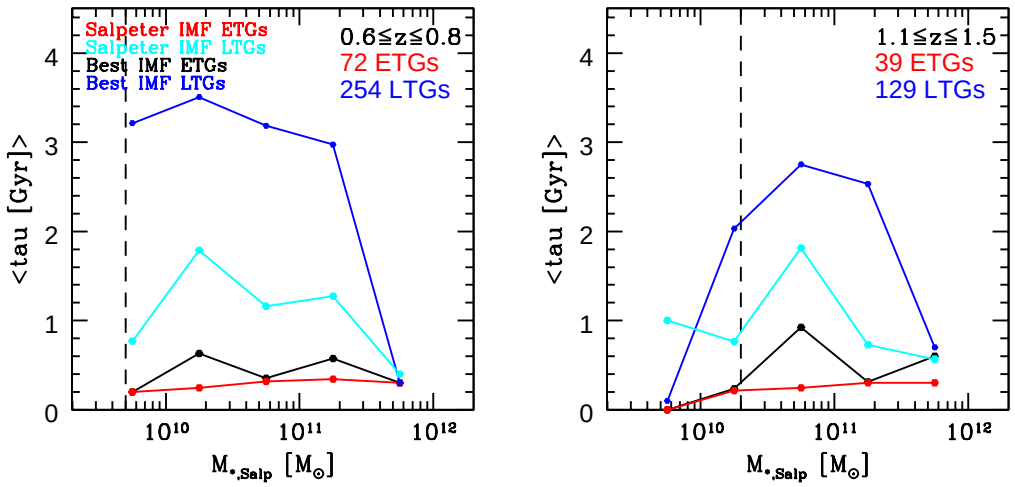

Figure 5.6: Star formation time-scale as a function of the galaxy stellar mass; the latter is derived adopting the Salpeter IMF in the models. The τ are derived both with the best-fitting IMF (blue and black lines) and assuming a Salpeter IMF (red and cyan lines). The left and right panels refer to the two redshift intervals $0.6 \leq z \leq 0.8$ and $1.1 \leq z \leq 1.5$. The vertical dotted lines represent the limit in mass completeness: $M_* > 5 \times 10^9$ $M_\odot$ for the interval $0.6 \leq z \leq 0.8$ and, $M_* > 2 \times 10^{10}$ $M_\odot$ for the interval $1.1 \leq z \leq 1.5$.

respect to fixing the Salpeter IMF, in the derived ages of the stellar component. Furthermore, in Fig. 5.5, the same trend observed in Sec. 4.6 is found also with variable IMFs: namely, the galaxies with greater mass have stellar population older than the galaxies with lower mass both for ETGs and LTGs (*downsizing scenario*).

For what concerns the star formation time-scale τ, the Fig. 5.6 shows its dependence as a function of the stellar mass derived with a Salpeter IMF in the same redshift ranges adopted above for the description of the age. For the spheroidal population, the values of τ derived assuming the Salpeter IMF (red line) or the IMF$_{BEST}$ (black line) are very similar, indicating that the mean properties of their stellar population are very uniform. The same trend is not verified for the late-type galaxies that present a large scatter between the τ estimated with the fixed or the variable IMFs, with τ_{Salp} always smaller than the τ_{BEST}. In Fig. 5.7 the SF time-scale for late and early type galaxies is shown as a function of redshift. The trends observed in the above analysis are also present over the whole redshift range: short time scales for the ETGs, longer and non uniform time scales for LTGs, depending on the adopted IMF.

Summarizing, no significant differences in the estimation of the physical

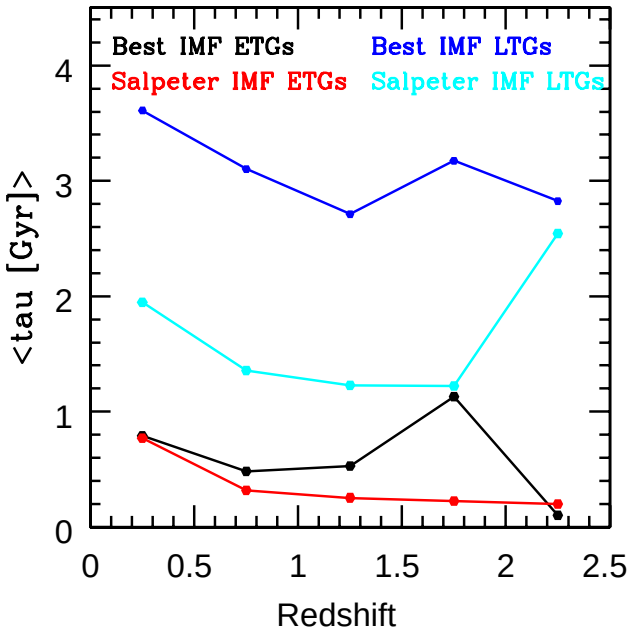

Figure 5.7: Star formation time-scale as a function of redshift. The τ are derived both with the best-fitting IMF (blue and black lines) and assuming a Salpeter IMF (red and cyan lines).

parameters of the spheroidal population are produced with different IMFs. Conversely, the properties of the late-type population seem more affected by the choice of the IMF, testifying that the stellar content of the LTGs is more heterogeneous with respect to the uniform stellar population contained in ETGs.

5.4 Constraining the IMF through observable properties

Until now, I studied the influence of the possible IMF variation as a function of the redshift and of the galaxy stellar mass, and I investigated how the physical parameters are affected by the IMF choice. However, both age, mass and SF time-scale are derived, at different redshift, by comparing observations with stellar population synthesis models strictly dependent on IMF. Hence, an intrinsic degeneracy exists between the IMF and the derived properties of a stellar population.

The only observable that we have in hand, not depending on any assumption or models, is the flux of the galaxies, measured in different bands and, consequently, the galaxy colours. For this reason, a colour-colour diagram was adopted to investigate if the abundance of low-to-high mass stars changes

with the colour of the galaxies. Indeed, the galaxy colours depend on the stellar populations present in the galaxies, each of them contributes in a different way to the galaxy emission at different wavelengths. Hence, the connection between the galaxy colours and the stellar component can provide indication on the possible IMF variation.

For this goal, the rest-frame U-V versus rest frame V-J colours, already adopted in Sec. 3.5, were used. The K22 sample was divided into five different redshift bins and, the galaxies were separated by means of their morphological classification. Then, to each galaxy was associated its best-fitting IMF, each with a different colours.

The resulted UVJ diagrams are shown in Fig. 5.8, for the ETG (top panels) and the LTG (bottom panels) populations. The different best IMFs were indicated with points with different colours. From the analysis of these plots no particular indication that connect the stellar component to a specific IMF seems to appear. The spheroidal galaxies, that occupy the redder region of the UVJ plane, have IMFs distributed without a particular trend in the planes at each redshift. However, a tendency of the flatter IMF ($s = 1.5$, $s = 2.0$, $s = 2.5$, black, blue and, cyan points, respectively) to populate the region with higher $(\text{U-V})_{rest}$ colours seems to appear. This means that the SEDs of the spheroidal galaxies with redder $(\text{U-V})_{rest}$ colours are well reproduced by an IMF with a higher relative fraction of high mass stars (represented by the $\text{IMF}_{1.5}$) up to $z \sim 1.5$. At higher redshift the trend is not present anymore, both for the low statistics and for the colour spread existing at high redshift, consequence of the gradual approaching to the time at which galaxies have quenched their star formation (see Sec. 3.5). The same tendency in preferring an IMF with a great fraction of high mass stars is not retrieved for the LTG population. Indeed, the UVJ diagrams of the LTGs are more spread than those of ETGs, with all the IMFs that occupy the entire plane. Hence, for this population it is not possible to connect the properties of a very heterogeneous stellar component to the initial mass function.

Another tool to describe the galaxy evolution trough physical parameters not coming from the SED fitting is the size-luminosity (SL) relation, that describes the dependence of the characteristic size of galaxies on their luminosity. The SL relation was estimated for the sample of early-type galaxies at $0.5 \lesssim z \lesssim 2.5$, for which were measured the R-band absolute

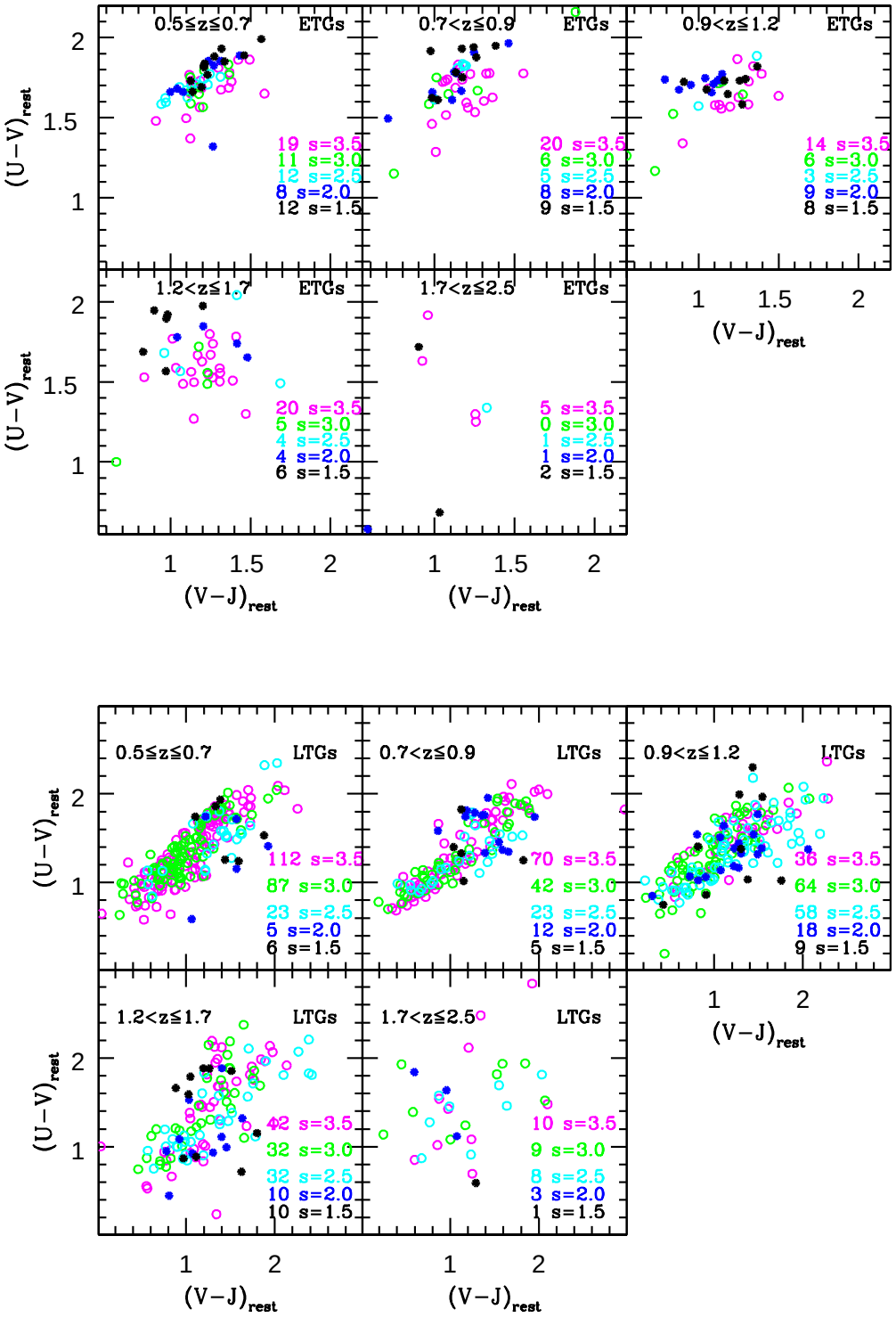

Figure 5.8: Rest frame colour-colour diagrams in different redshift bins for ETGs (top panels) and LTGs (bottom panel). The different colours in the figures refer to the different slope of the best fitting IMF associated to the galaxies: magenta for $IMF_{3.5}$, green for $IMF_{3.0}$, cyan for $IMF_{2.5}$, blue for $IMF_{2.0}$ and, black for $IMF_{1.5}$. The numbers of galaxies with the different IMFs are reported in the figures.

magnitudes M_R, and the effective radii, R_e, calculated through the fitting of the light profiles (see Sec.2.3.1). The resulted size-luminosity relation, for the population of spheroidal galaxies in different redshift bins, is shown in Fig. 5.9, where to each galaxy is associated its best fitting IMF with a different colour.

It can be seen that, for lower redshift bins the galaxies have progressively lower magnitudes. On the one hand, this effect is due to the passive evolution of the galaxy luminosity as the redshift decreases. Indeed, as the time passes, the stellar population becomes progressively older, and as consequence the galaxy luminosity changes. On the other hand, as shown in Sec. 4.1, the fainter galaxies are progressively lost for increasing redshift due to the mass selection function. Hence, in Fig. 5.9 the fainter magnitudes are more populated at lower redshift intervals due to the effects of the passive luminosity evolution and of the mass selection function.

Keep in mind these effects, the aim of this analysis is to investigate if in each redshift bin the brighter and bigger galaxies prefer a particular IMF compared to the fainter and smaller galaxies; since their different properties can testify different formation histories, that may have influenced also the IMF. From Fig. 5.9 it is clearly evident that no clear trend in the SL is observed for different IMFs, since the different colours reproducing the various IMF are spread in the same random way along the plane. Namely, the ETGs are distributed in the size-luminosity plane without a dependence on their abundance of low-to-high mass stars.

This result does not necessarily means that the luminosity of a galaxy does not depend on its IMF, but the current synthesis population models, that reproduce the observed SED for different high-to-low mass stars ratios, could not be enough detailed to provide this information (Sec. 5.2). On the other hand, a variation of the IMF must not be necessarily connected to the luminosity of the galaxy but can be linked to other physical properties.

New preliminary studies tried to constrain the IMF in massive ETGs at different redshift using asymmetric dynamical models that connect the IMF variation to the galaxy velocity dispersion (Shetty & Cappellari 2014, Gargiulo et al. 2014). These pioneering studies suggest a variation of the IMF even if the main driver of the variation is unclear.

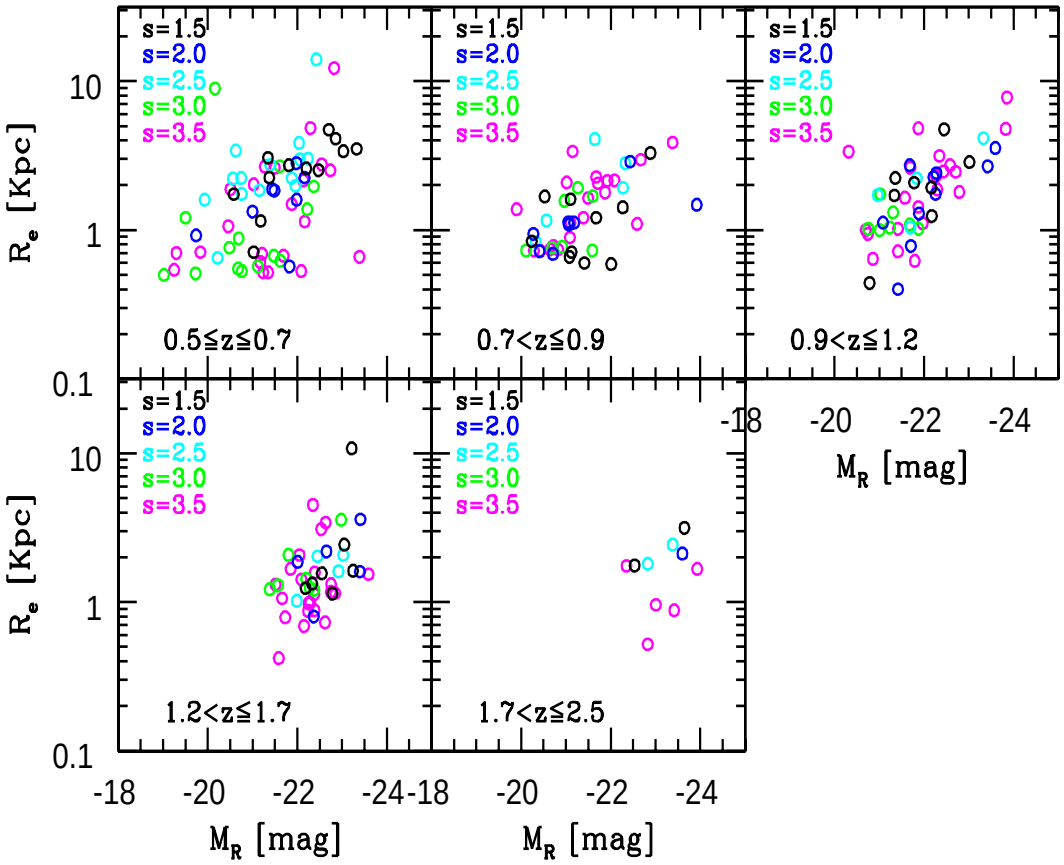

Figure 5.9: Size luminosity relation for the sample of ETGs at different redshift intervals. The different colours in the figures refer to the different slope of the best fitting IMF associated to the galaxies: magenta for $IMF_{3.5}$, green for $IMF_{3.0}$, cyan for $IMF_{2.5}$, blue for $IMF_{2.0}$ and, black for $IMF_{1.5}$. The numbers of galaxies with the different IMFs are reported in the figures.

Nowadays, the issue of the IMF variation remains still an open issue, since the current data do not provide a final proof of the non-universality of the IMF. If the IMF evolves with time and/or with environment remains a crucial point for understanding the stellar mass formation history and for interpreting the stellar population properties of ETGs.

Conclusion

In this thesis it has been presented a detailed study of the early-type galaxies aimed on the one hand to provide a robust approach to select this morphological class of galaxies, and on the other hand to follow the evolution of their properties across the cosmic time.

To understand the formation and evolution of ETGs first of all they must be defined and selected in the same way from low to high redshift. To this aim, starting from a sample of 1302 galaxies (Sec. 2.2), limited at Ks$\leq$ 22, with spectroscopic coverage of 76 % selected in the GOODS-South field, a sample of early-type galaxies (i.e. elliptical and spheroidal galaxies) classified on the basis of their morphology has been selected. The visual morphological classification (Sec. 3.1), performed on the deep ACS/F850LP images, was sustained by a visual inspection of the residual images, obtained by fitting the galaxy surface brightness profiles with a Sérsic model. **The analysis allowed to select 247 ETGs in the redshift range** $0.1 \lesssim \mathbf{z} \lesssim 2.5$**.**

This sample of ETGs was used to perform an accurate comparison with a sample of galaxies selected on the basis of their photometric properties (e.g. quiescence, red colours, high Sérsic index). Indeed, often in literature these methods are used to select ETGs from large sample of galaxies and/or to select ETGs at high redshift, where the morphological classification could be more challenging. However, we demonstrated that these photometric properties are not able to select ETGs at different redshift, and galaxies with different morphologies can be classified as ETGs. We proved that a classification based only on the Sérsic index is not an efficient method to distinguish between spheroidal types ($n > 2.5$) and late-type galaxies ($n < 2.5$) as often happen in literature (e.g. Ravindranath et al. 2004, Barden et al. 2005), since the fitting of the luminosity profile can provide high n values for a considerable fraction of spirals, and can miss ETGs with lower values of n. Also the classification based on two galaxy colours is not able to efficiently separate spheroidals

from discs (Sec. 3.5), nevertheless this criterion is widely adopted to separate different morphological classes with the aim of performing evolutionary studies of singular galaxy type (e.g. Williams et al. 2009, Brammer et al. 2011, Ilbert et al. 2010, 2013, Muzzin et al. 2013). Also a method based on the passivity of the galaxies, estimated through a fixed threshold of sSFR (sSFR=SFR/M_* $\leq 10^{11}$ yr^{-1}), is not able to select only spheroidal galaxies. In particular, taking as reference the passive sample derived with sSFR which assumes a Salpeter IMF in the models, we quantified the differences with the morphological sample in terms of selected galaxies and main sample properties. The results shows that:

- $\sim$ 35 % of passive galaxies have a late-type morphology;
- $\sim$ 26 % of the ETGs were not passive galaxies, hence they would be missed in the passive selection. However, these galaxies are basically equal to the other passive ETGs, but due to the sSFR threshold they have been excluded from the selection;
- no significant differences in stellar masses, ages, radii and SFR were found between the sample of passive galaxies and that of morphological ETGs. Median values of $M_* \sim 5 \times 10^{11}$ M$_\odot$, $r_e \sim 1.5$ Kpc, $SFR \sim 0.1$ M$_\odot$/yr were found;
- ages, stellar masses and SFR of the passive LTGs are highly comparable with the same measurements done for the passive ETGs, due to the similarity of their SEDs fitted with the same spectrophotometric templates (Fig. 3.11). The only marked difference between passive LTGs and ETGs is the axis ratio ($< b/a >_{LTG} \sim 0.5$, $< b/a >_{ETG} \sim 0.8$), witnessing of their different morphology;
- the presence of passive discs in the sample of passive galaxies does not depend on the redshift and on the galaxy mass.

In the light of the above analysis, we also tested the dependence of the selection criterion based on the sSFR from the choice of the stellar initial mass function, recurring to the use of IMFs with a different proportion of low-to-high mass stars. This study produced two main results; first, the selection of passive galaxies with the fixed sSFR threshold ($sSFR \leq 10^{11}$ yr^{-1}) never includes only and all the spheroidal galaxies, irrespective of the assumed IMF. Second, since

different IMFs imply different values of stellar mass and star formation rate used to estimate the sSFR, the sSFR threshold should be rescaled according to the used IMF. However, also in this case none of the selection of passive galaxies allows to collect all the ETGs. In conclusion, morphology and passivity are not equivalent: a selection of passive galaxies is highly dependent on the assumed IMF, produces samples with a high fraction of LTGs, and misses a significant fraction of ETGs.

We used the visually classified sample of 196 ETGs compared with the broad class of 723 LTGs to follow their evolution over the redshift range $0.6 \leq z \leq 2.5$ (Chapter 4). The main results of our analysis can be summarized as follows.

1. The relative fraction of ETGs and LTGs is constant at $0.6 \leq z \leq 2.5$, with spheroidal galaxies settled at 20-30 % and LTGs at 70-80 %, in agreement with previous results. Hence, the population of galaxies does not change significantly their composition across the time at least for masses $< 10^{11}$ $M_{\odot}$, suggesting that the Hubble sequence was already in place more than 10 Gyr ago. For galaxies with $M_{*} \geq 10^{11}$ $M_{\odot}$ at $z < 1$ we found a significant change in the composition of the morphological fraction; in particular we observe an increase in the fraction of massive ETGs to more than 40 % of the massive population.

2. We also investigate the number density evolution of the two classes, finding that irrespective of their morphology and mass, both spheroids and discs have significantly increased their number density from z=2.5 to z=0.6, with LTGs being always the richer population. For the complete sample of massive galaxies ($M_{*} \geq 10^{11}$ $M_{\odot}$), we found that between $z = 2.5$ and $z = 0.6$ the whole population of galaxies increased by a factor of ~ 8. This growth was faster for the massive ETGs population whose number density increases by a factor of $\sim$12, than for the massive LTGs that increased by a factor of ~ 7. This difference, however, is mainly due to the steepening we observe for spheroidal galaxies between $z \sim 1$ and $z \sim 0.6$.

3. We examined the mass fraction evolution for different stellar mass bins and we found that for the low-intermediate mass regime ($M_{*} < 10^{11}$ $M_{\odot}$) the mass fractions follow the same constant evolution, with similar

percentage of the number fractions. For the massive ETGs we observe an increase in the mass fraction toward lower redshift and a growth in the mass density with a similar rate of the number densities. On the contrary, the late-type population increases its number by a factor of ~ 7 while its mass by a factor of ~ 3.5. This implies that new massive late-type objects are progressively added with smaller masses, in agreement with Muzzin et al. (2013).

4. We found that the extremely-massive galaxies ($M_* \gtrsim 4 \times 10^{11}$ $M_\odot$) were in place at high redshift ($z > 2.5$) and that their number did not increase as the less massive ones did ($10^{11} < M_* < 4 \times 10^{11}$ $M_\odot$), but remained approximately constant, suggesting a scenario in which extremely-massive galaxies were mostly formed in the early Universe. Moreover, as the redshift decreases we observe a deviation toward the low-mass end of the stellar mass distribution of the massive LTGs, also recovered in their mass function distribution. The presence of extremely-massive LTGs only at higher redshift suggests a disc-to-spheroid transformation, through one or more processes that quench the star formation and remove the disc such as the dynamical instabilities mechanism (Kormendy & Kennicut 2004).

5. We found that the formation epochs of massive galaxies span a broad range of time with no particular indication towards a privileged time for star formation and with mean ages of a few Gyr younger than the observation redshift. This is not surprising considering the rise of the number density and suggests that new massive galaxies both ETGs and LTGs are assembled as the time flows, with stellar populations of a few Gyr old.

6. We observe that galaxies with greater mass have stellar population older than their counterpart with lower mass. This trend reproduces the expectation of the downsizing scenario (Cowie et al. 1996), where massive galaxies are the first to form stars and populate the galaxy mass function.

Finally, in Chapter 5, the issue of a possible variation of the IMF has been tackled, thanks to the availability of a set of models, that adopt as IMFs a power law form with different slopes. This functional form allows to directly probe if any variation of the relative number of low-to-high mass occurs as

function of time, galaxy mass and galaxy morphology. From this analysis it has been found that the bulk (> 80 %) of the 1302 galaxies in the flux limited sample are best-fitted with IMFs that contain a greater relative number of low mass stars compared to a Salpeter IMF. However, we found that the Salpeter IMF is statistically compatible to reproduce the observed SED of the bulk of the galaxies (~ 85 %). From our studies, no significant variation of the IMF at different cosmic epochs and for different galaxy mass has been detected, with galaxies that at any redshift and mass prefer IMF with high ratio of low-to-high mass stars. Even the analysis of the galaxy colours, that are not dependent on any assumption, did not show a particular trend in preferring a particular IMF. We observe only a slight evidence of the ETGs with redder $U - V_{rest}$ colours to be best-fitted with IMF with a greater abundance of high mass stars, the same trend was not found for the LTGs.

Even if several recent studies point to a varying IMF, we do not observe such variation. We are conscious that the spectrophotometric models suffer from incomplete spectral libraries, as well as poorly calibrated stellar stages (e.g. asymptotic giant branch) and that the spectral energy distribution of a galaxy provides constraints poorer than gravitational sensitive spectral features. Hence, if the issue of a variable or universal IMF want to be solved, better calibrated models coupled with suited spectral data are required.

Publication

A&A 570, A102 (2014)
DOI: 10.1051/0004-6361/201424040

Astronomy & Astrophysics

The population of early-type galaxies: how it evolves with time and how it differs from passive and late-type galaxies

S. Tamburri[1,2], P. Saracco[1], M. Longhetti[1], A. Gargiulo[1], I. Lonoce[1,2], and F. Ciocca[1,2]

[1] INAF – Osservatorio Astronomico di Brera, via Brera 28, 20121 Milano, Italy
e-mail: sonia.tamburri@brera.inaf.it
[2] Dipartimento di Scienza e Alta Tecnologia, Universitá degli Studi dell'Insubria, via Valleggio 11, 22100 Como, Italy

Received 21 April 2014 / Accepted 2 September 2014

ABSTRACT

Aims. There are two aims to our analysis. On the one hand we are interested in addressing whether a sample of morphologically selected early-type galaxies (ETGs) differs from a sample of passive galaxies in terms of galaxy statistics. On the other hand we study how the relative abundance of galaxies, the number density, and, the stellar mass density for different morphological types change over the redshift range $0.6 \leq z \leq 2.5$.
Methods. From the 1302 galaxies brighter than $Ks(\mathrm{AB}) = 22$ selected from the GOODS-MUSIC catalogue, we classified the ETGs, i.e. elliptical (E) and spheroidal galaxies (E/S0), on the basis of their morphology and the passive galaxies on the basis of their specific star formation rate ($sSFR \leq 10^{-11}$ yr^{-1}). Since the definition of a passive galaxy depends on the model parameters assumed to fit the spectral energy distribution of the galaxy, in addition to the assumed sSFR threshold, we probed the dependence of this definition and selection on the stellar initial mass function (IMF).
Results. We find that spheroidal galaxies cannot be distinguished from the other morphological classes on the basis of their low star formation rate, irrespective of the IMF adopted in the models. In particular, we find that a large fraction of passive galaxies (>30%) are disc-shaped objects and that the passive selection misses a significant fraction (~26%) of morphologically classified ETGs. Using the sample of 1302 galaxies morphologically classified into spheroidal galaxies (ETGs) and non-spheroidal galaxies (LTGs), we find that the fraction of these two morphological classes is constant over the redshift range $0.6 \leq z \leq 2.5$, being 20–30% the fraction of ETGs and 70–80% the fraction of LTGs. However, at $z < 1$ these fractions change among the population of the most massive ($M_* \geq 10^{11} M_\odot$) galaxies, with the fraction of massive ETGs rising up to 40% and the fraction of massive LTGs decreasing to 60%. Parallel to this trend, we find that the number density and the stellar mass density of the whole population of massive galaxies increase by almost a factor of ~10 between $0.6 \leq z \leq 2.5$, with a faster increase of these densities for the ETGs than for the LTGs. Finally, we find that the number density of the highest-mass galaxies both ETGs and LTGs ($M_* > 3{-}4 \times 10^{11}\ M_\odot$) does not increase from $z \sim 2.5$, contrary to the lower mass galaxies. This suggests that the most massive galaxies formed at $z > 2.5{-}3$ and that the assembly of such high-mass galaxies is not effective at lower redshift.

Key words. galaxies: evolution – galaxies: elliptical and lenticular, cD – galaxies: formation – galaxies: high-redshift

Bibliography

Abel, T., Bryan, G. L., & Norman, M. L. 2002, Science, 295, 93

Abraham, R. G., Valdes, F., Yee, H. K. C., & van den Bergh, S. 1994, ApJ, 432, 75

Abraham, R. G., van den Bergh, S., Glazebrook, K., et al. 1996a, ApJS, 107, 1

Abraham, R. G., van den Bergh, S., Glazebrook, K., et al. 1996b, ApJS, 107, 1

Abraham, R. G., van den Bergh, S., & Nair, P. 2003, ApJ, 588, 218

Arimoto, N. & Yoshii, Y. 1987, A&A, 173, 23

Arnouts, S., Walcher, C. J., Le Fèvre, O., et al. 2007, A&A, 476, 137

Baldry, I. K., Glazebrook, K., Brinkmann, J., et al. 2004, ApJ, 600, 681

Balestra, I., Mainieri, V., Popesso, P., et al. 2010, A&A, 512, A12

Barden, M., Rix, H.-W., Somerville, R. S., et al. 2005, ApJ, 635, 959

Barnes, J. E. & Hernquist, L. 1996, ApJ, 471, 115

Barnes, J. E. & Hernquist, L. E. 1991, ApJ, 370, L65

Bastian, N., Covey, K. R., & Meyer, M. R. 2010, ARA&A, 48, 339

Baugh, C. M., Lacey, C. G., Frenk, C. S., et al. 2005, MNRAS, 356, 1191

Baum, W. A. 1959, PASP, 71, 106

Bell, E. F. 2008, ApJ, 682, 355

Bell, E. F., Wolf, C., Meisenheimer, K., et al. 2004, ApJ, 608, 752

Bender, R., Burstein, D., & Faber, S. M. 1992, ApJ, 399, 462

Bernardi, M., Sheth, R. K., Annis, J., et al. 2003, AJ, 125, 1866

Bertin, E. & Arnouts, S. 1996, A&AS, 117, 393

Bezanson, R., van Dokkum, P. G., Tal, T., et al. 2009, ApJ, 697, 1290

Binney, J. & Tremaine, S. 2008, Galactic Dynamics: Second Edition (Princeton University Press)

Birnboim, Y. & Dekel, A. 2003, MNRAS, 345, 349

Blumenthal, G. R., Faber, S. M., Primack, J. R., & Rees, M. J. 1984, Natur, 311, 517

Bolzonella, M., Miralles, J.-M., & Pelló, R. 2000, A&A, 363, 476

Bournaud, F., Daddi, E., Elmegreen, B. G., et al. 2008, A&A, 486, 741

Bower, R. G., Lucey, J. R., & Ellis, R. S. 1992, MNRAS, 254, 601

Bower, R. G., Terlevich, A., Kodama, T., & Caldwell, N. 1999, in Astronomical Society of the Pacific Conference Series, Vol. 163, Star Formation in Early Type Galaxies, ed. P. Carral & J. Cepa, 211

Boylan-Kolchin, M., Springel, V., White, S. D. M., Jenkins, A., & Lemson, G. 2009, MNRAS, 398, 1150

Brammer, G. B., Whitaker, K. E., van Dokkum, P. G., et al. 2011, ApJ, 739, 24

Bressan, A., Chiosi, C., & Fagotto, F. 1994, ApJS, 94, 63

Bromm, V., Coppi, P. S., & Larson, R. B. 2002, ApJ, 564, 23

Bruzual, G. & Charlot, S. 2003, MNRAS, 344, 1000

Buitrago, F., Trujillo, I., Conselice, C. J., & Häu
ler, B. 2013, MNRAS, 428, 1460

Bundy, K., Ellis, R. S., & Conselice, C. J. 2005, ApJ, 625, 621

Bundy, K., Ellis, R. S., Conselice, C. J., et al. 2006, ApJ, 651, 120

Calzetti, D., Armus, L., Bohlin, R. C., et al. 2000, ApJ, 533, 682

Cappellari, M., McDermid, R. M., Alatalo, K., et al. 2012, Nature, 484, 485

Cassata, P., Cimatti, A., Franceschini, A., et al. 2005, MNRAS, 357, 903

Cassata, P., Giavalisco, M., Guo, Y., et al. 2011, ApJ, 743, 96

Cattaneo, A., Dekel, A., Devriendt, J., Guiderdoni, B., & Blaizot, J. 2006, MNRAS, 370, 1651

Ceverino, D., Dekel, A., Mandelker, N., et al. 2012, MNRAS, 420, 3490

Chabrier, G. 2003, PASP, 115, 763

Chiosi, C. & Carraro, G. 2002, MNRAS, 335, 335

Cimatti, A. 2009, in American Institute of Physics Conference Series, Vol. 1111, American Institute of Physics Conference Series, ed. G. Giobbi, A. Tornambe, G. Raimondo, M. Limongi, L. A. Antonelli, N. Menci, & E. Brocato, 191–198

Cimatti, A., Daddi, E., & Renzini, A. 2006, A&A, 453, L29

Ciotti, L. 1991, A&A, 249, 99

Cole, S., Aragon-Salamanca, A., Frenk, C. S., Navarro, J. F., & Zepf, S. E. 1994, MNRAS, 271, 781

Colless, M., Dalton, G., Maddox, S., et al. 2001, MNRAS, 328, 1039

Conroy, C. & van Dokkum, P. G. 2012, ApJ, 760, 71

Conselice, C. J. 2003, ApJS, 147, 1

Conselice, C. J. 2006, MNRAS, 373, 1389

Conselice, C. J., Bluck, A. F. L., Buitrago, F., et al. 2011, MNRAS, 413, 80

Conselice, C. J., Bundy, K., Trujillo, I., et al. 2007, MNRAS, 381, 962

Cowie, L. L., Songaila, A., Hu, E. M., & Cohen, J. G. 1996, AJ, 112, 839

Daddi, E., Alexander, D. M., Dickinson, M., et al. 2007, ApJ, 670, 173

Daddi, E., Cimatti, A., Renzini, A., et al. 2004, ApJ, 617, 746

De Lucia, G. & Blaizot, J. 2007, MNRAS, 375, 2

De Lucia, G. & Borgani, S. 2012, MNRAS, 426, L61

De Lucia, G., Springel, V., White, S. D. M., Croton, D., & Kauffmann, G. 2006, MNRAS, 366, 499

De Santis, C., Grazian, A., Fontana, A., & Santini, P. 2007, NewA, 12, 271

de Vaucouleurs, G. 1948, Annales d'Astrophysique, 11, 247

Dekel, A. & Birnboim, Y. 2006, MNRAS, 368, 2

Dekel, A., Birnboim, Y., Engel, G., et al. 2009, Nature, 457, 451

Di Matteo, T., Springel, V., & Hernquist, L. 2005, Natur, 433, 604

Djorgovski, S. & Davis, M. 1987, ApJ, 313, 59

Dressler, A., Lynden-Bell, D., Burstein, D., et al. 1987, ApJ, 313, 42

Drory, N., Salvato, M., Gabasch, A., et al. 2005, ApJ, 619, L131

Eggen, O. J., Lynden-Bell, D., & Sandage, A. R. 1962, ApJ, 136, 748

Ellis, R. 1998, Natur, 395, A3

Elmegreen, B. G. 2009, in The Evolving ISM in the Milky Way and Nearby Galaxies

Elmegreen, B. G. & Elmegreen, D. M. 2005, ApJ, 627, 632

Faber, S. M., Willmer, C. N. A., Wolf, C., et al. 2007, ApJ, 665, 265

Ferreras, I., La Barbera, F., de la Rosa, I. G., et al. 2013, MNRAS, 429, L15

Feulner, G., Goranova, Y., Drory, N., Hopp, U., & Bender, R. 2005, MNRAS, 358, L1

Fioc, M. & Rocca-Volmerange, B. 1997, A&A, 326, 950

Fontana, A., D'Odorico, S., Poli, F., et al. 2000, AJ, 120, 2206

Fontana, A., Pozzetti, L., Donnarumma, I., et al. 2004, A&A, 424, 23

Fontana, A., Salimbeni, S., Grazian, A., et al. 2006, A&A, 459, 745

Fontana, A., Santini, P., Grazian, A., et al. 2009, A&A, 501, 15

Fontanot, F., De Lucia, G., Monaco, P., Somerville, R. S., & Santini, P. 2009, MNRAS, 397, 1776

Franceschini, A., Rodighiero, G., Cassata, P., et al. 2006, A&A, 453, 397

Franx, M., Labbé, I., Rudnick, G., et al. 2003, ApJ, 587, L79

Franzetti, P., Scodeggio, M., Garilli, B., et al. 2007, A&A, 465, 711

Freeman, K. C. 1970, ApJ, 160, 811

Fritz, A., Scodeggio, M., Ilbert, O., et al. 2014, A&A, 563, A92

Fukugita, M., Hogan, C. J., & Peebles, P. J. E. 1998, ApJ, 503, 518

Gargiulo, A., Saracco, P., Longhetti, M., La Barbera, F., & Tamburri, S. 2012, MNRAS, 425, 2698

Genzel, R., Burkert, A., Bouché, N., et al. 2008, ApJ, 687, 59

Giallongo, E., D'Odorico, S., Fontana, A., et al. 1998, AJ, 115, 2169

Giavalisco, M., Ferguson, H. C., Koekemoer, A. M., et al. 2004, ApJ, 600, L93

Graham, A. W. & Driver, S. P. 2005, PASA, 22, 118

Granato, G. L., De Zotti, G., Silva, L., Bressan, A., & Danese, L. 2004, ApJ, 600, 580

Grazian, A., Fontana, A., de Santis, C., et al. 2006, A&A, 449, 951

Hennebelle, P. & Chabrier, G. 2008, ApJ, 684, 395

Hopkins, A. M. & Beacom, J. F. 2006, ApJ, 651, 142

Hopkins, P. F. 2013, MNRAS, 433, 170

Hopkins, P. F., Bundy, K., Hernquist, L., Wuyts, S., & Cox, T. J. 2010, MNRAS, 401, 1099

Hubble, E. P. 1926, ApJ, 64, 321

Hubble, E. P. 1936, Realm of the Nebulae

Ilbert, O., McCracken, H. J., Le Fèvre, O., et al. 2013, A&A, 556, A55

Ilbert, O., Salvato, M., Le Floc'h, E., et al. 2010, ApJ, 709, 644

Ilbert, O., Tresse, L., Arnouts, S., et al. 2004, MNRAS, 351, 541

Ilbert, O., Tresse, L., Zucca, E., et al. 2005, A&A, 439, 863

Jimenez, R., Bernardi, M., Haiman, Z., Panter, B., & Heavens, A. F. 2007, ApJ, 669, 947

Jones, D. H., Peterson, B. A., Colless, M., & Saunders, W. 2006, MNRAS, 369, 25

Kauffmann, G. & White, S. D. M. 1993, MNRAS, 261, 921

Kauffmann, G., White, S. D. M., & Guiderdoni, B. 1993, MNRAS, 264, 201

Kereš, D., Katz, N., Weinberg, D. H., & Davé, R. 2005, MNRAS, 363, 2

Khochfar, S. & Silk, J. 2006, ApJ, 648, L21

Kodama, T., Arimoto, N., Barger, A. J., & Arag'on-Salamanca, A. 1998, A&A, 334, 99

Kodama, T., Yamada, T., Akiyama, M., et al. 2004, MNRAS, 350, 1005

Kroupa, P. 2001, MNRAS, 322, 231

Kroupa, P., Weidner, C., Pflamm-Altenburg, J., et al. 2013, The Stellar and Sub-Stellar Initial Mass Function of Simple and Composite Populations, ed. T. D. Oswalt & G. Gilmore, 115

La Barbera, F., Ferreras, I., Vazdekis, A., et al. 2013, MNRAS, 433, 3017

Labbé, I., Huang, J., Franx, M., et al. 2005, ApJ, 624, L81

Larson, R. B. 1974, MNRAS, 166, 585

Larson, R. B. 1998, MNRAS, 301, 569

Larson, R. B. 2005, MNRAS, 359, 211

Larson, R. B. & Tinsley, B. M. 1978, ApJ, 219, 46

Laureijs, R., Amiaux, J., Arduini, S., et al. 2011, ArXiv e-prints

Le Borgne, J.-F., Bruzual, G., Pelló, R., et al. 2003, A&A, 402, 433

Lilly, S. J., Le Brun, V., Maier, C., et al. 2009, ApJS, 184, 218

Lilly, S. J., Le Fèvre, O., Renzini, A., et al. 2007, ApJS, 172, 70

Lisker, T. 2008, ApJS, 179, 319

Longhetti, M. & Saracco, P. 2009, MNRAS, 394, 774

Lonoce, I., Longhetti, M., Saracco, P., Gargiulo, A., & Tamburri, S. 2014, MNRAS, 444, 2048

López-Sanjuan, C., Le Fèvre, O., Ilbert, O., et al. 2012, A&A, 548, A7

Lotz, J. M., Primack, J., & Madau, P. 2004, AJ, 128, 163

Madau, P., Ferguson, H. C., Dickinson, M. E., et al. 1996, MNRAS, 283, 1388

Mancini, C., Daddi, E., Renzini, A., et al. 2010, MNRAS, 401, 933

Maraston, C. 2005, MNRAS, 362, 799

Maraston, C., Daddi, E., Renzini, A., et al. 2006, ApJ, 652, 85

Marchesini, D., van Dokkum, P. G., Förster Schreiber, N. M., et al. 2009, ApJ, 701, 1765

McCracken, H. J., Capak, P., Salvato, M., et al. 2010, ApJ, 708, 202

Mei, S., Blakeslee, J. P., Stanford, S. A., et al. 2006, ApJ, 639, 81

Mei, S., Stanford, S. A., Holden, B. P., et al. 2012, ApJ, 754, 141

Menci, N., Fontana, A., Giallongo, E., Grazian, A., & Salimbeni, S. 2006, ApJ, 647, 753

Moresco, M., Pozzetti, L., Cimatti, A., et al. 2013, A&A, 558, A61

Mortlock, A., Conselice, C. J., Bluck, A. F. L., et al. 2011, MNRAS, 413, 2845

Mortlock, A., Conselice, C. J., Hartley, W. G., et al. 2013, MNRAS, 433, 1185

Muzzin, A., Marchesini, D., Stefanon, M., et al. 2013, ApJ, 777, 18

Naab, T., Johansson, P. H., & Ostriker, J. P. 2009, ApJ, 699, L178

Naab, T., Johansson, P. H., Ostriker, J. P., & Efstathiou, G. 2007, ApJ, 658, 710

Nipoti, C., Treu, T., Leauthaud, A., et al. 2012, MNRAS, 422, 1714

Nonino, M., Dickinson, M., Rosati, P., et al. 2009, ApJ, 183, 244

Norberg, P., Cole, S., Baugh, C. M., et al. 2002, MNRAS, 336, 907

Ostriker, J. P., Peebles, P. J. E., & Yahil, A. 1974, ApJ, 193, L1

Padoan, P. & Nordlund, Å. 2002, ApJ, 576, 870

Papovich, C., Moustakas, L. A., Dickinson, M., et al. 2006, ApJ, 640, 92

Peng, C. Y., Ho, L. C., Impey, C. D., & Rix, H. 2002, AJ, 124, 266

Pérez-González, P. G., Rieke, G. H., Egami, E., et al. 2005, ApJ, 630, 82

Perlmutter, S., Aldering, G., Goldhaber, G., et al. 1999, ApJ, 517, 565

Popesso, P., Dickinson, M., Nonino, M., et al. 2009, A&A, 494, 443

Pozzetti, L., Bolzonella, M., Zucca, E., et al. 2010, A&A, 523, A13

Pozzetti, L., Cimatti, A., Zamorani, G., et al. 2003, A&A, 402, 837

Prugniel, P. & Simien, F. 1997, A&A, 321, 111

Raichoor, A., Mei, S., Nakata, F., et al. 2011, ApJ, 732, 12

Raichoor, A., Mei, S., Stanford, S. A., et al. 2012, ApJ, 745, 130

Rasera, Y. & Teyssier, R. 2006, A&A, 445, 1

Ravindranath, S., Ferguson, H. C., Conselice, C., et al. 2004, ApJ, 604, L9

Renzini, A. 2006, ARA&A, 44, 141

Renzini, A. & Ciotti, L. 1993, ApJ, 416, L49

Retzlaff, J., Rosati, P., Dickinson, M., et al. 2010, A&A, 511, A50

Riess, A. G., Filippenko, A. V., Challis, P., et al. 1998, AJ, 116, 1009

Roberts, M. S. & Haynes, M. P. 1994, ARA&A, 32, 115

Rubin, V. C., Thonnard, N., & Ford, Jr., W. K. 1978, ApJ, 225, L107

Salimbeni, S., Giallongo, E., Menci, N., et al. 2008, A&A, 477, 763

Salpeter, E. E. 1955, ApJ, 121, 161

Sandage, A. & Visvanathan, N. 1978a, ApJ, 225, 742

Sandage, A. & Visvanathan, N. 1978b, ApJ, 223, 707

Santini, P., Fontana, A., Grazian, A., et al. 2009, A&A, 504, 751

Saracco, P., Fiano, A., Chincarini, G., et al. 2006, MNRAS, 367, 349

Saracco, P., Gargiulo, A., & Longhetti, M. 2012, MNRAS, 422, 3107

Saracco, P., Longhetti, M., & Gargiulo, A. 2011, MNRAS, 412, 2707

Scarlata, C., Carollo, C. M., Lilly, S. J., et al. 2007, ApJS, 172, 494

Schade, D., Lilly, S. J., Crampton, D., et al. 1999, ApJ, 525, 31

Schawinski, K., Khochfar, S., Kaviraj, S., et al. 2006, Natur, 442, 888

Schechter, P. 1976, ApJ, 203, 297

Schiavon, R. P., Faber, S. M., Konidaris, N., et al. 2006, ApJ, 651, L93

Scoville, N., Aussel, H., Brusa, M., et al. 2007, ApJS, 172, 1

Sersic, J. L. 1968, Atlas de galaxias australes, ed. Sersic, J. L.

Shen, S., Mo, H. J., White, S. D. M., et al. 2003, MNRAS, 343, 978

Shetty, S. & Cappellari, M. 2014, ApJ, 786, L10

Spiniello, C., Trager, S. C., Koopmans, L. V. E., & Chen, Y. P. 2012, ApJL, 753, L32

Springel, V. 2005, MNRAS, 364, 1105

Stanford, S. A., Eisenhardt, P. R., & Dickinson, M. 1998, ApJ, 492, 461

Strateva, I., Ivezić, Ž., Knapp, G. R., et al. 2001, AJ, 122, 1861

Szomoru, D., Franx, M., Bouwens, R. J., et al. 2011, ApJ, 735, L22

Thomas, D., Maraston, C., Bender, R., & Mendes de Oliveira, C. 2005, ApJ, 621, 673

Thomas, D., Maraston, C., Schawinski, K., Sarzi, M., & Silk, J. 2010, MNRAS, 404, 1775

Tinsley, B. M. 1972, ApJ, 178, 319

Treu, T., Auger, M. W., Koopmans, L. V. E., et al. 2010, ApJ, 709, 1195

Treu, T., Ellis, R. S., Liao, T. X., & van Dokkum, P. G. 2005, ApJ, 622, L5

van den Bergh, S., Abraham, R. G., Ellis, R. S., et al. 1996, AJ, 112, 359

van der Wel, A., Rix, H.-W., Wuyts, S., et al. 2011, ApJ, 730, 38

van Dokkum, P. G. & Conroy, C. 2010, Natur, 468, 940

van Dokkum, P. G. & Franx, M. 1996, MNRAS, 281, 985

van Dokkum, P. G. & Stanford, S. A. 2003, ApJ, 585, 78

Vanzella, E., Cristiani, S., Dickinson, M., et al. 2008, A&A, 478, 83

Visvanathan, N. & Sandage, A. 1977, ApJ, 216, 214

Wechsler, R. H. 2008, in Astronomical Society of the Pacific Conference Series, Vol. 399, Panoramic Views of Galaxy Formation and Evolution, ed. T. Kodama, T. Yamada, & K. Aoki, 82

Weinberg, D. H., Mortonson, M. J., Eisenstein, D. J., et al. 2013, PhR, 530, 87

White, S. D. M. & Rees, M. J. 1978, MNRAS, 183, 341

Wilkins, S. M., Hopkins, A. M., Trentham, N., & Tojeiro, R. 2008, MNRAS, 391, 363

Williams, R. J., Quadri, R. F., Franx, M., van Dokkum, P., & Labbé, I. 2009, ApJ, 691, 1879

Willmer, C. N. A., Faber, S. M., Koo, D. C., et al. 2006, ApJ, 647, 853

Wuyts, S., Labbé, I., Franx, M., et al. 2007, ApJ, 655, 51

York, D. G., Adelman, J., Anderson, Jr., J. E., et al. 2000, AJ, 120, 1579

Zel'dovich, Y. B. 1970, A&A, 5, 84

Zucca, E., Bardelli, S., Bolzonella, M., et al. 2009, A&A, 508, 1217

Zucca, E., Ilbert, O., Bardelli, S., et al. 2006, A&A, 455, 879

Zwicky, F. 1933, Helvetica Physica Acta, 6, 110